Polymetallic mineralization at the Toyoha Mine, Hokkaido, Japan

Eijun Ohta

1991

(1)

Polymetallic mineralization at the Toyoha Mine, Hokkaido, Japan

by

Eijun Ohta

Geological Survey of Japan

A Thesis Submitted to the Faculty of Science

DEPARTMENT OF GEOLOGY AND MINERALOGY

In Partial Fulfillment of the Requirements
For the Degree of

DOCTOR OF SCIENCE

HOKKAIDO UNIVERSITY

1991

ACKNOWLEDGMENTS

I am very grateful to Professors S. Yui and Y. Hariya, and Assistant Professors H. Matsueda and T. Kikuchi at Hokkaido University for advising and providing me a chance to complete this study. Sincere thanks are due to Dr. J. Yajima for encouragement, support, and critical reading of the manuscript throughout this study. The cooperation of successive directors and many geologists of the Exploration Section of the Toyoha Mines Co. Ltd. during underground survey is also gratefully acknowledged. Finally I would like to express my sincere thanks to my fellows at Hokkaido Branch of Geological Survey of Japan; Y. Watanabe, M. Nakagawa and N. Fujibayashi for everyday discussions on geology and mineralogy, T. Sato for preparing hundreds of excellent polished and thin sections for the laboratory works, T. Hasaka for his important suggestions on data processing with personal computers.

TABLE OF CONTENTS

LIST OF ILLUSTRATIONS

LIST OF TABLES

ABSTRACT

Toyoha is the largest lead-zinc-silver vein-type deposit in Japan. A remarkable feature of this deposit is occurrence of rare metals; tin, indium, wolfram, cobalt, nickel, bismuth, gallium, antimony and arsenic. Among them, indium concentration is extraordinary high enough to make the mine a leading indium producer in the world. Trace amounts of molybdenum, vanadium, selenium and tellurium are also detected in the veins and drill cores from the mining area.

Two stages of the mineralization at Toyoha, the earlier and the later, are recognized as cutting relations of the veins, and the later is classified into successive five substages A, B, C, D and E. Detailed underground and microscopic observations, and EPMA analyses have revealed that the rare metals derived from the ore solution during the substage B. Tin and indium are detected in cassiterite, stannite, kesterite, rhodostannite, roquesite, an unnamed Zn-In mineral, an unnamed Ag-In mineral, hocartite, pirquitasite, toyohaite (Ag analogue of rhodostannite), berndtite, herzenbergite, teallite, sphalerite, chalcopyrite and solid solutions among these phases. Bismuth is in matildite, bismuthinite, gustavite, native bismuth, galena and solid solutions among these minerals, and in tetrahedrite. Cobalt and nickel exist in the cobaltite-arsenopyrite solid solution, and are detected also in pyrite as minor component. Arsenic does not make sulfosalt with silver as main component in the Toyoha deposit, though silver-antimony and silver-lead-antimony sulfosalts are common ore minerals. Gallium is detected as a minor component in sphalerite, though no germanium is

found to date. Wolframite and two types of unknown Mo-Pb-Sb sulfides also occur.

Silver occurs as native silver, argentite and electrum in the earlier veins which have been significantly modified by the later-stage mineralization, while it exists in the silver-antimony and silver-lead-antimony sulfosalts, the tetrahedrite-tennantite solid solution, Ag-Sn minerals, the Ag-In mineral, Bi-Pb-Ag-S minerals, and electrum in the later veins. Formation of argentite in the earlier veins is attributed to the later-stage mineralization. That is, deposition of argentite in the earlier veins and the silver sulfosalts in the later veins proceeded simultaneously; as oxidation of silver-sulfide complexes by reaction with hematite in the earlier veins, and as dissociation of silver-chloride complexes by dilution of the ore solution in the later veins; during the substage C.

Deposition of the metals occurred upon mixing of the hydrothermal fluid from a granitic source with ambient geothermal water of meteoric origin. The temperature and NaCl equivalent concentration of the initial ore solution before the mixing were higher than 250°C and 2.3 weight percent for the Harima-Tajima trend (earlier-stage mineralization), and higher than 300°C and 4.2 weigh percent for the Izumo trend (later-stage mineralization). Especially for the rare-metal mineralization, initial hydrothermal fluid at 350 to 400°C, salinity of 5 to 7 equivalent weight percent NaCl, fo_2 below the upper limit of pyrrhotite, fs_2 at around the pyrrhotite-pyrite boundary, is consistent with data from fluid inclusions and mineral-assemblages at Toyoha. The temperature and salinity of the ambient water are estimated to be 160 to 210°C

and 0.35 weight percent for the earlier stage, and 210 to 250°C and 0.5 weight percent for the later.

The earlier- and the later-stage evolution trends of the ore solutions on the temperature versus fs_2 diagram correspond to the trends caused by magnetite- and ilmenite-series granitoids respectively. These trends and the occurrence of tin and indium in the later veins suggest that the later-stage mineralization was initiated by an ore solution emanated from an intrusion of ilmenite-series granitoid, and that the earlier was derived from a magnetite-series granitoid. The ilmenite-series granitoid may have been evolved through local reduction of a magnetite-series magma by contamination of organic materials in the Usubetsu Formation. The chronological data, the zonal distribution of minerals, grades of metals and fluid inclusions, and the flow vector of the currently active hydrothermal solution found in the Shinano vein imply that the source of the ore solution is a latent granitoid intrusion below the Muineyama Andesite.

Key words: Toyoha, Polymetallic vein, Silver, Lead, Zinc, Tin, Indium, Bismuth, Cobalt, Formation condition.

CHAPTER 1

INTRODUCTION

Toyoha is the largest among the vein-type deposits in Japan. The veins are situated about 40 kilometers on road to the southwest of the center of Sapporo. More than 15 million metric tons of crude ore has been mined since 1915, and the metal amounts of silver, lead and zinc produced exceed 1,560, 330,000 and 870,000 metric tons (Tani et al., 1985) respectively. In addition, copper, manganese, antimony and arsenic are common metals occur in the mine. Both mining and exploration have been quite active at this mine, and recent successive discovery of the Izumo and Shinano veins indicates the great potentiality of the deposit in the future. As Figure 1a and Figure 1c show, the Izumo, Shinano and Sorachi veins, and southern half of the Soya vein are in the southeast of the deposit, and are marked by occurrence of rare elements; tin, tungsten (Yajima, 1977), indium (Ohta, 1980), bismuth, molybdenum (Ohta et al., 1987), cobalt, nickel (Narui et al., 1988) and gallium (this study). Moreover, recent studies detected tellurium, selenium and vanadium in drill cores recovered by MMAJ, Metal Mining Agency of Japan, (1988; JTU1 and JTU2 in Figure 1a and Figure 1c), and by the Toyoha Mines Co. Ltd. from southwest of the current mining area (Ohta, unpublished data). Among the elements listed above, indium concentration in these veins is about 250 ppm in average (Yoshie et al., 1986), which is comparable to that in zinc concentrates (not in crude ore) of some representative indium producers in central Peru (Soler, 1987). This figure and the current production tonnage of crude ore (about 500,000 metric tons/year) indicate that Toyoha is currently the

largest indium producer in the world. The grades of lead (2.32 wt%), zinc (7.48 wt%) and silver (148 ppm) in the crude ore are also high (Yoshie et al., 1986). Because of the high reserve potentiality, the high grade ore and the occurrences of rare metals, many geological and mineralogical arguments have been focused on this deposit in this decade.

The present investigation is aimed at giving detailed descriptions of the rare-metal occurrence, understanding the process of mineralization in and around the mining area, and interpreting the physicochemical environment of metal deposition, within the framework of both macro- and microscopic observations of ores and host rocks, and chemical analyses by means of EPMA. As a result, a model for the formation of the rare-metal bearing high-grade ore is proposed.

CHAPTER 2

OUTLINE OF GEOLOGY

Geology:

The Toyoha deposit is hosted by Tertiary sediments, andesite, basalt and rhyolite (Figure 1a, Figure 1b, Table 1). The basement of the mining area is the Usubetsu Formation, which is unconformably overlain by the Early Miocene Shiramizugawa and Koyanagizawa Formations, the Middle Miocene Motoyama and Nagato Formations, the Late Miocene Oheyama Formation, the Pliocene Suberizawa Formation, and the Pliocene to Pleistocene Muineyama Andesite. The Usubetsu and the Shiramizugawa Formations are exposed along the Shiramizugawa, about 6 to 9 kilometers to the southeast of the mining office (Figure 1b), but is not observed around the mining area. Drill data after NEDO, New Energy and Industrial Technology Development Organization (1988; see Figure 1b), however, indicate that these Formations contain significant volumes of underlying rocks of the area.

Alteration:

Andesite of the Motoyama and the Nagato Formations are overprinted by pervasive propylitic alteration, whose genetic relation to the ore mineralization is not known. Sawai (1986), however, discriminated vertical progressive zonation of the alteration mineral assemblage in the propylitic zone distributed between the mining area and the Yunosawa Creek, two kilometers to the east of the mining office, and considered the alteration of diagenetic origin caused by the extensive geothermal

activity of the area. This indicates that, at least, a part of the propylitic zone is of the same origin with the ore mineralization, which also is related to the current geothermal activity (Yajima and Ohta, 1979; Kanbara et al., 1989). Assemblages of gangue minerals are similar to those of alteration minerals distributed in close vicinity to the veins, and three types are discriminated; propylitic (quartz + chlorite + pyrite ± sericite ± calcite ± rutile ± epidote ± apatite), phyllic (sericite + quartz + pyrite ± chlorite), and argillic (kaolin minerals + quartz + pyrite ± pyrophyllite ± sericite ± alunite ± jarosite ± wavellite). The argillic assemblage is common only in the southeastern veins which produce the rare metals listed above.

Chronology:

Absolute ages of rocks around Toyoha have been determined by Igarashi et al. (1978), Watanabe and Iwata (1986), Sawai and Ganzawa (1988), NEDO (1988), Watanabe (1990b). Marumo and Sawai (1986), Sawai and Itaya (1988), and Sawai et al. (1989) determined K-Ar ages of sericite from the major veins, and from the Okuiburi and Yunosawa alteration zones around Toyoha. The results indicate that the mineralization (2.93 - 0.49 Ma) and alteration (2.90 Ma for Okuiburi, 2.39 and 2.40 Ma for Yunosawa) started about 3 million years ago, at around the time of the eruption of the Muineyama Andesite, to which Watanabe (1990b) ascribed the mineralization at Toyoha. These chronological data are summarized in Table 1.

Table 1. Rock facies and their absolute ages around Toyoha.

FT: fission-track KA: potassium-argon FS: fossils

Formation	rock facies	age(Ma)	method	reference
Nagaoyama*1	two pyroxene andesite	1.9	FT	Igarashi et al.(1978)
Andesite		3.5	KA	NEDO(1988)
Muineyama Andesite	ditto	3.0, 3.1	KA	Watanabe(1990b)
Sanbonmata*2	dacite lava etc.	3.3	FT	Sawai and Ganzawa(1988)
Oshidorizawa*3	felsic tuff, mudstone	8.8	FT	ditto
Nagato	andesite lava etc.			
Motoyama	acidic tuff tuffaceous sandstone	13.3, 14.2	FT	Sawai and Ganzawa(1988)
	mudstone conglomerate	12 to 15	FS	Watanabe and Iwata(1986)
Koyanagizawa	rhyolite, basalt andesite	15	FT	Igarashi et al.(1978)
Usubetsu	acidic welded tuff shale, sandstone	24	FT	Koshimizu and Narita(1987)
Intrusions				
granodiorite from drill TH-7		15.8, 9.1	KA	NEDO(1988)
granodiorite from drill TH-5		12.1, 14.0	KA	ditto
granodiorite from drill TH-4		18.2	KA	ditto
quartz porphyry at Jozankei		8.5	KA	ditto
ditto		10.9	KA	Watanabe et al. (1989)
Dikes				
basalt and rhyolite intrude into the Motoyama Formation				
andesite intrudes into the Nagato Formation				

*1 Corresponds to the lower unit of the Muineyama Andesite
*2 Equivalent to the Suberizawa Formation in Figure 1
*3 Equivalent to the Oheyama Formation in Figure 1

CHAPTER 3

VEIN SYSTEM AND MINERALIZATION STAGES

Vein System:

More than fifty veins have been found to date in the Toyoha deposit. Two formation stages of the veins have been discriminated (Akome and Haraguchi, 1963, 1967; Miyajima et al., 1971; Hashimoto et al., 1977; Yajima and Ohta, 1979). The veins formed in the earlier- and the later-stage mineralizations are expressed as "earlier veins" and "later veins" respectively in this paper. It should be noted, however, that the "earlier veins" have been significantly modified by the later-stage mineralization (e.g. Yajima and Ohta, 1979), and are defined as "the veins which have been formed mainly by the earlier-stage mineralization" (Ohta, 1980). In this sense, the Harima, Tajima, Chikugo (No.1, 2 and 3) and Rebun veins are defined as the earlier, and the Shinano, Izumo, Sorachi and Soya are the later (Figure 1c). In addition to zinc, lead and silver, the veins of both stages produce subordinate amount of manganese especially in the northwest of the vein swarm, while a high-grade (more than one weight percent) copper zone is recognized in the Shinano and Izumo veins on the southeast of the vein swarm (Kanbara et al., 1989). The distribution of the rare elements such as tin, indium, bismuth and cobalt in the current mining area is centered on the southeastern border of the vein swarm, at around the boundary between the Izumo and Shinano veins, and is limited mostly in the later-stage veins except northern half of the Soya (Figure 1c) where these rare elements are scarce though manganese abounds. Watanabe (1990a)

summarized previous discussions on formation of the vein system at Toyoha, and introduced a new idea of "pull-apart vein system".

Mineralization Stages:

The earlier-stage ore is characterized by coarse-grained aggregate of brown to amber sphalerite, galena, pyrite and quartz disseminated by fine-grained hematite. Banded pyrite-hematite ore described by Yajima and Okabe (1971) is also characteristic of this stage. Manganese of the earlier stage occurs as both carbonates and silicates, and is associated with pyrite (Yoshie et al., 1986). Evident cutting relations between the earlier- and later-stage mineralizations is observed at the crossing points of Tajima and Soya veins, and of Harima and Sorachi (e.g. Akome and Haraguchi, 1967). Based on underground survey and microscopic observations of ores of the Izumo and Sorachi veins, Ohta (1980) classified the later stage into three substages (Figure 2), and two substages are added and defined by Ohta (1989) and this study. Kanbara et al. (1989) classified the earlier stage into two (I, II), and the later into five substages (III to VII). The two classifications can be correlated and summarized as follows:

A (Substage of pyrrhotite and iron-rich sphalerite; III-a in Kanbara et al., 1989) is characterized by a simple assemblage of pyrrhotite and sphalerite. Though the pyrrhotite has been mostly altered to marcasite and pyrite by later ore solutions, large masses of tabular pseudomorphs of pyrrhotite are frequently observed in the later-stage veins. Sphalerite of the substage A occurs as fine-grained dark-colored aggregate together with the pseudomorphs of pyrrhotite, and also has been partly replaced by minerals of the later substages B

and C (mostly by coarse-grained brown sphalerite).

B (Substage of the rare metals such as Sn, In, W, Co, Ni, Bi, Mo and Ga; III-b and IV) is characterized by the rare metals listed above. The individual minerals which contain the rare metals, however, are not easily distinguishable from others under naked eyes in most cases. A typical major-mineral assemblage of this substage is coarse-grained brown sphalerite, galena and pyrite (Figure 2). Although chalcopyrite of this substage is minor in amount at upper levels, it is a major component at deep levels of the Shinano and Izumo veins where bismuth concentration in the chalcopyrite-rich ore reaches up to 0.n wt% (Kanbara et al., 1989). Majority of the fine-grained milky quartz which dominates over the coarse crystals of quartz in the later-stage veins seems to have precipitated at the beginning of this substage, and is associated with cassiterite. Underground observations revealed that ore solution of this substage has largely modified the mineral assemblage of the substage A.

C (Substage of silver sulfosalts; V) is characterized by abundant galena, colloform sphalerite and wurtzite, and subordinate amount of chalcopyrite. Although silver minerals are identifiable only under microscope in most cases, large masses of diaphorite banded together with galena and the colloform sphalerite are observed at the Sorachi vein -350 mL (point 4 in Figure 1c), where sphalerite of the substage B is cut by the band and is fouled with sericite. The cutting relation or the tectonic boundary between the substages B and C is frequently observed.

D (Substage of kaolin minerals and decomposition of preexisting sulfides; VI ?) is characterized by kaolin minerals associated with pyrite, sulfates and minor amount of rare minerals such as toyohaite, rhodostannite, teallite, herzenbergite, berndtite, lead-antimony sulfosalts and wavellite. Wherever the kaolin minerals are observed, the ore minerals of the previous substages are partly or entirely corroded. Kanbara et al. (1989) describe that sphalerite and galena in their substage VI are not associated with silver, tin nor indium minerals, and are recognized only in northern half of the Soya vein. Therefore the correlation between the substages D and VI is only on the apparent simultaneity between them.

E (Substage of manganese minerals; VII). Although small amounts of rhodochrosite and manganocalcite observed in the Izumo and Shinano veins are the only minerals of this substage in the southeastern rare-metal producing veins, they increase their percentages northwestwards along the Soya vein. The manganese minerals apparently postdate the kaolin minerals of the substage D, and therefore are the latest production of the mineralization at Toyoha.

Details of the sequence will be discussed in Chapter 5 (Table 22).

Stages of Manganese and Silver Mineralization in Northern Veins:

Because the above classification is largely based on the assemblages of minerals and metals in the southeastern veins of the Toyoha deposit, the change in the assemblages reflect the change in stage or time only in that limited area. The ore-formation conditions (temperature, salinity, sulfur fugacity, oxygen fugacity etc. of the ore solution) in the northwestern later veins and the earlier veins during

the later-stage mineralization might have been significantly different from those in the southeastern veins as discussed later in Chapter 5. Therefore, the classification is not adaptable without consideration to the veins distributed in the north and northwest of the vein swarm. For example, mineralization sequences of Fe-Sb-As-S minerals and carbonates;

pyrrhotite + arsenopyrite + Mn-calcite -→ native As -→ berthierite

observed in the veinlets cutting the Tajima vein (Ohta, 1979), and

pyrrhotite + arsenopyrite -→ native As + pyrargyrite -→
Pb-Sb sulfosalts -→ rhodochrosite

commonly observed in the later veins are similar to, but not same with each other. These sequences and the occurrence of the silver-containing manganese ore described below suggest that the deposition of manganese minerals in the northwestern later veins and veinlets started at the time of the substage B or C.

Argentite and native silver constitute sporadic silver-rich zones in the earlier veins. Argentite occurs as euhedral to subhedral crystals of which largest ones reach a few centimeters in diameter. Such large grains of argentite are observed on the crystal surface of coarse-grained geode quartz or in veinlets cutting through the earlier-stage lead-zinc ore, and is generally associated with magnetite replacing hematite (Figure 3). Native silver occurs as irregularly curved aggregate of whiskers grown on argentite whose crystal edges have been rounded. Thus it is likely that native silver in Toyoha has

formed by secondary decomposition of argentite as is denoted by Shikazono (1975). Silver is contained in black sulfide-rich bands in a manganese-carbonate ore which existed at the Tajima vein 0 mL (W36; see Figure 46), and was defined as a product of the later-stage mineralization by Haraguchi and Tajima (1969). Based on the occurrence mode of silver, Yajima and Ohta (1979) denoted that argentite in the earlier veins is a product of the later-stage mineralization. On the other hand, some studies concluded that argentite deposition is attributed to the earlier-stage mineralization (e.g. Yoshie et al., 1986). This discrepancy will be discussed in Chapter 5.

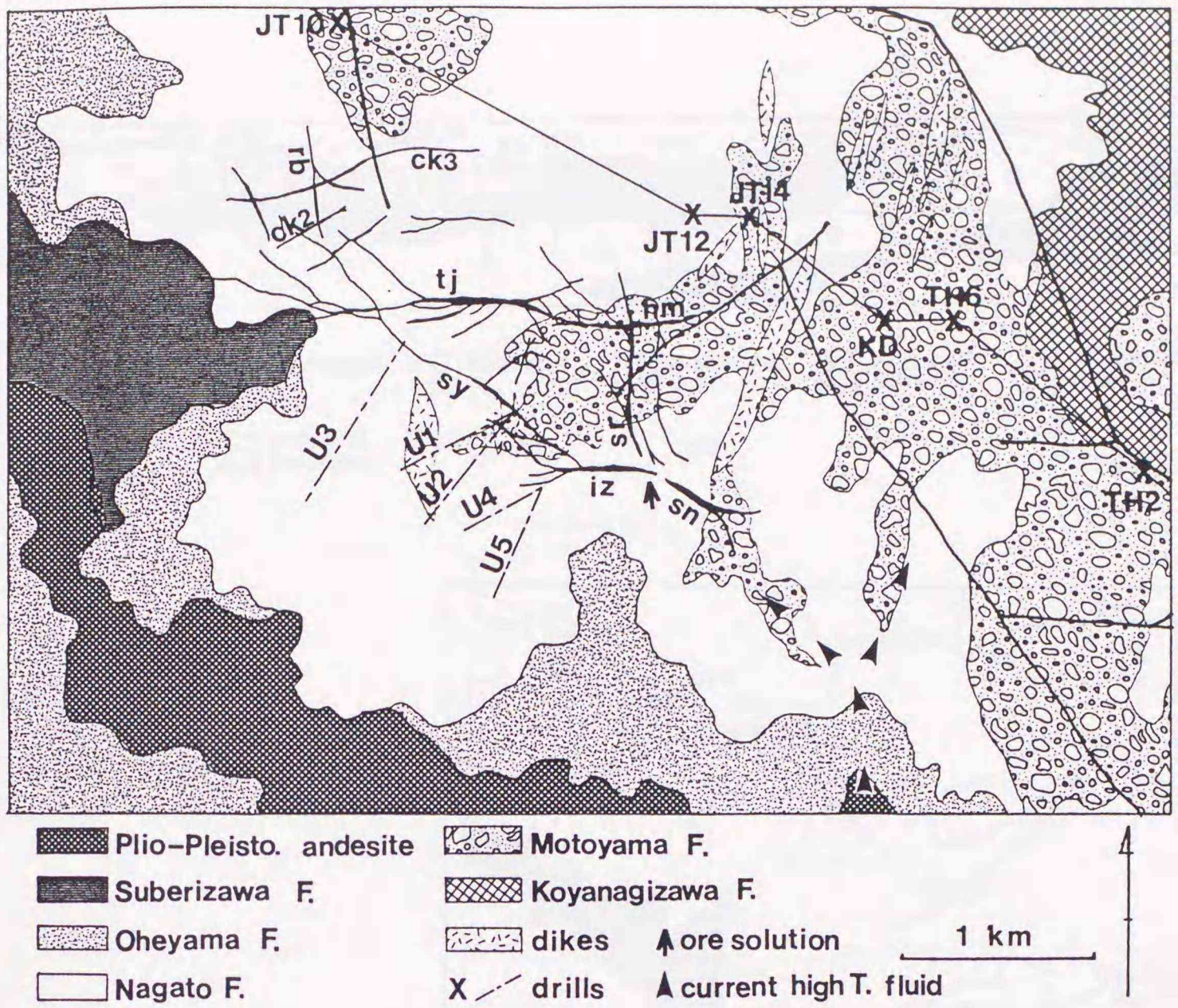

Figure 1a. Geology, vein pattern and drill locations of the Toyoha deposit modified after NEDO (1988), Watanabe and Iwata (1986) and Kanbara et al. (1989).

Plio-Pleisto. andesite corresponds to Muineyama and Nagaoyama andesites in the text and Table 1. U1 to U5 are drills JTU1 to JTU5 (MMAJ, 1990). JT10, JT12 and JT14 are drills proceeded by MMAJ (1976, 1977). Drills TH2 and TH6 are by NEDO (1990). KD is a drill by the Toyoha Mines Co. Ltd. Fairly straight thick lines are faults, and thin lines connecting the drills TH2 to JT10 are the pass of the section in Figure 1b.

Veins; rb:Rebun, ck2, ck3:Chikugo No.2 and 3, tj:Tajima, hm:Harima (earlier) sy:Soya, sr:Sorachi, iz:Izumo, sn:Shinano (later)

ore solution: influx of the initial ore solution suggested by Yajima and Ohta (1979) and Kanbara et al. (1989).

current high T. fluid: flow of the currently active high temperature solution suggested by Kanbara et al. (1989)

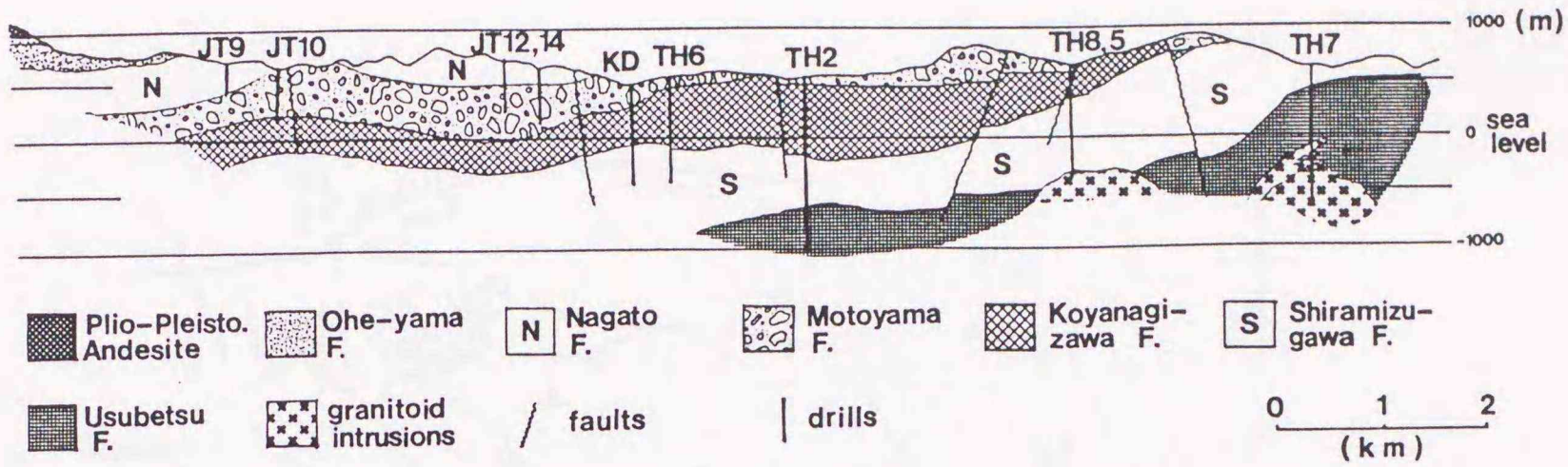

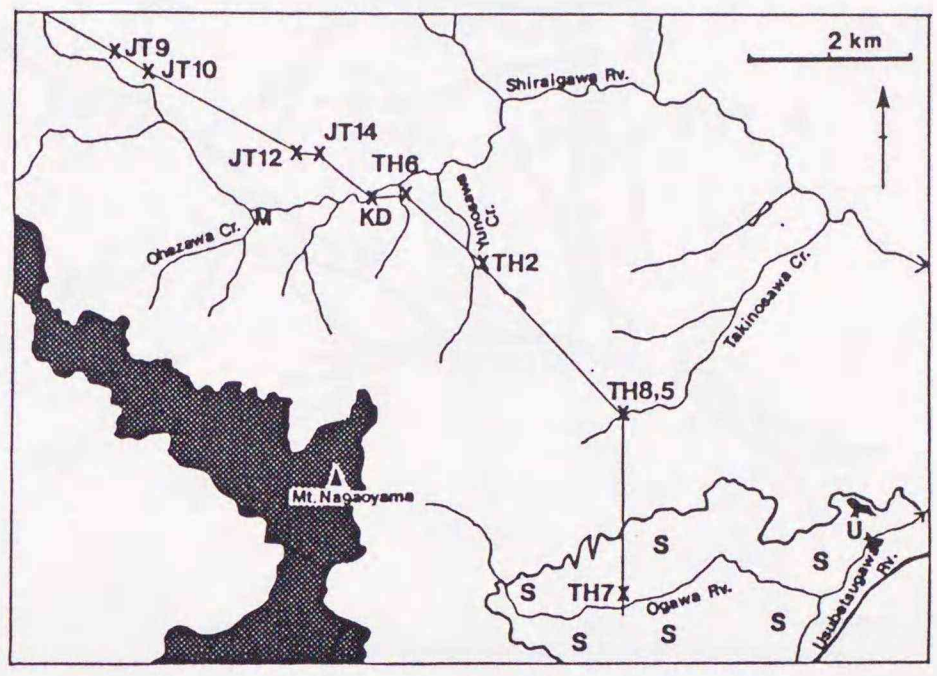

Figure 1b. Geological section modified after NEDO (1988).
The attached map shows the path of the section, and distributions of the Pliocene to Pleistocene andesite, the Usubetsu Formation (U) and the Shiramizugawa Formation (S).
The Plio-Pleisto. andesite corresponds to the Muineyama and the Nagaoyama andesites in the text and Table 1. The level of the mining office (0 mL of the drift system) is at around 500 meters above sea level. Approximate position of the vein system is between JT9 and JT14, and between the 500-meter and sea level lines on the section if projected north.
Abbreviations for the attached map; Rv.:river, Cr.:creek, M: mining office of Toyoha, U: the Usubetsu Formation.

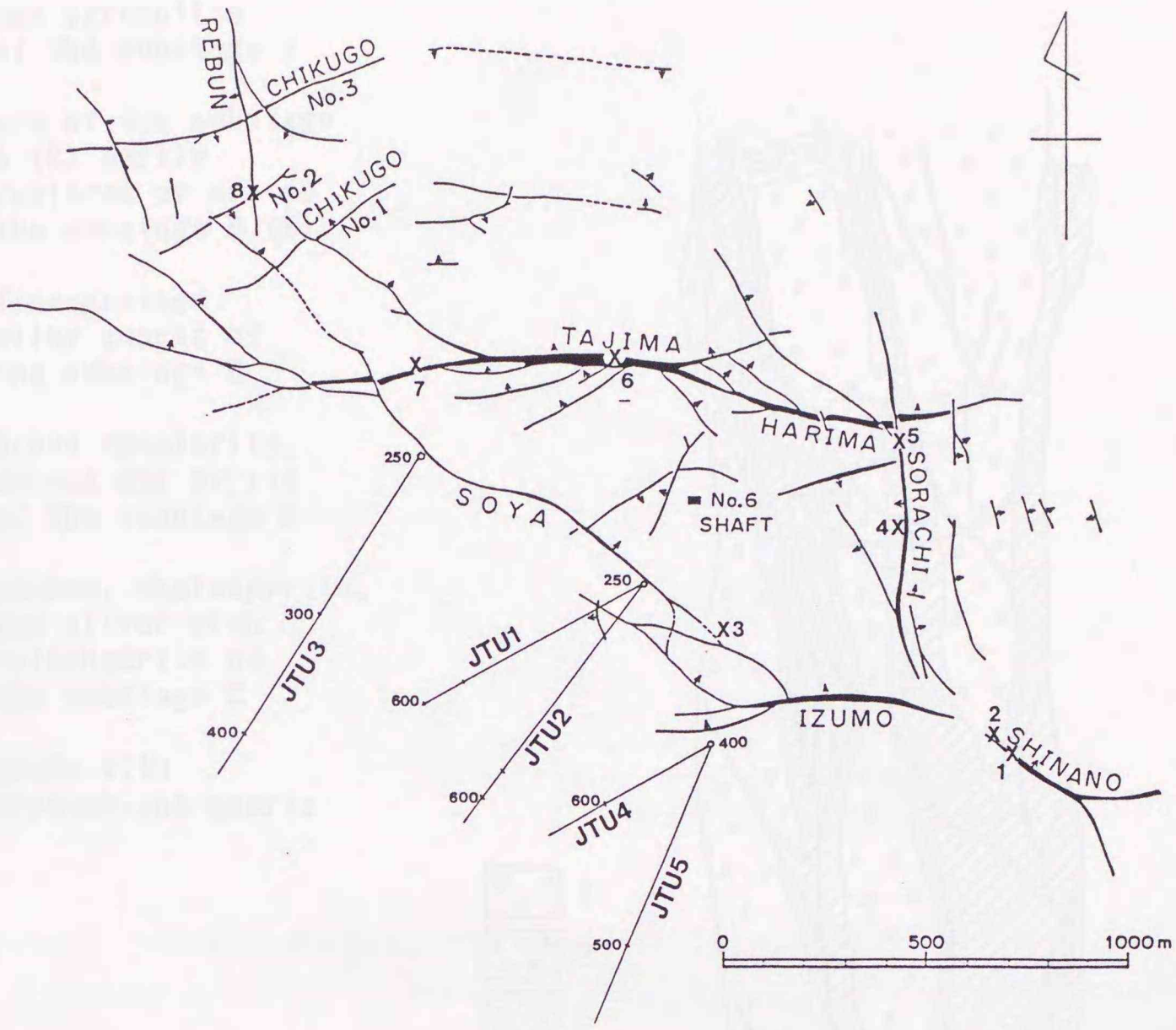

Figure 1c. Locality reference map for the veins and MMAJ drills in the Toyoha Mine.

This map is only for approximate horizontal locations. Crosses (X) numbered from 1 to 8 are referred in the text. Levels for the locations are specified in the text where this map is referred. Numerals by drills indicate levels in meters which correspond to those of the drift system at Toyoha.

1:altered host rock

2:fine-grained
black sphalerite
and pyrrhotite
of the substage A

3:ore of the substage
A (2) partly
replaced by ore of
the substage B (5)

4:fine-grained
milky quartz of
the substage B

5:brown sphalerite,
galena and pyrite
of the substage B

6:galena, chalcopyrite,
and silver-rich
tetrahedrite of
the substage C

7:geode with
crystalline quartz

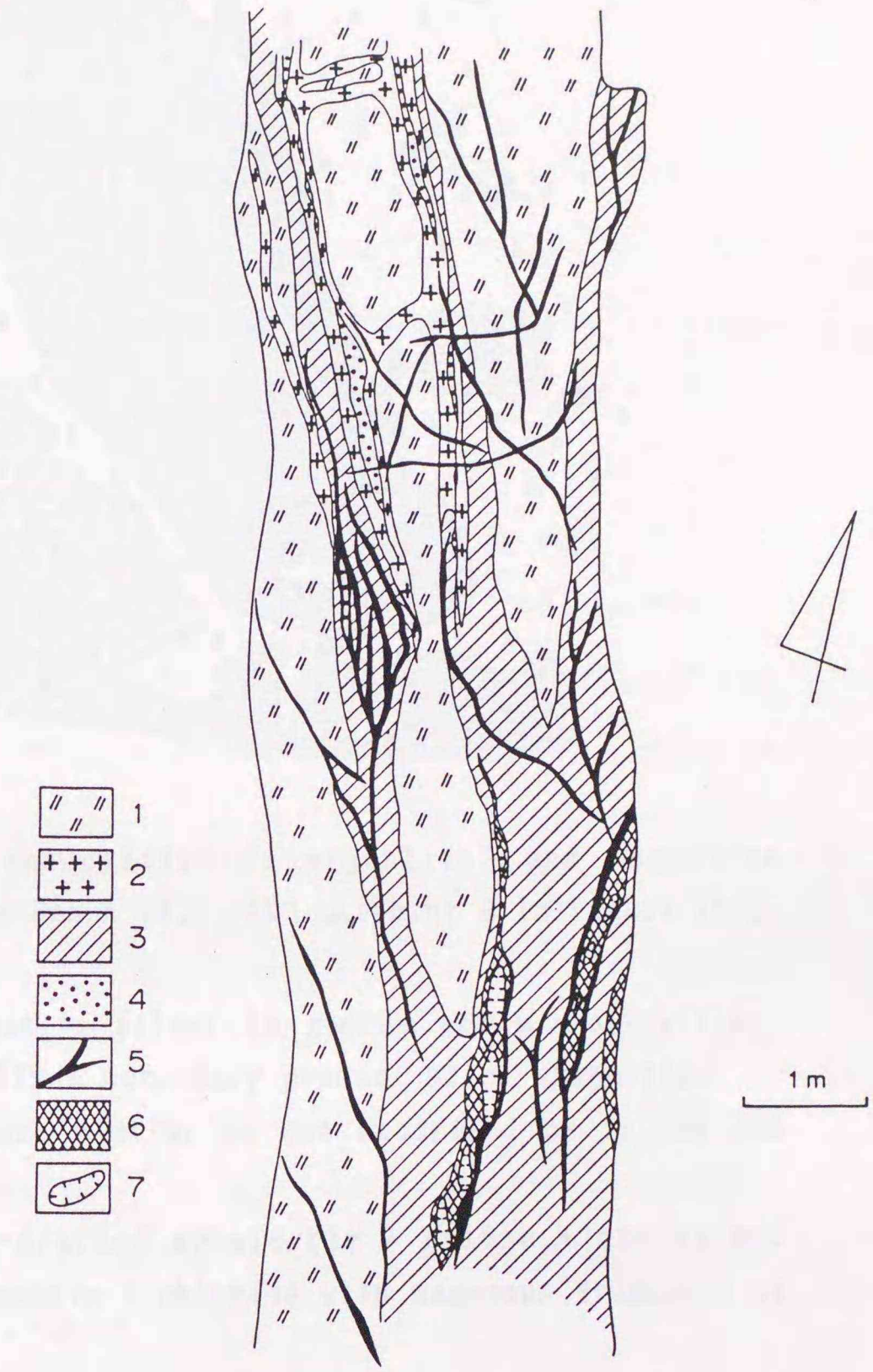

Figure 2. Sketch showing the substages A, B and C at the Sorachi vein -250 mL (point 4 in Figure 1c; after Ohta, 1980).

Figure 3. Sketch showing association of argentite, and magnetite replacing hematite at the Rebun vein -150 mL(point 8 in Figure 1c).

A (black): Argentite and native silver in geodes and micro-cavities. Native silver is apparently a secondary product after argentite.

B: Banded pyrite-hematite ore similar to one described by Yajima and Okabe (1971).

C: Ore consists of coarse-grained sphalerite + galena + quartz and fine-grained pyrite + hematite + chlorite with numerous fragments of the host rock.

CH: Massive aggregate of chlorite formed at the margin of F.

F: Ore consists of fine-grained sphalerite + galena + pyrite + quartz.

G: Geode with quartz crystals. The silver minerals are seen in most of the geodes.

M: Magnetite replaced or replacing hematite.

R: Host rock silicified and chloritized.

CHAPTER 4

OCCURRENCE AND CHEMISTRY OF ORE MINERALS

4-1. Analytical Procedure

Shimadzu EPMA-8705 electron microprobe analyzer with X-ray take off angle 52.5 degrees has been employed to obtain chemical data for characteristic ore minerals from the Toyoha deposit. Accelerating voltage and sample current for the analyses were 20 kV and 10 to 20 nA on the MgO standard. Several points for each of the minerals were qualitatively analyzed. A set of characteristic X rays were selected for each kind of minerals, and measured in accordance with the result, and ZAF - atomic number (Z; Duncumb-Reed), absorption (A; Philibert) and fluorescence (F; Reed) - corrections were made. Amounts of oxygen in oxide minerals are calculated assuming the valences of the metals in the course of the ZAF corrections. Standards for the analyses are listed in Table 2. Element maps were made for several phases to distinguish complex internal textures which are invisible under optical microscope in most cases. Basically, quantitative data which total in the range of 100±1 weight percent were employed to make the tables and diagrams, though some others in the range of 100±2 were also used because of their unique compositions.

Table 2. Analyses conditions employed in this study.

Machine	Shimadzu EPMA-8705	
X-ray take off angle	52.5 degrees	
Accelerating voltage	20 kV	
Sample current	10 to 20 nA on MgO standard	
Correction	ZAF	Z = atomic number (Duncumb-Reed)
		A = absorption (Philibert)
		F = fluorescence (Reed)

Standards for sulfides and sulfosalts

Ag, Bi, Cd, Co, Ge, Mn, Mo: metal
Ni, Sb, Se, Sn, Te, V, Zn: metal
As, Ga: synthetic GaAs
Cu: chalcopyrite
Fe: pyrite for Fe-Co-Ni-As-Sb sulfides,
chalcopyrite for others
In: synthetic InP
Pb: galena
S: galena for minerals which contain
Pb or Bi as a major component
chalcopyrite for others

Standards for oxides*

Al: Al_2O_3
Ca: $CaSiO_3$
Fe: Fe_2O_3
Mn: MnO
Sn, W, Mo: metal
Ti: TiO_2

* Amounts of oxygen in oxide minerals are calculated assuming the valences of the metals in the course of the ZAF corrections.

4-2. Sn-In-containing Sulfides

Tin sulfides are generally accompanied by indium minerals, and those from Toyoha are not exceptions. By this time eighteen tin and/or indium minerals have been recognized in the Toyoha deposit (Table 3).

Stannite and Kesterite (Substage B):

Optical characters of stannite and kesterite from Toyoha are similar to those described in Uytenbogaardt and Burke (1971). Comparison of the microscopic observations and chemical analyses have proved that Zn/Fe+Zn ratios of these minerals are negatively correlated to strength of both anisotropism and bireflectance. Stannite and kesterite are as common as the Zn-In mineral (Ohta, 1980, 1989) in the later veins. Stannite dominates over kesterite at upper levels, while the amount of kesterite and maximum Zn/Fe+Zn ratios in kesterite increase downward and southeastward (Ohta, 1989). At deep levels, stannite frequently shows concentric parallel intergrowth bands with anisotropic chalcopyrite (Figure 4, Figure 5) or sphalerite (Figure 6, Figure 7), while kesterite typically occurs together with indium-bearing sphalerite (hereafter expressed as indium sphalerite), the Zn-In mineral, and roquesite as discrete grains or concentric parallel bands within sphalerite (Figure 8, Figure 9, Figure 10). Observed maximum weight percentages of indium in kesterite and stannite are 16.51 and 20.0 respectively, though these high concentrations may be partly attributed to evenly mixed minute grains of roquesite and chalcopyrite (Ohta, 1989). Representative chemical compositions of stannite and kesterite are listed in Table 4.

Table 3. Tin and indium minerals recognized in the Toyoha deposit.

name	ideal formula	reference
cassiterite	SnO_2	Yajima, 1977
herzenbergite	SnS	Ohta et al., 1987
berndtite	SnS_2	Ohta et al., 1987
teallite	$PbSnS_2$	Sugaki and Hayashi, 1986
canfieldite?*1	Ag_8SnS_6	Ohta and Yajima, 1979
stannite	Cu_2FeSnS_4	Yajima, 1977
kesterite	Cu_2ZnSnS_4	Ohta, 1989
hocartite	Ag_2FeSnS_4	Kojima et al., 1979
pirquitasite	Ag_2ZnSnS_4	ditto; Johan and Picot, 1982
rhodostannite	$Cu_2FeSn_3S_8$	Narita et al., 1977
toyohaite*2	$Ag_2FeSn_3S_8$	Ohta et al., 1987
Zn-In mineral*3	$CuZn_2InS_4$	Ohta, 1980
Ag-In mineral*3	$AgInS_2$	Ohta, 1980
roquesite	$CuInS_2$	Ohta, 1989
indium sphalerite	$(1-x)Zn_2S_2 + xCuInS_2$	Ohta, 1989
sakuraiite	$(Cu,Fe,Zn)_3(In,Sn)S_4$	Ohta, 1989
cp-st ss.*4	$0.7Cu_2FeSnS_4 + 0.3Cu_2Fe_2S_4$?	Ohta, 1989
colusite*5	$Cu_3(As,Sn,V,Fe,Sb)S_4$	MMAJ, 1988

*1 not confirmed because of slight difference of composition

*2 new mineral (YAJIMA et al. in press)

*3 unnamed yet

*4 a chalcopyrite-stannite solid solution (see the text)

*5 observed only as small inclusions within pyrite in drill cores from JTU1 (496.3 to 500.2 m).

Table 4. Representative EPMA analyses of stannite(st) and kesterite(ks).

Abbreviations; Atom:atomic composition, IZ:Izumo, SN:Shinano, SR:Sorachi, SY:Soya, TA:Tajima
Numerals after the vein name abbreviations indicate levels in meters below the mining office at Toyoha.

Loc.	Name	Fe	Zn	Cu	Ag	In	Sn	S	Total
TA450	st	12.62	1.52	28.93	0.27	0.04	27.53	29.89	100.79
Atom		0.97	0.10	1.95	0.01	0.00	0.99	3.98	8
TA450	st	11.98	1.20	29.01	0.77	0.06	27.78	29.70	100.49
Atom		0.92	0.08	1.97	0.03	0.00	1.01	3.99	8
IZ300	st	11.46	2.07	29.84	0.00	0.00	27.53	29.48	100.38
Atom		0.88	0.14	2.02	0.00	0.00	1.00	3.96	8
SR500	st	10.66	2.62	29.68	0.04	0.17	27.64	29.28	100.08
Atom		0.83	0.17	2.02	0.00	0.01	1.01	3.96	8
SN450	st	10.35	5.47	28.89	0.05	0.49	25.32	29.30	99.88
Atom		0.80	0.36	1.96	0.00	0.02	0.92	3.94	8
SR500	st	9.59	3.80	28.66	0.54	0.24	27.57	28.63	99.02
Atom		0.76	0.26	1.99	0.02	0.01	1.02	3.94	8
SN350	st	8.14	3.03	28.99	0.37	16.35	14.26	28.58	99.72
Atom		0.65	0.21	2.02	0.01	0.63	0.53	3.95	8
SR450	st	7.62	6.11	27.95	0.66	0.11	28.22	29.20	99.87
Atom		0.60	0.41	1.93	0.03	0.00	1.04	3.99	8
SR350	st	7.47	6.76	29.19	0.20	1.01	26.93	28.74	100.31
Atom		0.58	0.45	2.01	0.01	0.04	0.99	3.92	8
IZ300	st	6.93	5.31	28.14	0.31	0.78	29.75	29.38	100.60
Atom		0.54	0.36	1.94	0.01	0.03	1.10	4.02	8
SN350	ks	6.11	9.24	28.96	0.24	0.14	25.98	29.22	99.90
Atom		0.48	0.61	1.98	0.01	0.01	0.95	3.96	8
SN350	ks	5.21	9.62	29.20	0.23	0.12	26.81	29.05	100.32
Atom		0.41	0.64	2.00	0.01	0.00	0.98	3.95	8
SR350	ks	5.13	11.29	27.48	0.45	0.97	25.98	28.48	99.78
Atom		0.40	0.76	1.90	0.02	0.04	0.96	3.91	8
SY550	ks	4.93	9.94	27.44	0.33	6.71	22.84	28.49	100.67
Atom		0.39	0.67	1.90	0.01	0.26	0.85	3.92	8
SY550	ks	4.73	9.96	27.22	0.43	7.00	22.46	28.29	100.08
Atom		0.38	0.68	1.90	0.02	0.27	0.84	3.92	8
SR250	ks	4.47	10.50	28.57	0.54	1.16	26.04	29.29	100.57
Atom		0.35	0.70	1.96	0.02	0.04	0.95	3.98	8
SR350	ks	3.91	10.40	28.99	0.15	1.41	26.84	28.93	100.63
Atom		0.31	0.70	2.00	0.01	0.05	0.99	3.95	8
SR350	ks	3.65	11.04	28.67	0.35	0.72	27.19	28.53	100.16
Atom		0.29	0.74	1.99	0.01	0.03	1.01	3.92	8
SY550	ks	2.53	9.54	26.34	1.27	16.51	16.41	27.67	100.28
Atom		0.21	0.66	1.88	0.05	0.65	0.63	3.92	8
SY550	ks	1.94	12.65	27.04	0.94	7.02	22.56	28.18	100.34
Atom		0.15	0.86	1.90	0.04	0.27	0.85	3.92	8
SY550	ks	1.68	12.76	27.48	1.05	6.26	23.17	28.25	100.64
Atom		0.13	0.87	1.92	0.04	0.24	0.87	3.92	8

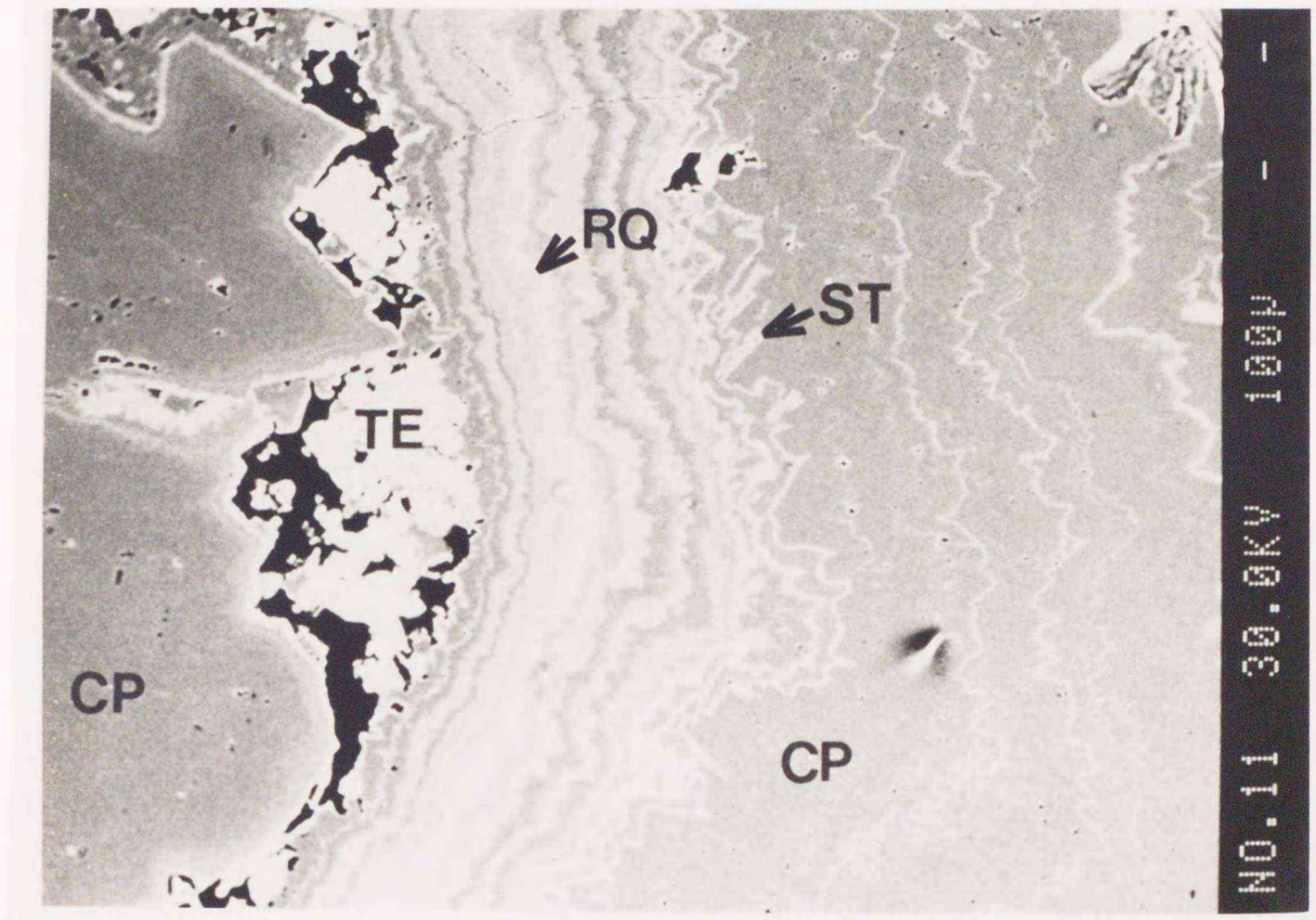

Figure 4. Back-scattered electron (BSE) image showing rhythmic growth (colloform) banding of the anisotropic chalcopyrite (CP), presumed roquesite (RQ) and indium-rich stannite (ST) in a chalcopyrite-rich sample of the substage B from the Shinano vein -350 mL (point 1 in Figure 1c).

The bands piled up from right to left, though tetrahedrite (TE) is presumably a replacement product in the later substage C.

Figure 5. Tin and indium maps of the central area shown in Figure 4. The two images cover exactly the same area. The band of highest indium concentration is presumably of roquesite with mixtures of minute grains of chalcopyrite and stannite. Bands with high tin and intermediate indium contents are of stannite with mixtures possibly of chalcopyrite and roquesite. Darkest areas correspond to the anisotropic chalcopyrite.

"X 0.200 mm" indicates that the width of the mapped area is 0.2 millimeters, and "STEP .001 mm" indicates that the samplings of the X rays were made for every 0.001 mm in both X and Y directions.

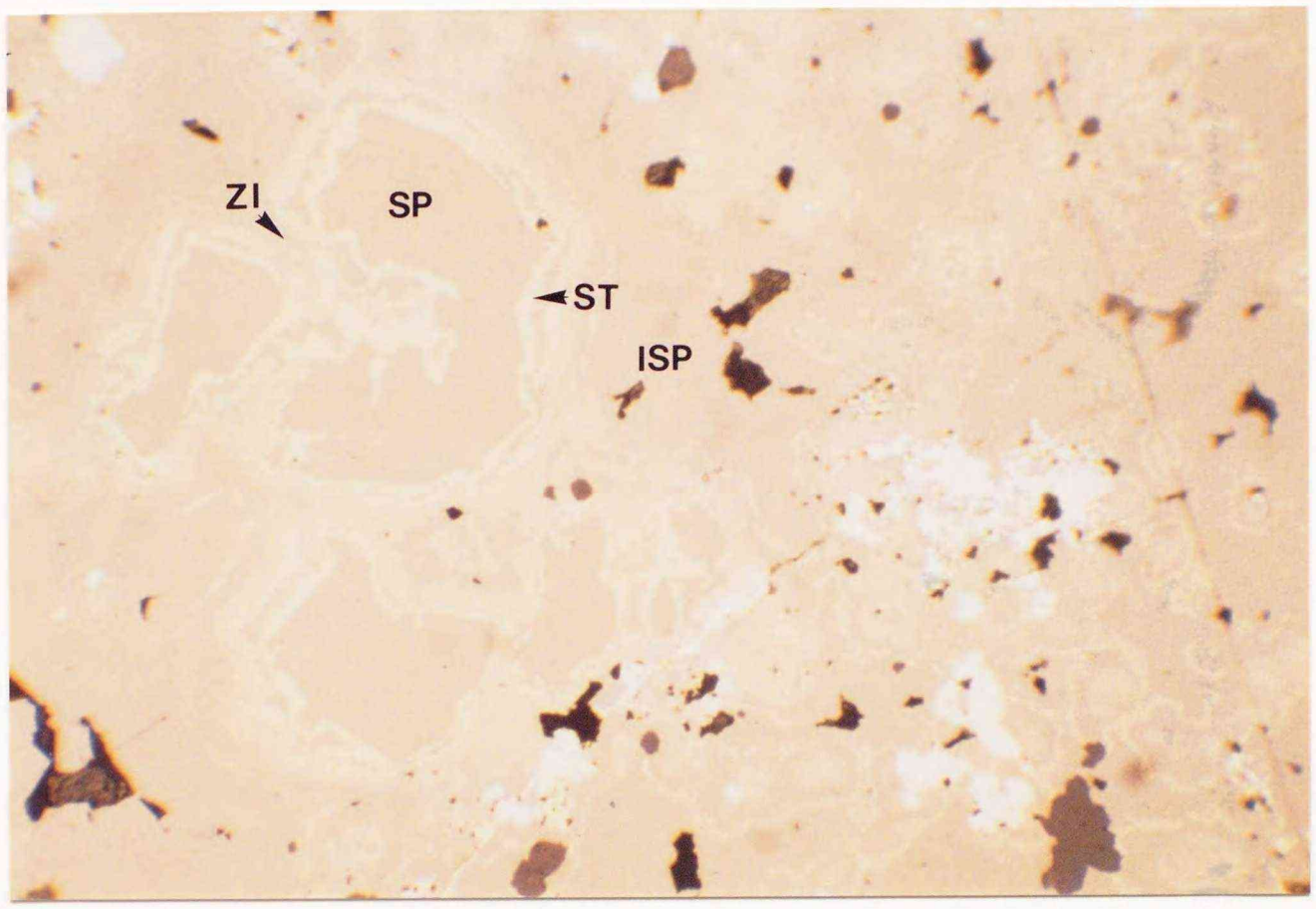

Figure 6. Photomicrograph of stannite (ST), the Zn-In mineral (ZI), indium-poor sphalerite (SP) and indium-containing sphalerite (ISP) intergrowth in a brown-sphalerite-rich sample of the substage B from the Sorachi vein -350 mL (about 100 m south of point 4 in Figure 1c). White grains are of pyrite.
Note that the indium-containing sphalerite is slightly brighter than the indium-poor sphalerite. Width of the pictured area is 0.6 mm.

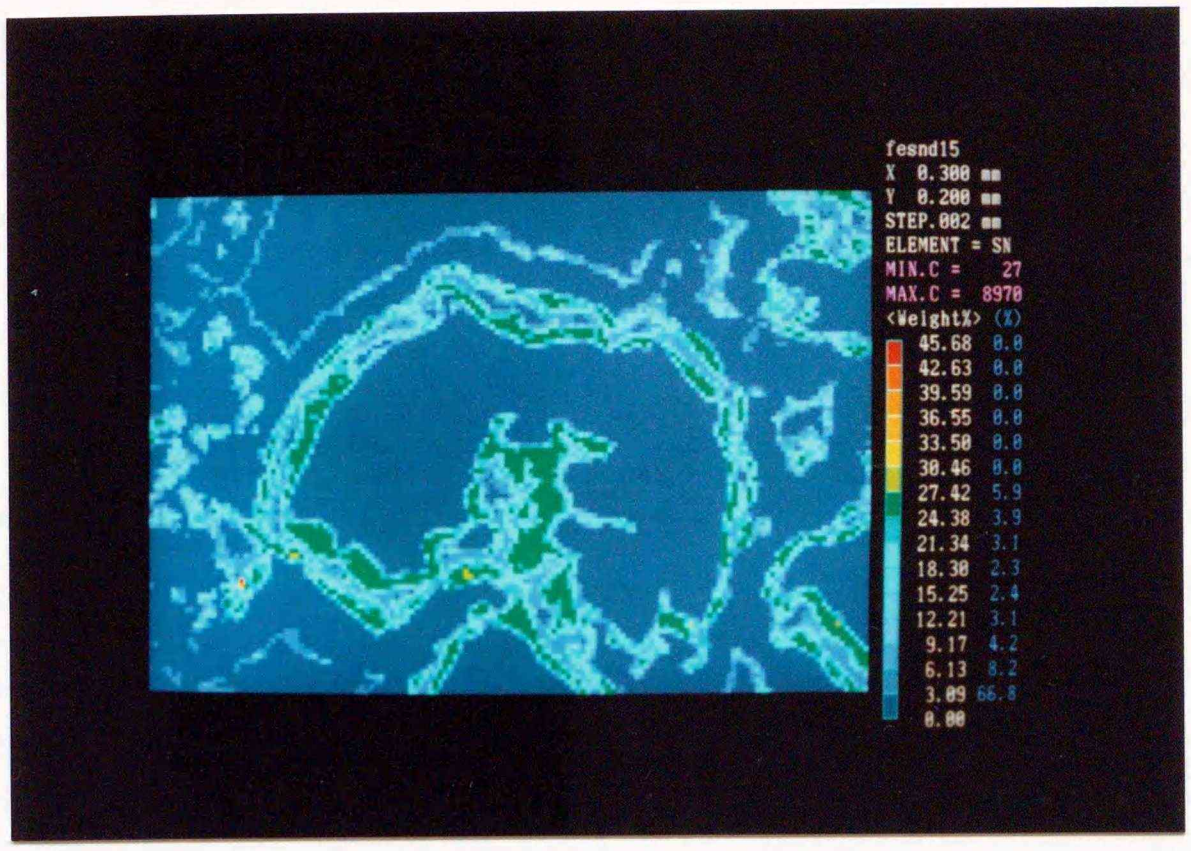

Figure 7. Tin and indium maps of a part of the area shown in Figure 6. The images in this figure are turned about 90° counterclockwise. The tin-rich bands (green in the upper image) are of stannite, the indium-rich bands (brown in the lower image) are of the Zn-In mineral, and other bands of low indium concentration are of indium-containing sphalerite.

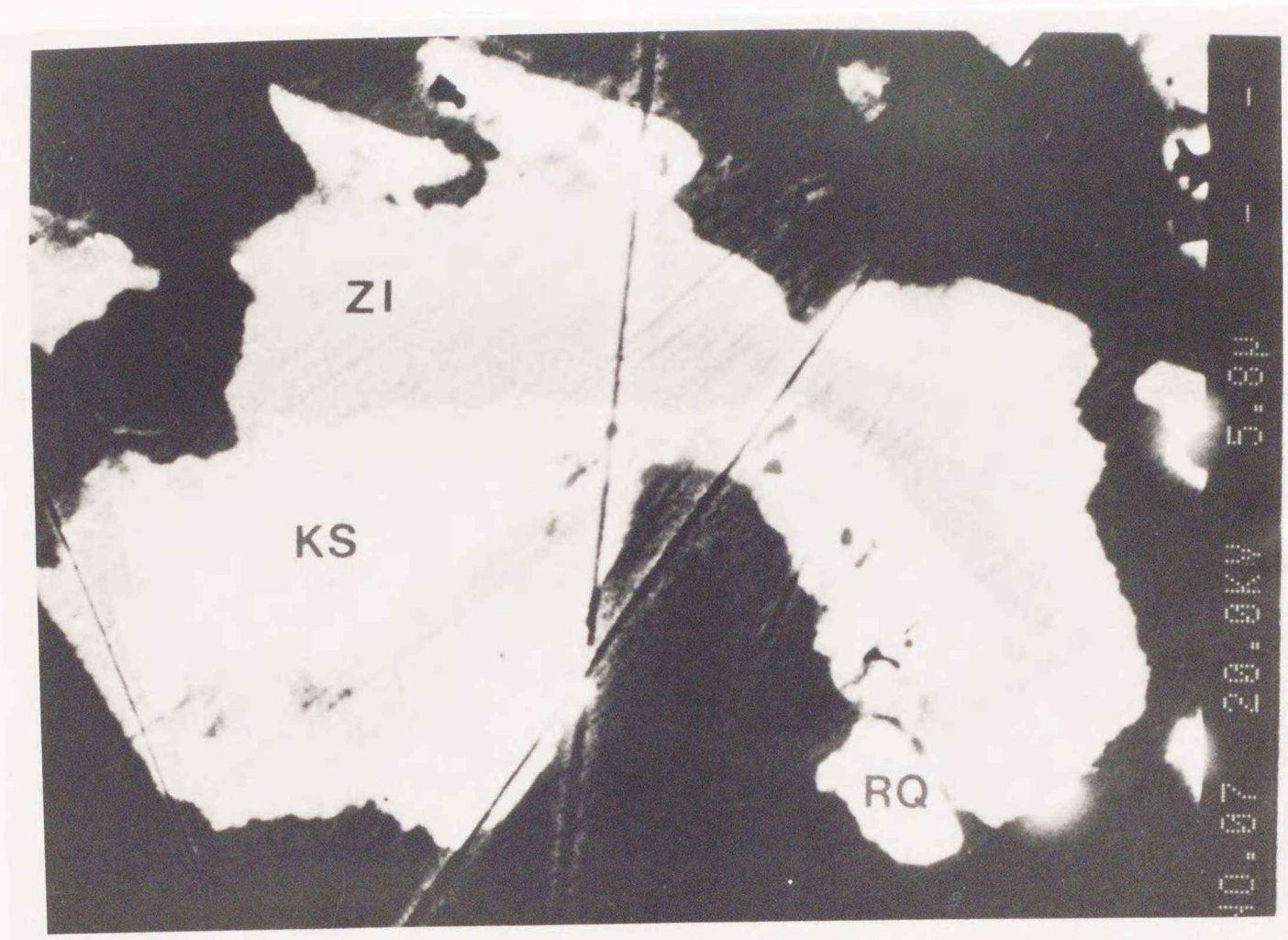

Figure 8. BSE image of aggregate of kesterite (KS), the Zn-In mineral (ZI) and roquesite (RQ) in a chalcopyrite-rich sample of the substage B from the Soya vein -550 mL (point 3 in Figure 1c).
The heterogeneity of each phase reflects change in its composition due to the solid solutions described in the text. Dark background surrounding the aggregate is sphalerite.

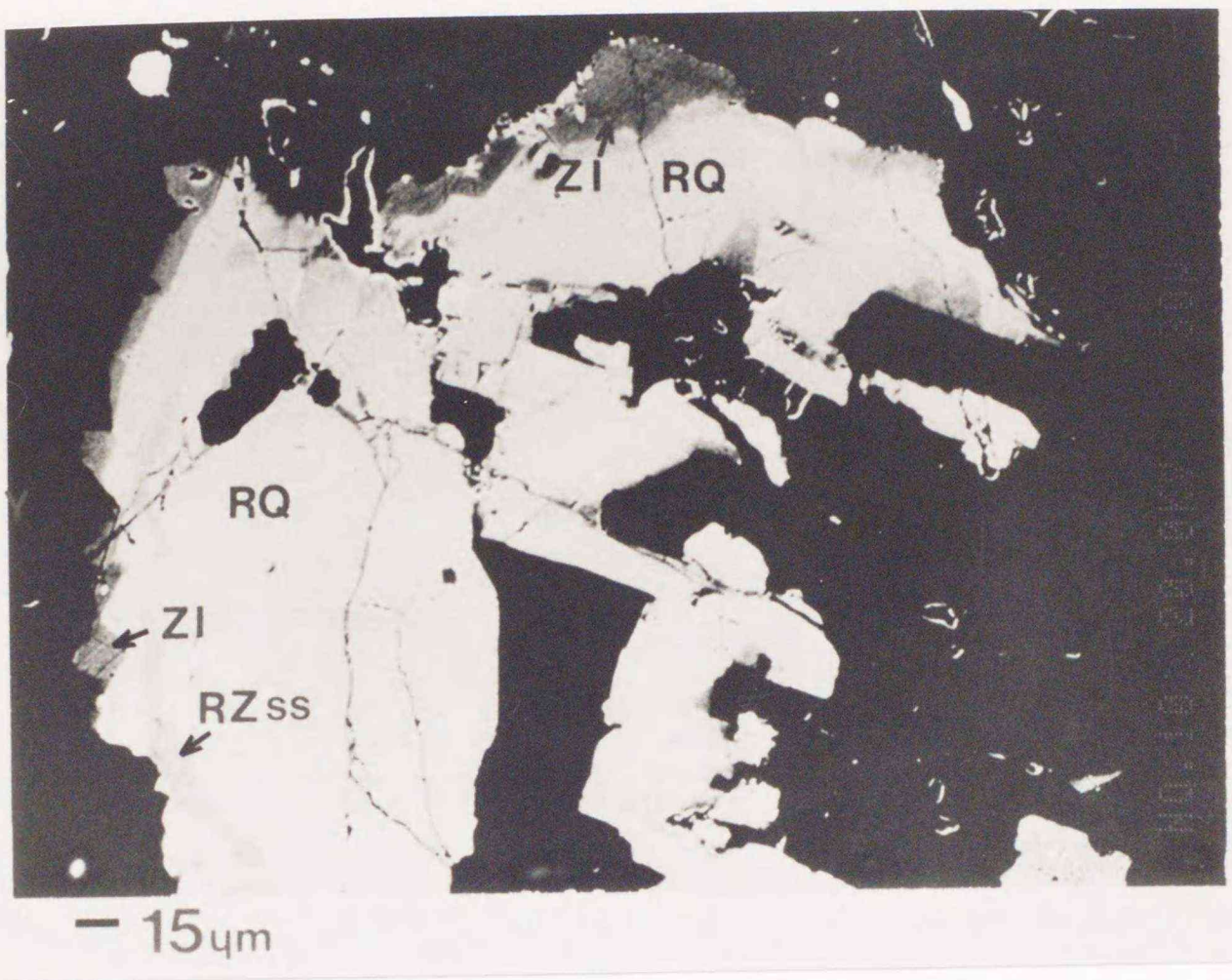

Figure 9. BSE image showing aggregate of roquesite (RQ), the Zn-In mineral (ZI) and a solid solution (RZ ss) between roquesite and the Zn-In mineral in the same sample as shown in Figure 8.

The heterogeneity of the roquesite reflects change in its composition due to the solid solution with an unreal phase of the Zn-In mineral composition. Dark background on the right is chalcopyrite, that on the left is sphalerite.

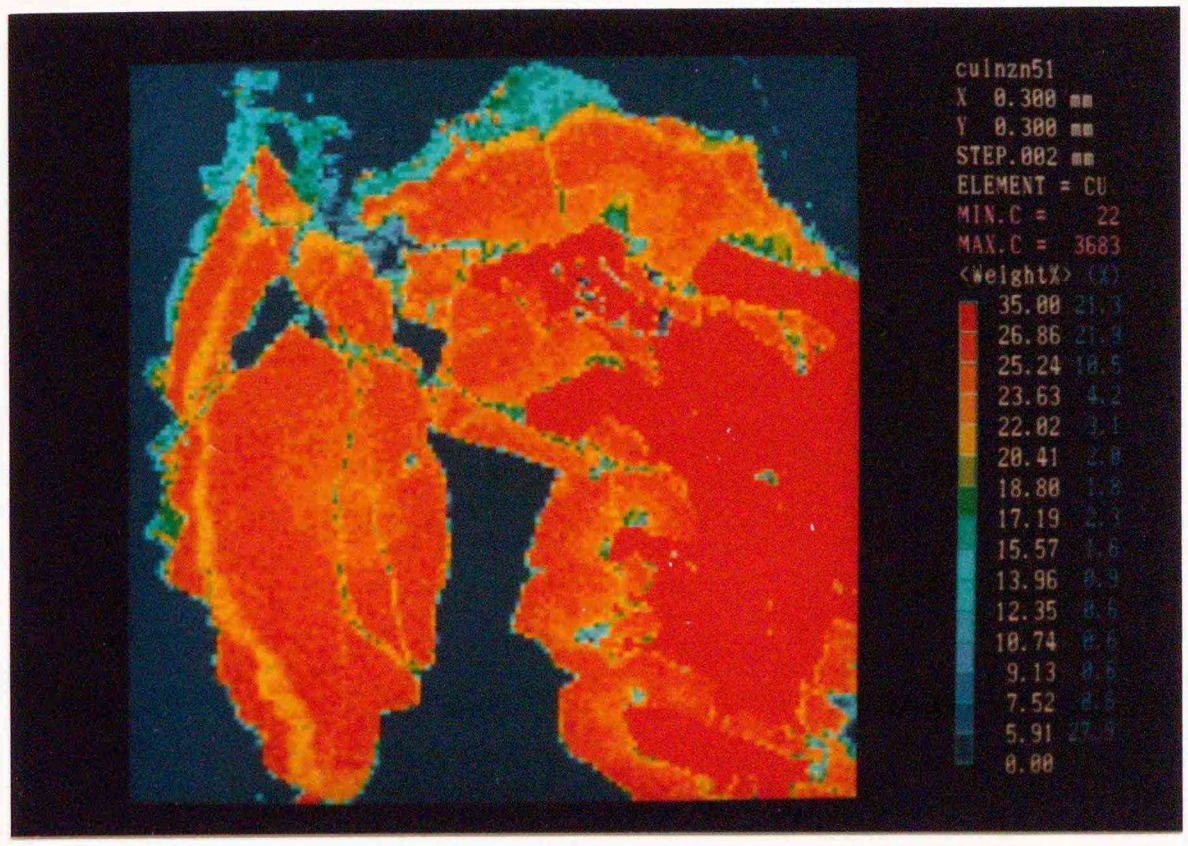

Figure 10. Copper and zinc maps of the aggregate shown in Figure 9. Note that the concentrations of copper and zinc in the aggregate are in negative correlation.

Chalcopyrite-Stannite Solid Solutions (Substage B):

Two optically different types of chalcopyrite, isotropic and anisotropic, occur in the Toyoha deposit (Kase, 1987). The isotropic one has an almost ideal chemical composition $CuFeS_2$, and occurs dominantly throughout the Toyoha deposit, while the anisotropic one is recognized only in the substage-B samples from deep levels of the southeastern veins. As shown in Figure 4, Figure 11 and Figure 12 the anisotropic chalcopyrite is always associated with tin and/or indium minerals, and contains tin, indium and zinc in itself. The chemical compositions (Table 5, Figure 13) indicate that these minor components in the anisotropic chalcopyrite exist as stannite molecule and as minor amount of roquesite molecule. The anisotropism is presumably due to distortion of the cell caused by these components. Observed maximum weight percentages of tin and indium in chalcopyrite are 3 and 1 weight percent respectively (Ohta, 1989). In addition to the anisotropic chalcopyrite, microprobe work has identified two unknown phases between chalcopyrite and stannite compositions; stannite with slightly more chalcopyrite molecule than normal one, and an unnamed phase (cp-st ss.) whose analysis data are plotted between chalcopyrite and stannite (Table 5; Figure 13, Figure 14). As well as the anisotropic chalcopyrite, this phase is distributed mainly in deep levels of the southeastern veins, always exhibits complex intergrowth with stannite, and generally includes small grains of cassiterite and the anisotropic chalcopyrite (Figure 15, Figure 16). Its color is similar to that of stannite, but anisotropism is much stronger. These phases are due to substitutions of $(Fe^{+2},Zn)Sn$ in stannite molecule for $2Fe^{+3}$ to form chalcopyrite molecule (Ohta, 1989).

Table 5. Representative EPMA analyses of chalcopyrite (cp) and the chalcopyrite-stannite solid solution (cp-st).

Abbreviations; Atom:atomic composition, SN:Shinano, SR:Sorachi, SY:Soya, TA:Tajima
Numerals after the vein name abbreviations indicate levels in meters below the mining office at Toyoha. Mn is less than 0.09 wt%, Cd is less than 0.12 wt% for all points analyzed.

Loc.	Name	Fe	Zn	Cu	Ag	In	Sn	S	Total
TA450	cp	29.89	0.10	34.84	0.12	0.07	0.00	34.90	99.93
	Atom	1.97	0.01	2.02	0.00	0.00	0.00	4.00	8
SY550	cp	30.24	0.11	33.82	0.24	0.13	0.09	34.57	99.20
	Atom	2.01	0.01	1.97	0.01	0.00	0.00	4.00	8
TA450	cp	29.88	0.68	34.49	0.09	0.03	0.10	35.25	100.52
	Atom	1.96	0.04	1.98	0.00	0.00	0.00	4.02	8
SY550	cp	30.33	0.09	34.23	0.24	0.25	0.11	34.79	100.04
	Atom	2.00	0.01	1.98	0.01	0.01	0.00	3.99	8
SY550	cp	30.57	0.13	34.48	0.16	0.13	0.18	34.98	100.63
	Atom	2.00	0.01	1.98	0.01	0.00	0.01	3.99	8
SY550	cp	29.44	0.29	34.33	0.13	0.34	0.23	34.96	99.72
	Atom	1.95	0.02	1.99	0.01	0.01	0.01	4.02	8
SY550	cp	30.59	0.27	34.35	0.12	0.28	0.23	34.78	100.62
	Atom	2.01	0.01	1.98	0.00	0.01	0.01	3.98	8
SR350	cp	28.91	0.77	34.61	0.11	0.39	0.34	34.55	99.70
	Atom	1.92	0.04	2.02	0.00	0.01	0.01	3.99	8
SR350	cp	28.72	1.63	34.08	0.09	0.30	0.41	34.34	99.56
	Atom	1.91	0.09	1.99	0.00	0.01	0.01	3.98	8
SN450	cp	29.01	0.32	34.86	0.05	0.08	1.64	34.76	100.71
	Atom	1.91	0.02	2.02	0.00	0.00	0.05	3.99	8
SN350	cp	27.04	0.31	34.22	0.09	0.64	2.87	34.29	99.46
	Atom	1.82	0.02	2.02	0.00	0.02	0.09	4.02	8
SN450	cp	27.33	0.49	34.32	0.10	0.07	2.99	34.13	99.44
	Atom	1.84	0.03	2.03	0.00	0.00	0.10	4.00	8
SN450	cp	27.84	0.45	34.65	0.11	0.06	2.72	34.29	100.11
	Atom	1.86	0.03	2.03	0.00	0.00	0.09	3.99	8
SN350	cp	26.66	0.63	33.96	0.12	1.01	4.06	34.22	100.67
	Atom	1.79	0.04	2.00	0.00	0.03	0.13	4.00	8
SN450	cp-st	15.85	1.63	31.46	0.09	0.13	19.61	30.15	99.17
	Atom	1.19	0.10	2.07	0.00	0.01	0.69	3.93	8
SN450	cp-st	15.88	1.42	31.13	0.08	0.08	21.87	30.09	100.74
	Atom	1.18	0.09	2.04	0.00	0.00	0.77	3.91	8
SN450	cp-st	15.04	2.48	31.11	0.09	0.10	21.32	30.09	100.44
	Atom	1.12	0.16	2.04	0.00	0.00	0.75	3.92	8
SN450	cp-st	12.94	8.00	28.97	0.14	0.20	18.77	30.89	100.04
	Atom	0.96	0.51	1.88	0.01	0.01	0.65	3.98	8
SN450	cp-st	12.72	8.29	28.37	0.14	0.24	20.06	30.64	100.60
	Atom	0.94	0.53	1.85	0.01	0.01	0.70	3.96	8
SN450	cp-st	14.42	5.19	30.04	0.14	0.08	19.81	30.50	100.32
	Atom	1.07	0.33	1.96	0.01	0.00	0.69	3.94	8

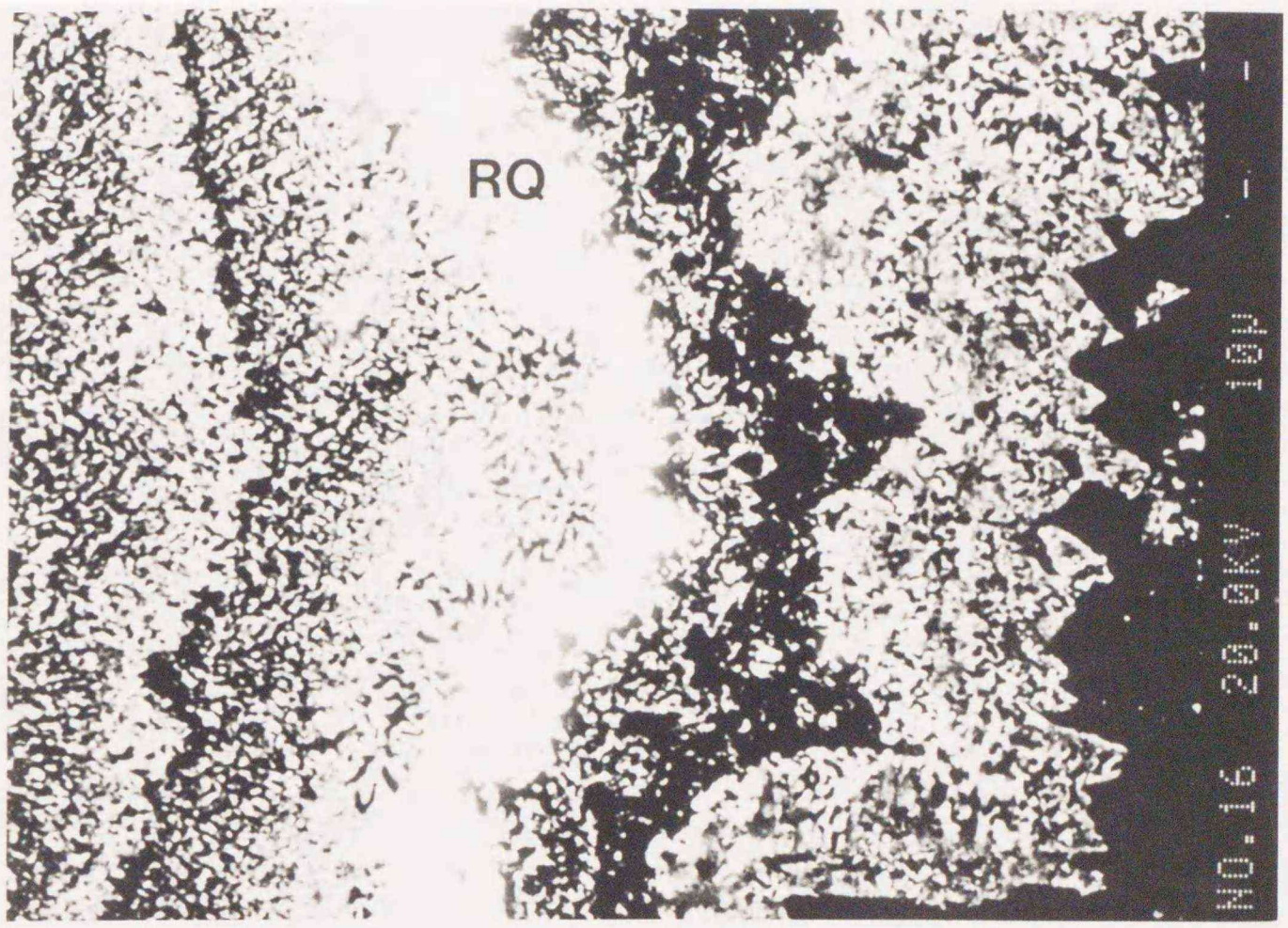

Figure 11. BSE image showing zoning of the anisotropic chalcopyrite, stannite, roquesite, and mixtures of their fine grains from the Shinano vein -350 mL.

Black part is the anisotropic chalcopyrite, gray is stannite. The brightest white band (RQ) is presumably of roquesite. The pictured area corresponds to the upper central part of those in Figure 5.

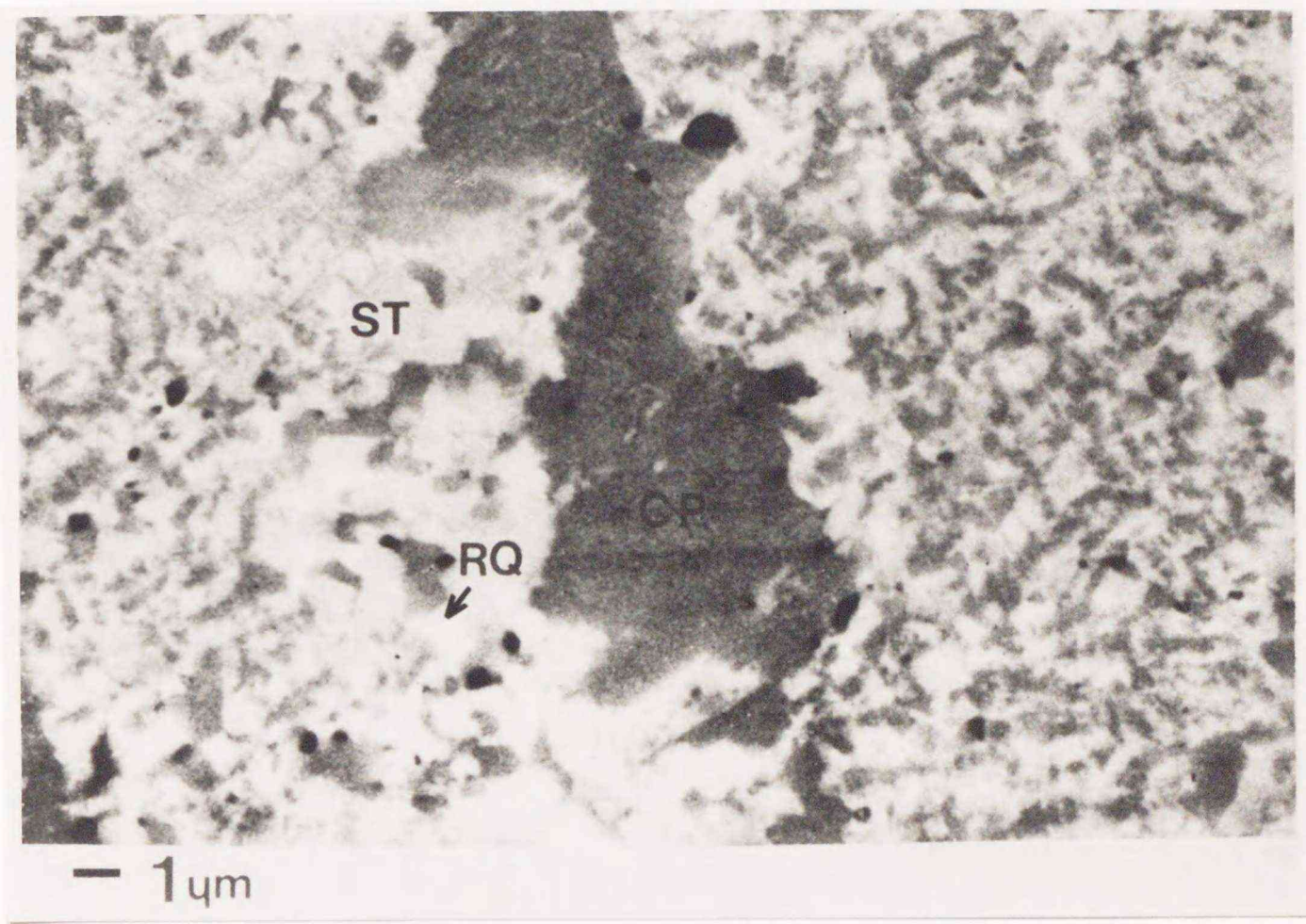

Figure 12. BSE image of a part of the area in Figure 11.
The complex mixture of chalcopyrite (CP, black), stannite (ST, gray), and roquesite (RQ, white) contains no piece of other phases.

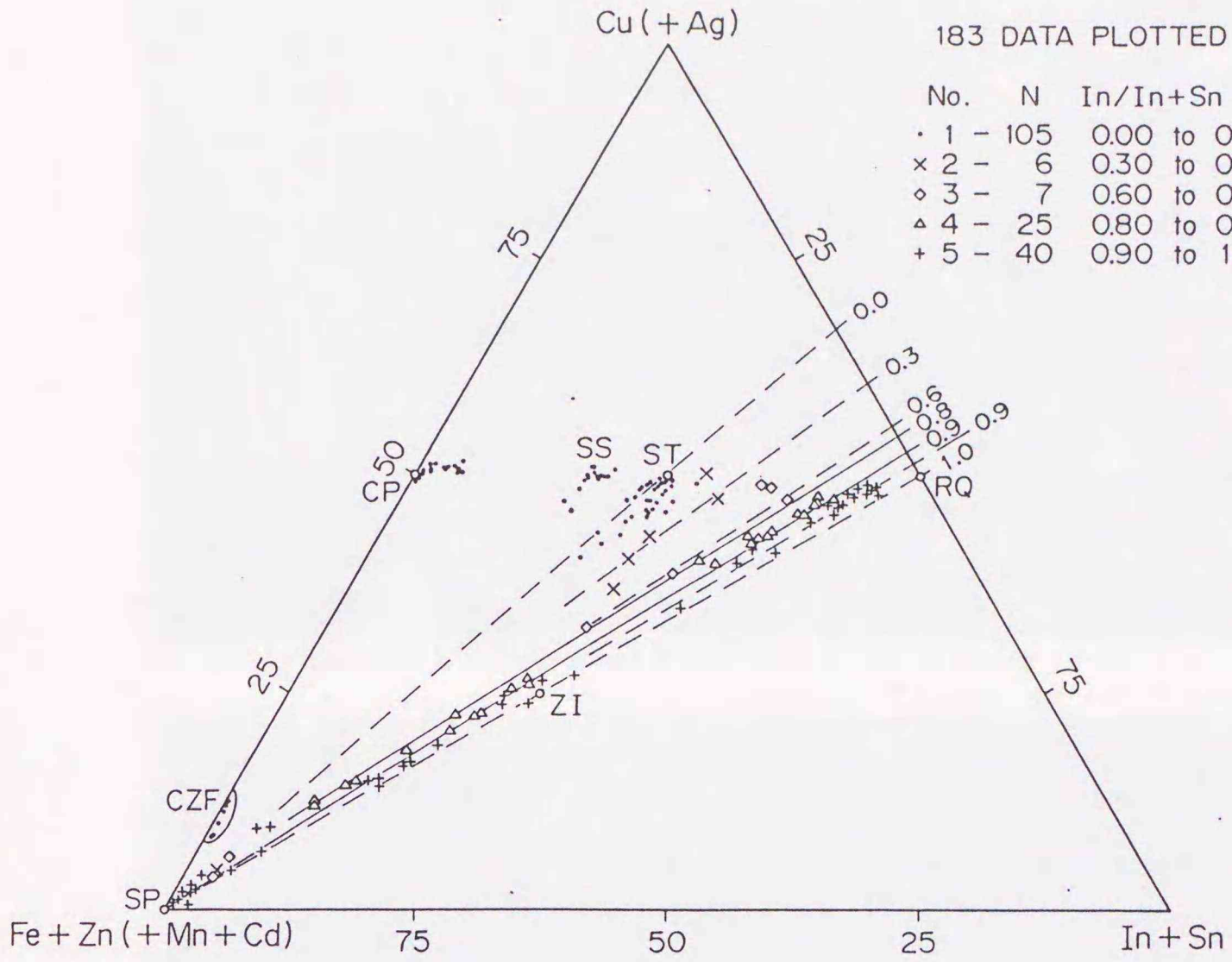

Figure 13. Cu - Fe+Zn - In+Sn (mol) diagram of the CSR (chalcopyrite - sphalerite - roquesite) group minerals from Toyoha (Ohta, 1989).
CP:chalcopyrite, SS:the cp-st ss., ST:stannite, RQ:roquesite, ZI:the Zn-In mineral, SP:sphalerite, CZF:the Cu-Zn-Fe mineral.
Solid lines in the diagram are isopleths of observed In/In+Sn, and broken lines are of calculated In/In+Sn assuming that Fe^{+3} is zero. Small open circles by the abbreviations in the figure are at ideal compositions of corresponding phases. Addition of minor Ag to Cu and Mn+Cd to Fe+Zn does not make any recognizable difference on this diagram. Dots around the CZF mineral and chalcopyrite include data which exhibit less that 0.1 In+Sn in 8 total atoms. Though their In/In+Sn are not necessarily in the range from 0.00 to 0.29, the ratios for those with such low In+Sn are beyond the scope of this discussion.

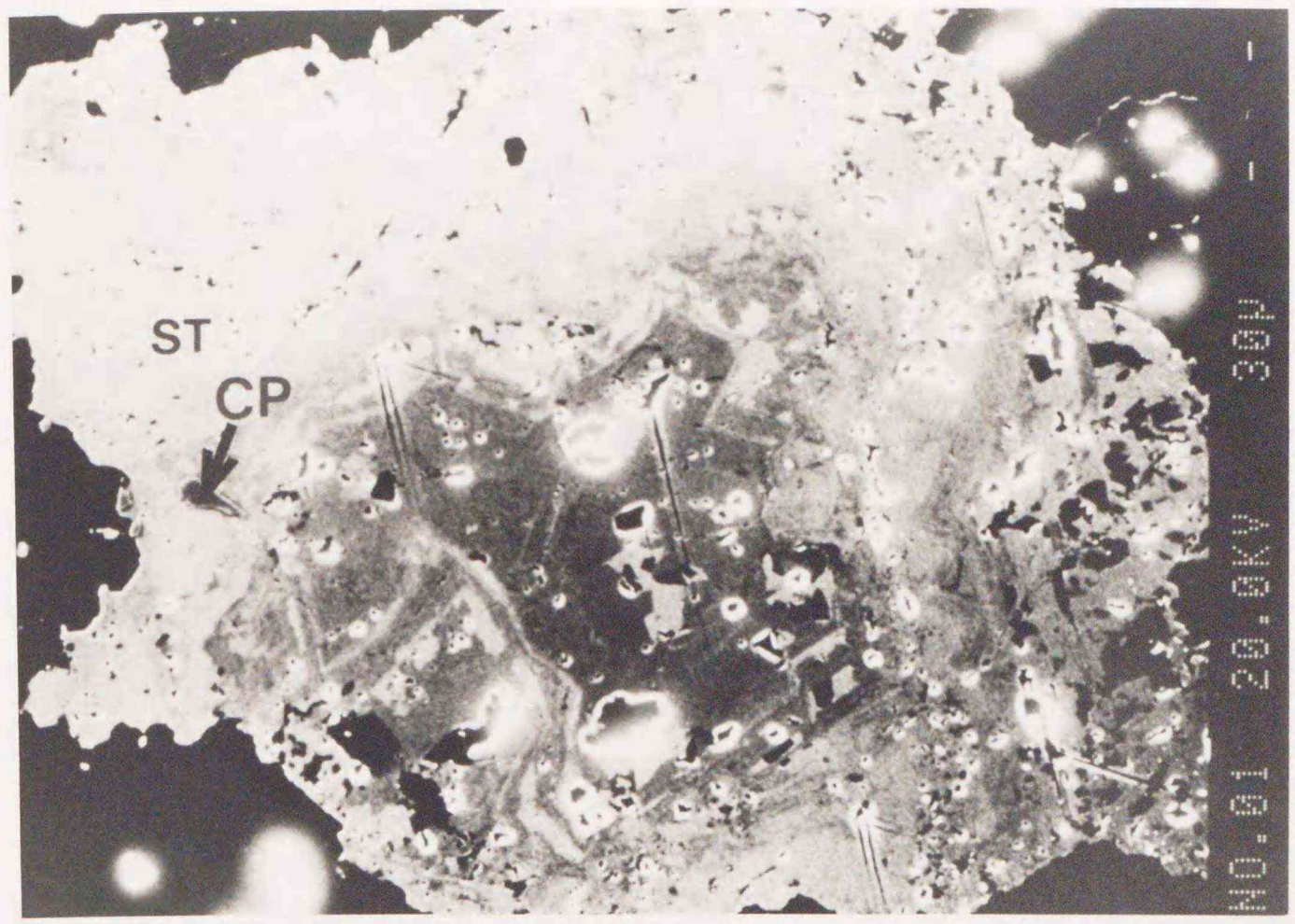

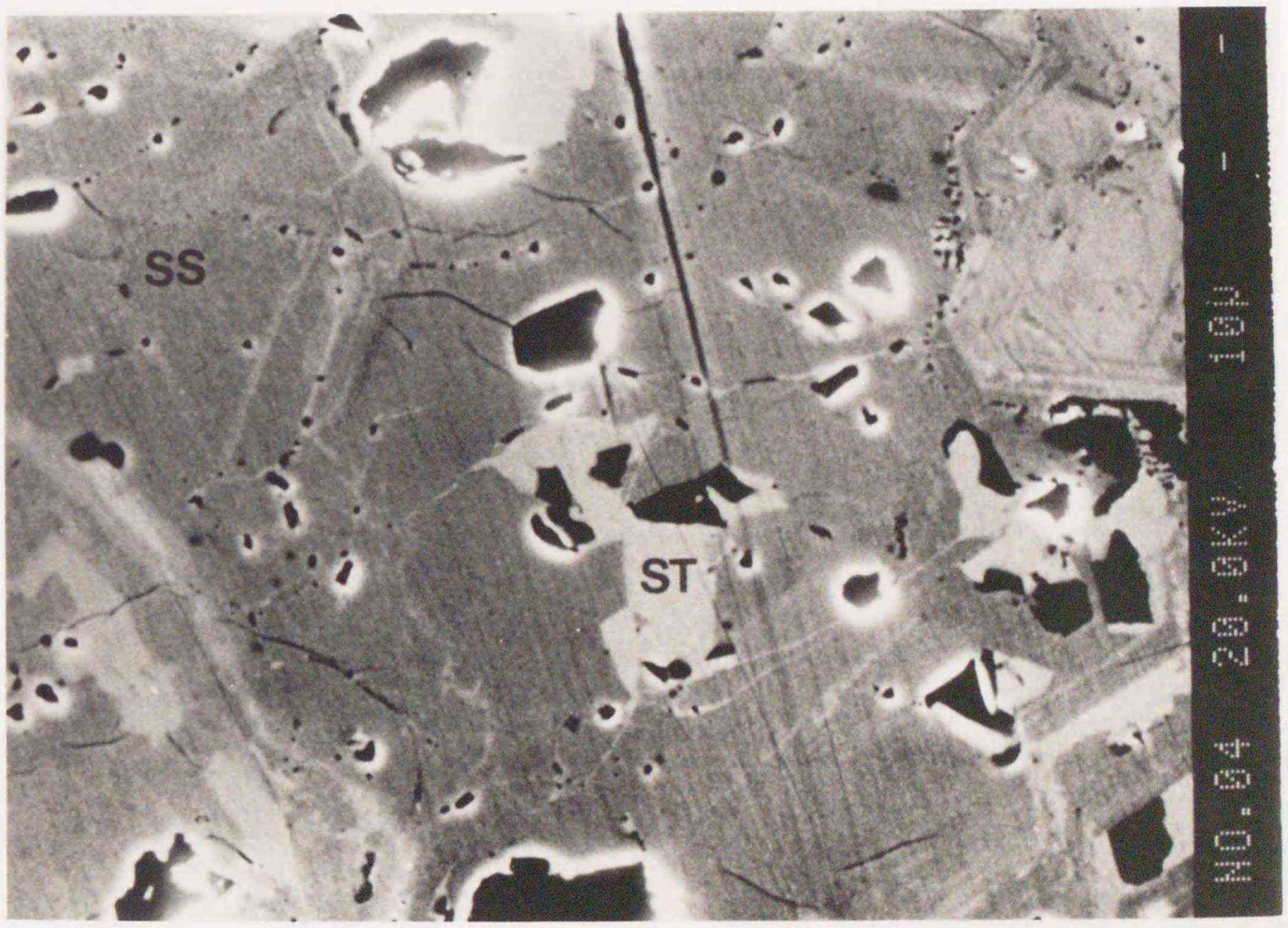

Figure 14. BSE images showing complex aggregate of stannite (ST), the chalcopyrite-stannite solid solution (SS) and chalcopyrite (CP) in a chalcopyrite-rich sample of the substage B from the Shinano vein -450 mL (point 2 in Figure 1c).

The lower image shows the central portion of the upper whose coverage corresponds to the area shown in Figure 16.

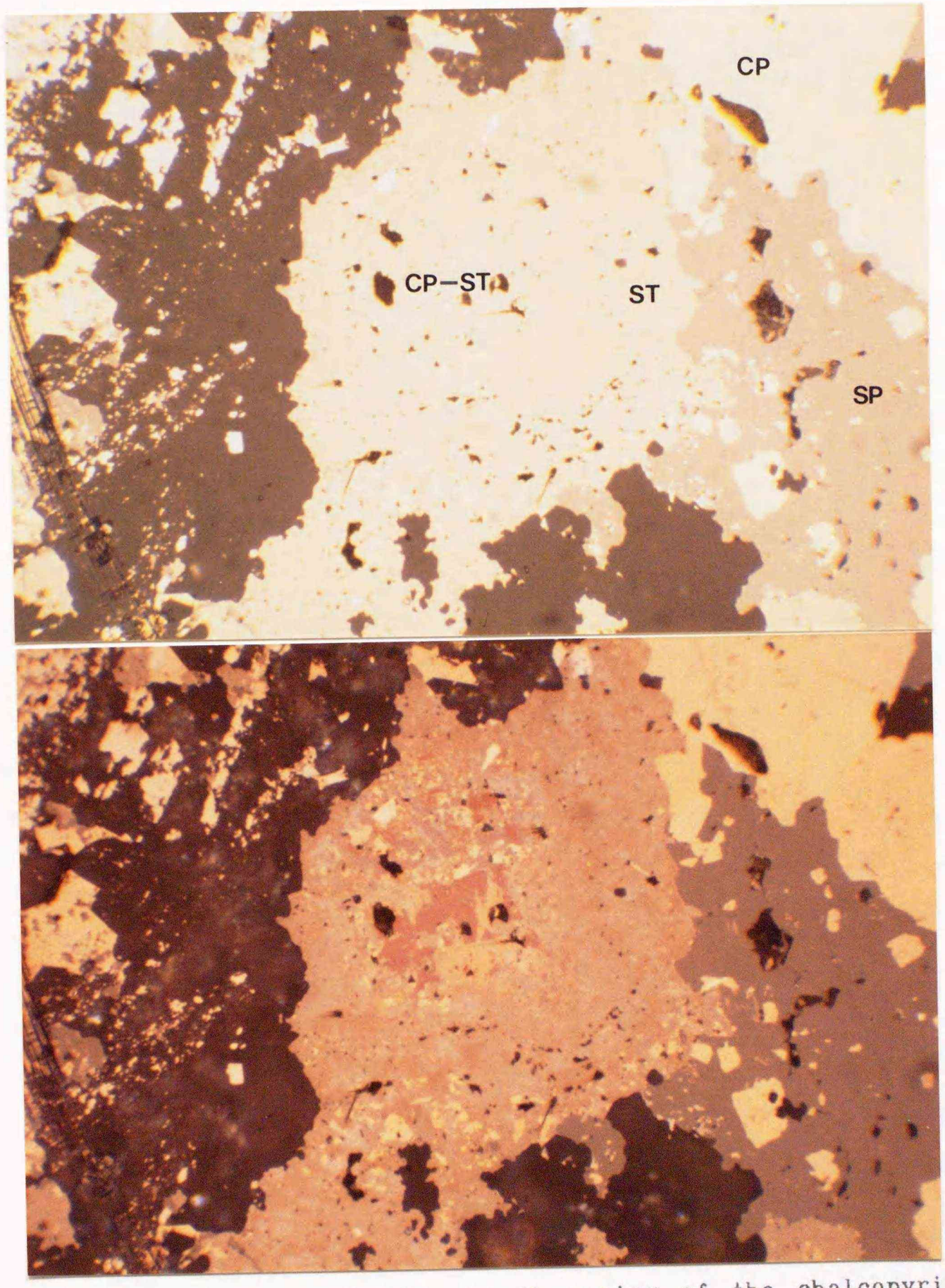

Figure 15. Photomicrograph showing growth zoning of the chalcopyrite-stannite solid solution (CP-ST, mostly at the core) and stannite (ST).

Boundaries between them are not easily recognizable on this picture. The upper picture is under plane polarized light, and the lower is under crossed polars. This aggregate is the same with that shown in Figure 14, but turned about 90° clockwise. Width of the pictured area is 0.6 mm. Note the small grains of the anisotropic chalcopyrite included in the solid solution. CP:chalcopyrite, SP:sphalerite.

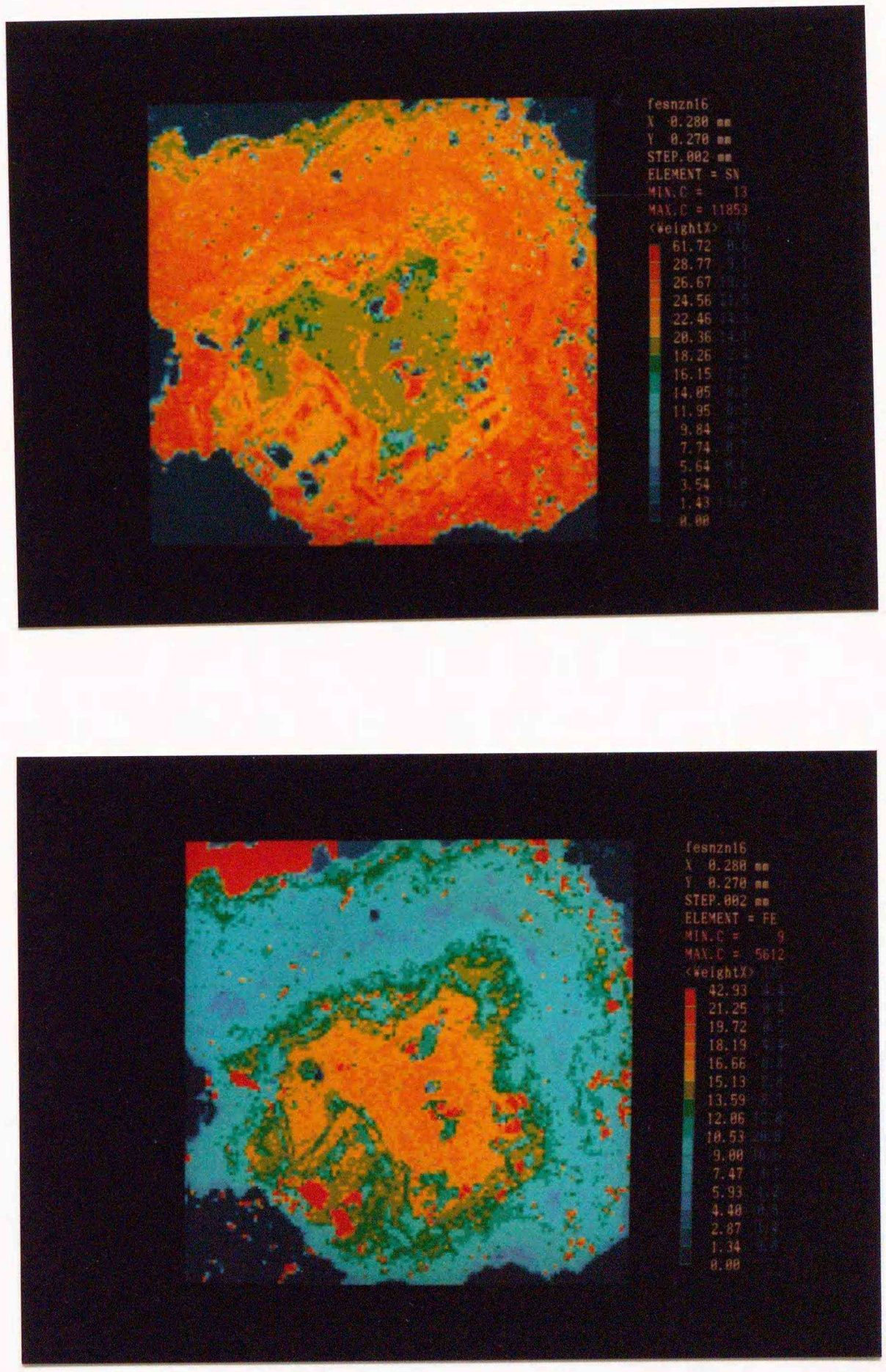

Figure 16. Tin and iron maps of the aggregate of stannite, the chalcopyrite-stannite solid solution and anisotropic chalcopyrite shown in Figure 14 and Figure 15.
The concentrations of iron and tin are in negative correlation.

Roquesite and Sakuraiite (Substage B):

Roquesite and sakuraiite are recognized in copper-rich ores of the substage B from deep levels of a southern part of the Soya vein (point 3 in Figure 1c). They occur as bands or grains intergrown with kesterite and the Zn-In mineral (Figure 8, Figure 9, Figure 10). Thin layers possibly of roquesite mixed with extremely fine grains of the anisotropic chalcopyrite and indium-rich stannite (Figure 11, Figure 12) are recognized also in a sample from the Shinano vein -350 mL. When compared with kesterite or the Zn-In mineral, roquesite shows a distinct blue tint and clear boundaries against them in some occasions, but in other occasions, the boundaries are almost invisible under microscope. In the latter case, the roquesite is actually a solid solution with composition close to sakuraiite which, in chemical term, is assumed as a solid solution between the Zn-In mineral and kesterite (Ohta, 1989). Moreover, the colors of kesterite and sakuraiite resemble that of the Zn-In mineral, and it is essentially impossible to discriminate between kesterite and sakuraiite under microscope, because there is no distinct gap in chemistry between these minerals from Toyoha, like as those from the Ikuno mine (Shimizu et al. 1986). Both roquesite and sakuraiite are weakly anisotropic, and show neither bireflectance nor internal reflection. It is notable that roquesite is observed only in chalcopyrite-rich ore, and generally in direct contact with the Zn-In mineral, kesterite or chalcopyrite, but rarely with sphalerite (Figure 9, Figure 10), while the Zn-In mineral is widely distributed in sphalerite. This fact indicates that the assemblage roquesite + sphalerite is unstable at least in the formation conditions of the Toyoha deposit (Ohta, 1989). Representative analyses of the solid solutions between the Zn-In mineral and roquesite, and between kesterite and the Zn-In mineral are shown in

Table 6. Observed mol percentages of roquesite in the solid solution between roquesite and the Zn-In mineral range from 37 to 90 (Ohta, 1989). This solid solution is due to a coupled substitution of 2(Zn, Fe) for CuIn, while the solid solution between kesterite and the Zn-In mineral is to a coupled substitutions of (Zn,Fe)In for CuSn (Ohta, 1989).

Sphalerite and Unnamed Zn-In Mineral (Substage B):

The unnamed Zn-In mineral has a chemical composition at the midst of sphalerite and roquesite (Ohta, 1980). It is common in the later veins, and usually occurs within sphalerite. It generally shows concentric parallel intergrowth with normal and indium sphalerite (Figure 6, Figure 7). Stannite, kesterite, and chalcopyrite often accompany them. A unit band of the Zn-In mineral is as wide as 50 microns at lower levels of the veins, but is quite thin, generally ten microns or less, at upper levels. Under ore microscope, the Zn-In mineral exhibits a slight brown tint as compared with sphalerite, and shows imperceptible to weak anisotropism, but no bireflectance nor internal reflection (Ohta, 1980, 1989). Indium sphalerite is commonly observed as thin growth bands within normal sphalerite, and exhibits various colors between those of normal sphalerite and the Zn-In mineral. Though boundaries of the Zn-In mineral against the other two are generally sharp, indium sphalerite frequently shows gradational boundaries to normal sphalerite. Figure 17 shows a back-scattered electron image of rhythmically zoned indium sphalerite. Figure 18 evidently shows that distribution patterns of indium and copper in sphalerite are essentially identical. Indium concentration in sphalerite ranges from 0.0n to a few weight percent in most case, but exceeds

ten weight percent at some points to bridge sphalerite and the Zn-In mineral (Table 7). All these facts reveal a continuous and complete solid solution between sphalerite and the Zn-In mineral (Ohta, 1989). Actually the range of the solid solution deviates slightly towards roquesite (Figure 13) up to a composition $48(Zn,Fe)_2S_2 + 52CuInS_2$. The solid solution between sphalerite and the Zn-In mineral (or roquesite) is attributed also to a coupled substitution of 2(Zn,Fe) for CuIn.

Manganese and cadmium contents in sphalerite of the later veins are generally less than 0.1 and 0.5 weight percents respectively, though they sporadically exceed 0.2 and 1 weight percents as element maps in Figure 19 show. The maps also show a complex compositional texture which is attributed to overgrowth of sphalerite of the substage B on iron-rich sphalerite of the substage A, and to replacement of the latter with the former along cracks. This replacement texture in sphalerite is common in the later veins (Ohta, 1980), but a careful observation is needed to identify it under normal optical microscope. Quantitative analyses preceded by careful qualitative analyses detected 0.01 to 0.23 weight percent of gallium in sphalerite associated with the unknown Mo-Pb-Sb sulfides at the Shinano vein -450 mL (Table 8).

Table 6. Representative EPMA analyses of the solid solutions among roquesite, kesterite and the Zn-In mineral from Toyoha (Ohta, 1989).

Abbreviations; Atom:atomic composition, SN:Shinano, SR:Sorachi, SY:Soya, rq:solid solutions between roquesite and the Zn-In mineral, ks: kesterite and sakuraiite or the solid solution between kesterite and the Zn-In mineral

Numerals after the vein name abbreviations indicate levels in meters below the mining office at Toyoha.

Locality	Name	Cu	Ag	Fe	Zn	In	Sn	S	Total
SY550	rq	24.68	0.92	0.38	2.44	42.68	2.16	26.07	99.33
Atom		1.89	0.04	0.03	0.18	1.81	0.09	3.96	8
SY550	rq	24.60	0.97	1.77	3.07	41.11	1.89	26.53	99.94
Atom		1.85	0.04	0.15	0.22	1.71	0.08	3.95	8
SY550	rq	23.84	0.68	0.78	6.63	37.88	3.31	27.19	100.31
Atom		1.76	0.03	0.07	0.48	1.55	0.13	3.98	8
SY550	rq	23.24	0.45	1.54	8.66	33.20	4.96	27.63	99.68
Atom		1.70	0.02	0.13	0.62	1.34	0.19	4.00	8
SY550	rq	21.76	0.49	1.04	11.95	34.54	2.38	27.77	99.93
Atom		1.58	0.02	0.09	0.84	1.39	0.09	3.99	8
SY550	rq	22.48	0.47	2.40	12.77	27.79	6.27	27.98	100.16
Atom		1.61	0.02	0.20	0.89	1.10	0.24	3.96	8
SY550	rq	21.84	0.42	1.37	16.03	25.37	7.06	27.85	99.94
Atom		1.56	0.02	0.11	1.11	1.00	0.27	3.93	8
SY550	ks	21.92	0.23	3.90	18.00	16.34	12.57	28.72	101.68
Atom		1.50	0.01	0.30	1.20	0.62	0.46	3.90	8
SY550	ks	23.63	0.28	3.87	15.76	11.98	16.32	29.07	100.91
Atom		1.62	0.01	0.30	1.05	0.46	0.60	3.96	8
SR350	ks	25.48	0.26	3.65	17.05	1.83	21.91	29.33	99.52
Atom		1.74	0.01	0.28	1.13	0.07	0.80	3.97	8
SR350	ks	26.47	0.34	3.14	15.03	0.32	25.97	28.63	99.89
Atom		1.83	0.01	0.25	1.01	0.01	0.96	3.92	8
SR450	ks	25.66	1.57	4.84	12.12	1.86	25.98	28.13	100.16
Atom		1.79	0.06	0.38	0.82	0.07	0.97	3.89	8
SY550	ks	27.44	0.33	4.93	9.94	6.71	22.84	28.49	100.68
Atom		1.90	0.01	0.39	0.67	0.26	0.85	3.92	8
SR350	ks	27.66	0.43	4.52	12.00	1.15	25.87	28.79	100.44
Atom		1.90	0.02	0.35	0.80	0.04	0.95	3.93	8
SN350	ks	28.96	0.24	6.11	9.24	0.14	25.98	29.22	99.89
Atom		1.98	0.01	0.48	0.61	0.01	0.95	3.96	8

Table 7. Representative EPMA analyses of the solid solution between sphalerite and the Zn-In mineral.

Abbreviations; Atom:atomic composition, IZ:Izumo, SR:Sorachi, SY:Soya, n.a.:not analyzed

Numerals after the vein name abbreviations indicate levels in meters below the mining office at Toyoha.

Loc.	Fe	Zn	Cu	Ag	In	Sn	S	Mn	Cd	Total
IZ400	4.33	59.17	1.17	0.12	1.12	0.43	32.57	0.05	0.50	99.47
Atom	0.30	3.56	0.07	0.00	0.04	0.01	3.99	0.00	0.02	8
SR350	1.27	61.40	2.29	0.70	1.62	0.46	32.42	n.a.	0.00	100.15
Atom	0.09	3.69	0.14	0.03	0.06	0.01	3.98		0.00	8
SY550	1.23	60.33	2.68	0.03	2.18	1.00	32.24	0.00	0.69	100.37
Atom	0.09	3.64	0.17	0.00	0.07	0.03	3.97	0.00	0.02	8
IZ400	8.56	50.98	1.90	1.01	2.61	1.01	32.46	0.07	1.01	99.61
Atom	0.60	3.08	0.12	0.04	0.09	0.03	4.00	0.01	0.04	8
IZ400	6.36	53.12	2.35	0.22	3.61	0.23	32.68	0.05	0.77	99.39
Atom	0.45	3.21	0.15	0.01	0.12	0.01	4.03	0.00	0.03	8
IZ400	7.24	48.02	4.16	0.41	6.98	0.36	32.30	0.06	0.69	100.22
Atom	0.52	2.92	0.26	0.01	0.24	0.01	4.01	0.00	0.03	8
SR350	2.41	43.88	9.15	0.12	10.85	2.42	31.13	n.a.	n.a.	99.97
Atom	0.18	2.76	0.59	0.01	0.39	0.08	3.99			8
SR350	1.48	44.32	9.13	0.20	13.21	1.41	30.76	n.a.	n.a.	100.52
Atom	0.11	2.80	0.59	0.01	0.47	0.05	3.96			8
SR350	1.80	42.49	9.15	0.26	13.99	1.47	30.72	n.a.	n.a.	99.87
Atom	0.14	2.71	0.60	0.01	0.51	0.05	3.99			8
SR350	1.53	40.54	9.96	0.20	15.89	1.25	30.43	n.a.	n.a.	99.80
Atom	0.12	2.60	0.66	0.01	0.58	0.04	3.99			8
SR250	4.43	32.36	13.58	0.20	17.24	2.55	30.17	n.a.	n.a.	100.53
Atom	0.33	2.08	0.90	0.01	0.63	0.09	3.96			8
SR350	1.57	37.27	11.32	0.16	18.12	1.40	30.28	n.a.	n.a.	100.11
Atom	0.12	2.41	0.75	0.01	0.67	0.05	3.99			8
SY550	2.26	30.31	14.57	0.25	21.06	2.22	29.14	n.a.	n.a.	99.81
Atom	0.18	2.01	0.99	0.01	0.80	0.08	3.94			8
SY550	1.28	29.44	15.24	0.26	22.73	2.66	28.91	n.a.	n.a.	100.51
Atom	0.10	1.96	1.04	0.01	0.86	0.10	3.93			8
SY550	3.90	27.44	14.52	0.22	23.07	1.29	29.57	0.03	0.40	100.45
Atom	0.30	1.81	0.98	0.01	0.86	0.05	3.97	0.00	0.01	8

Table 8. Representative EPMA analyses of sphalerite (sp), and the unnamed Cu-Zn-Fe mineral (cz).

Abbreviations; Atom:atomic composition, IZ:Izumo, SB:Soya Bunki (a branch of the Soya vein), SN:Shinano, SR:Sorachi, SY:Soya, TA:Tajima, n.a.:not analyzed

Numerals after the vein name abbreviations indicate levels in meters below the mining office at Toyoha.

Loc.	Name	Fe	Zn	Cu	Ag	In	Sn	S	Mn	Cd	Ga	Total
SR200	sp	22.52	43.48	n.a.	n.a.	n.a.	n.a.	33.87	n.a.	n.a.	n.a.	99.87
	Atom	1.52	2.50					3.98				8
SB280	sp	20.01	44.45	0.88	n.a.	0.09	0.07	34.06	0.05	0.08	n.a.	99.68
	Atom	1.35	2.57	0.05		0.00	0.00	4.01	0.00	0.00		8
SN450	sp	6.93	58.66	0.09	n.a.	0.01	0.00	33.05	0.07	0.09	0.23	99.19
	Atom	0.48	3.48	0.01		0.00	0.00	4.00	0.01	0.00	0.01	8
SR350	sp	3.86	62.13	0.53	0.19	0.09	0.08	32.85	n.a.	n.a.	n.a.	99.72
	Atom	0.27	3.70	0.03	0.01	0.00	0.00	3.99				8
SY550	sp	2.62	62.64	0.76	0.01	0.11	0.29	32.78	0.00	1.13	n.a.	100.33
	Atom	0.18	3.73	0.05	0.00	0.00	0.01	3.98	0.00	0.04		8
TA450	sp	2.54	63.75	0.55	0.02	0.50	0.10	33.08	n.a.	n.a.	n.a.	100.54
	Atom	0.18	3.77	0.03	0.00	0.02	0.00	4.00				8
IZ400	sp	1.67	64.23	0.61	0.06	0.00	0.50	32.73	0.06	0.38	n.a.	100.23
	Atom	0.12	3.83	0.04	0.00	0.00	0.02	3.98	0.00	0.01		8
TA450	sp	1.60	65.04	0.27	0.04	0.21	0.08	33.30	n.a.	n.a.	n.a.	100.56
	Atom	0.11	3.85	0.02	0.00	0.01	0.00	4.01				8
SN450	sp	1.50	65.72	0.08	n.a.	0.07	0.00	32.39	0.04	0.15	0.20	100.18
	Atom	0.10	3.92	0.01		0.00	0.00	3.94	0.00	0.01	0.01	8
SN450	sp	1.37	65.67	0.09	n.a.	0.08	0.00	32.44	0.04	0.07	0.23	100.05
	Atom	0.10	3.92	0.01		0.00	0.00	3.95	0.00	0.00	0.01	8.00
SN450	sp	1.13	65.97	0.12	n.a.	0.08	0.00	32.80	0.04	0.06	0.12	100.35
	Atom	0.08	3.92	0.01		0.00	0.00	3.98	0.00	0.00	0.01	8
SN450	sp	1.03	66.65	0.00	n.a.	0.06	0.00	32.53	0.10	0.08	0.18	100.68
	Atom	0.07	3.96	0.00		0.00	0.00	3.94	0.01	0.00	0.01	8
SN450	sp	0.72	65.41	0.56	n.a.	0.09	0.16	32.65	0.06	0.10	n.a.	99.75
	Atom	0.05	3.91	0.03		0.00	0.01	3.98	0.00	0.00		8
SY550	cz	9.75	49.28	6.47	0.14	0.56	0.12	33.67	n.a.	n.a.	n.a.	99.99
	Atom	0.67	2.89	0.39	0.01	0.02	0.00	4.02				8
SY550	cz	9.59	49.00	7.42	0.05	0.50	0.12	33.91	n.a.	n.a.	n.a.	100.59
	Atom	0.65	2.85	0.44	0.00	0.02	0.00	4.03				8
SY550	cz	10.76	47.05	8.28	0.08	0.31	0.08	33.83	n.a.	n.a.	n.a.	100.39
	Atom	0.73	2.74	0.50	0.00	0.01	0.00	4.02				8

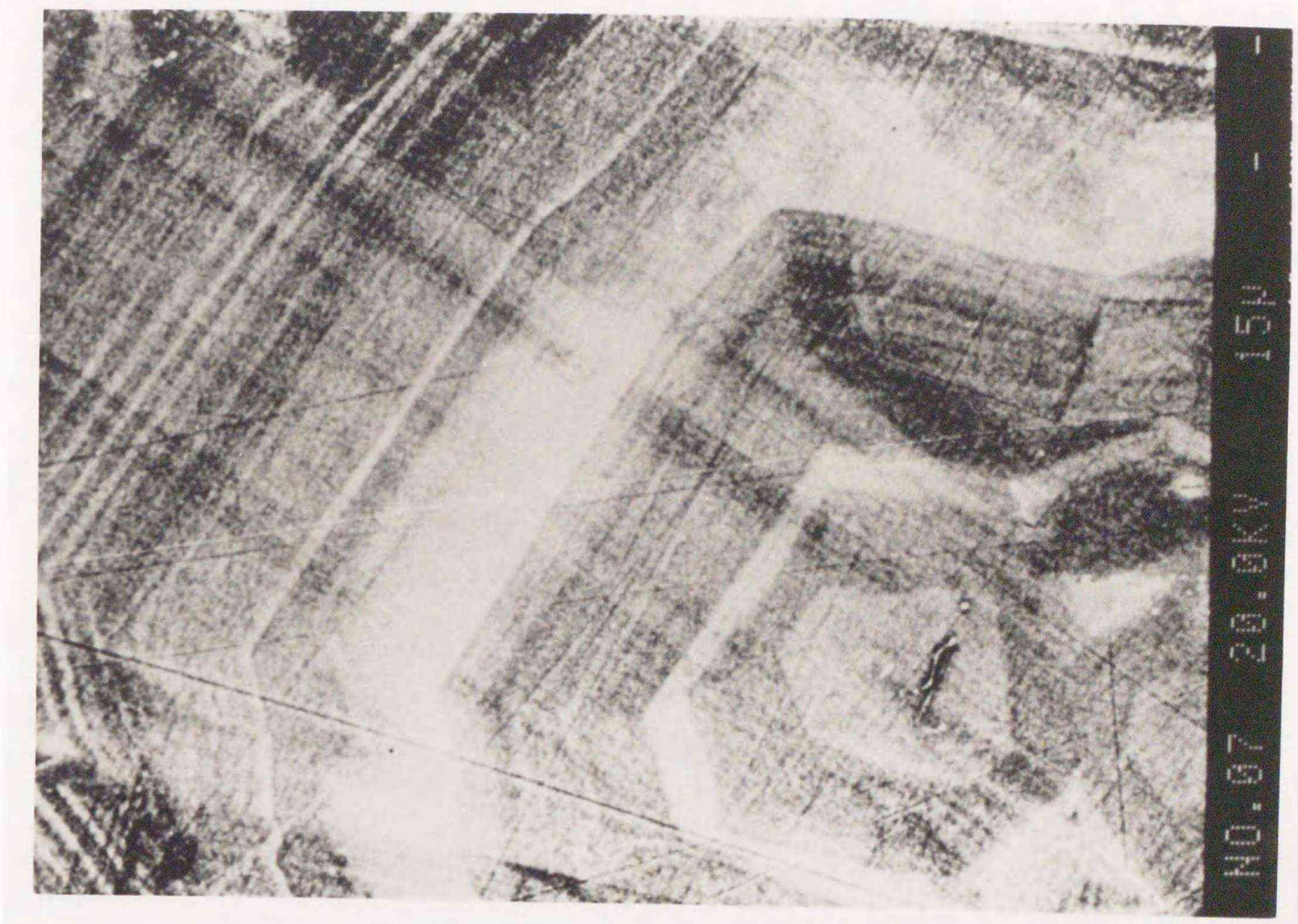

Figure 17. BSE image showing rhythmic zoning in sphalerite in a brown-sphalerite-rich sample of the substage B from the Sorachi vein -350 mL (about 100 m south of point 4 in Figure 1c).
The brighter zones contain more indium and copper (roquesite mol) than the darker zones. Sphalerite covers more than 99 percent of the scope, which corresponds to a part of the area shown in Figure 18.

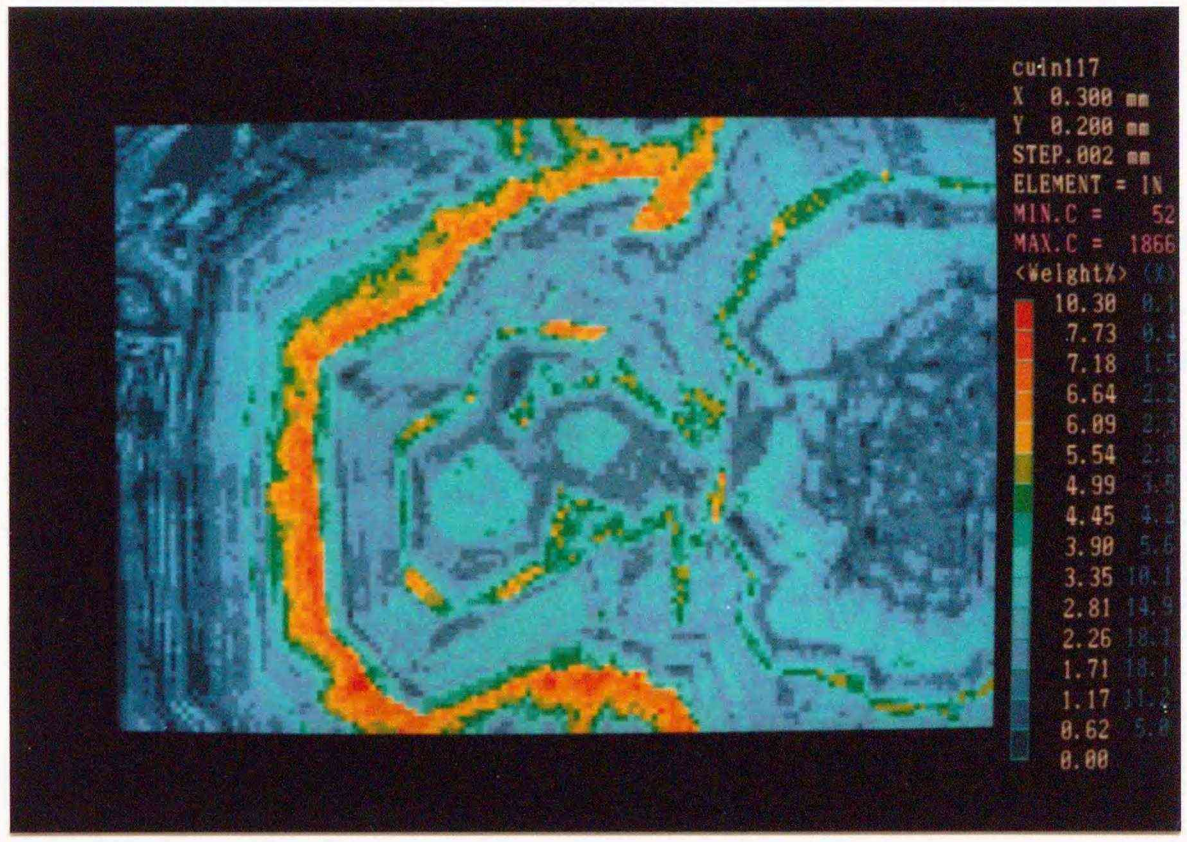

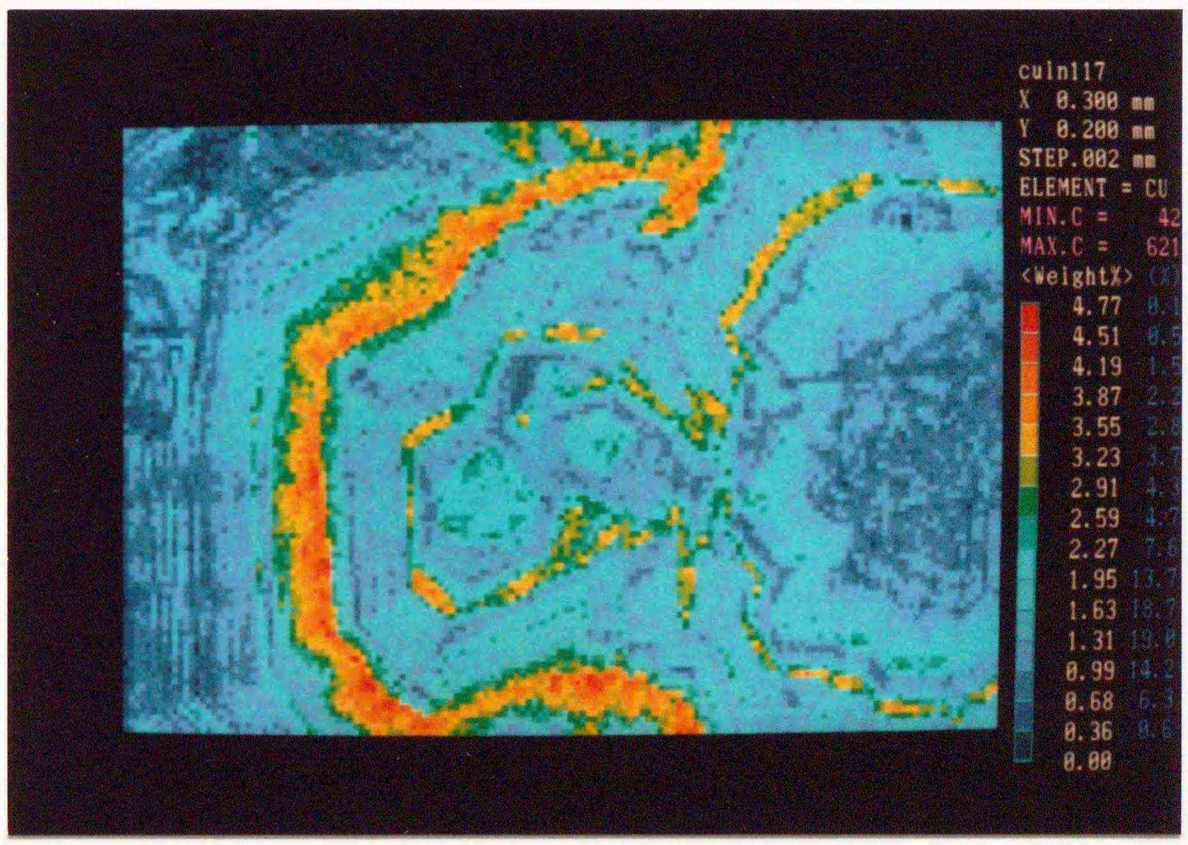

Figure 18. Indium and copper maps showing growth bands of the sphalerite in Figure 17.

Note the patterns almost identical. The Cu/In atomic ratio in this sample is about 1.1 in average.

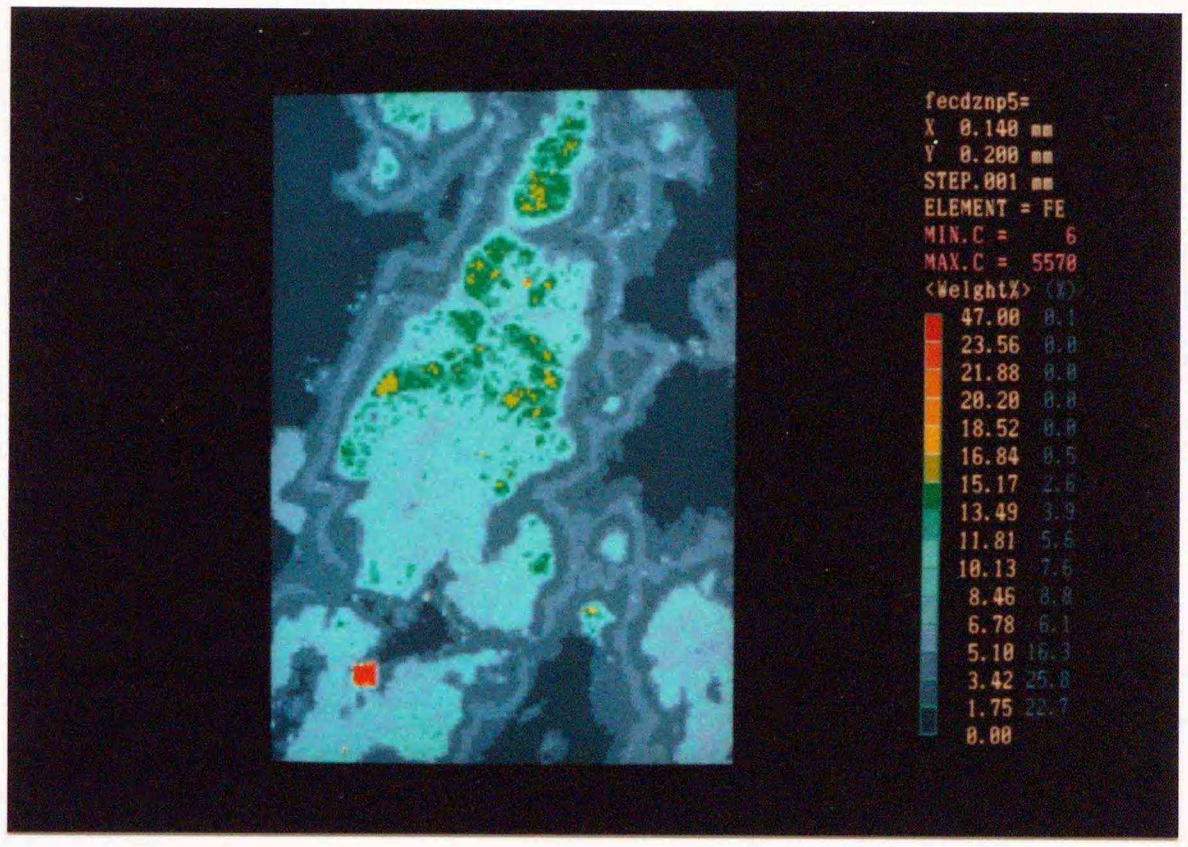

Figure 19a. Iron and indium maps of sphalerite in a toyohaite-containing sample (formed in the substage B, and modified in the substages C and D) from the Sorachi vein -450 mL (point 4 in Figure 1c). This sphalerite holds numerous pores of which some are filled with a kaolin mineral (possibly dickite). Dark background is quartz. Small red squares on the upper image are grains of pyrite.

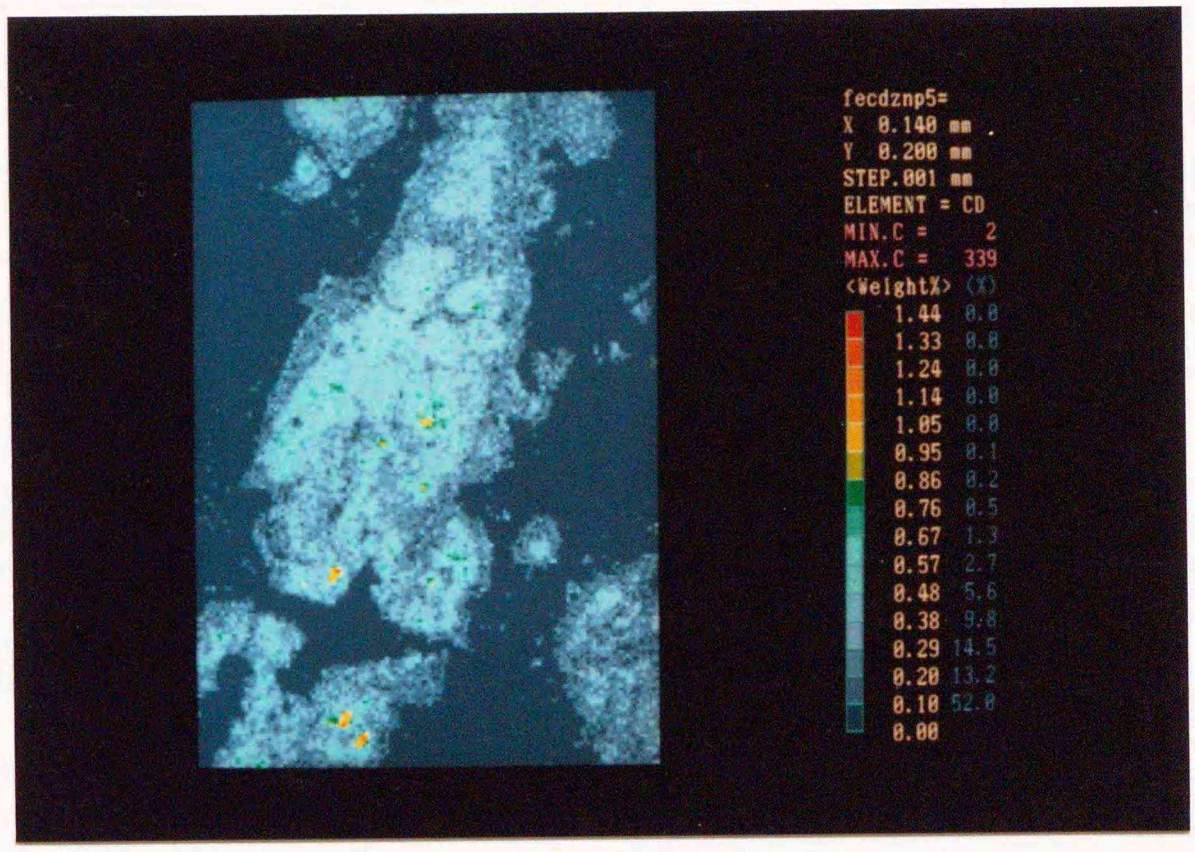

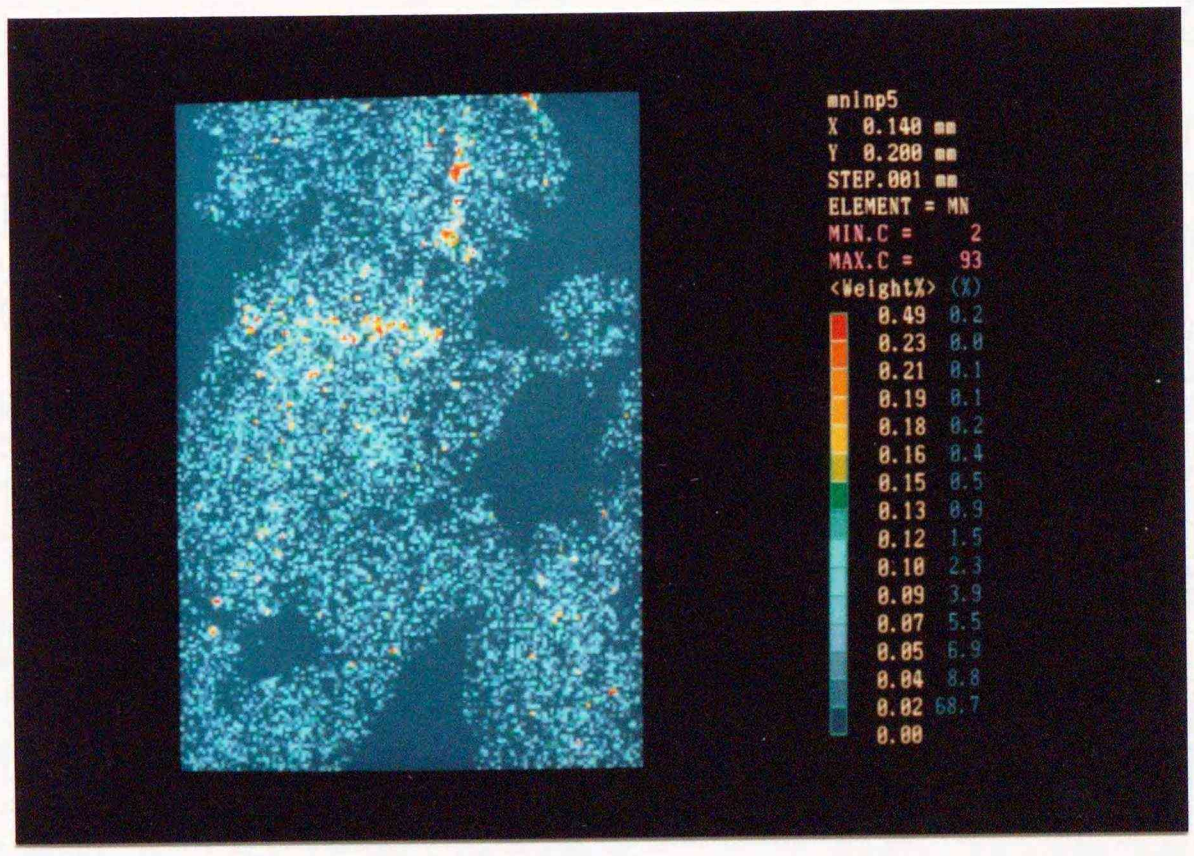

Figure 19b. Cadmium and manganese maps of the sphalerite shown in Figure 19a.

Unnamed Ag-In Mineral (Substage C):

The unnamed Ag-In mineral (Ohta, 1980, 1989) is the silver analogue of roquesite in chemical term (Table 9). It is rarely and locally recognized at middle to upper levels of the Sorachi vein where intense silver mineralization has followed that of tin and indium. It occurs in close association with hocartite, galena, pyrargyrite and pyrite as metasome which has partly replaced the Zn-In mineral or indium sphalerite. This suggests that the formation of the Ag-In mineral is due to a reaction between indium minerals of the substage B and the silver-rich ore solution of the substage C (Ohta, 1980, 1989). As compared with hocartite, the Ag-In mineral has similar polishing hardness, and shows a slightly more red tint. Its anisotropism is strong, but bireflectance is not observed.

Hocartite and Pirquitasite (Substage C):

Occurrences of hocartite and pirquitasite, the zinc analogue of hocartite (Johan and Picot, 1982), in Toyoha are described by Kojima et al.(1979). As well as toyohaite, these minerals are observed within hydrothermally etched pits in sphalerite which includes cassiterite and/or stannite grains. The occurrence modes of the Ag-In mineral, hocartite and pirquitasite are similar, and indicate that these minerals were formed by the same mechanism, reaction of the silver-rich ore solution of the substage C with tin- and indium-containing ore of the substage B. Observed Ag/Ag+Cu atomic ratios in these minerals are generally higher than 0.92 (Table 9, Table 10).

Table 9. EPMA analyses of the Ag-In mineral (AI), hocartite (hc) and pirquitasite (pq).

Abbreviations; Atom:atomic composition, SR:Sorachi, n.a.:not analyzed

Numerals after the vein name abbreviation indicate levels in meters below the mining office at Toyoha.

Loc.	Name	Fe	Zn	Cu	Ag	In	Sn	S	Mn	Cd	Total
SR250	AI	0.24	1.37	0.80	36.28	39.18	n.a.	21.74	n.a.	n.a.	99.61
	Atom	0.03	0.12	0.07	1.93	1.96		3.89			8
SR250	AI	0.17	0.95	0.82	37.86	38.40	n.a.	21.32	n.a.	n.a.	99.52
	Atom	0.02	0.08	0.07	2.03	1.94		3.85			8
SR250	AI	0.17	1.59	0.50	37.80	38.97	n.a.	20.27	n.a.	n.a.	99.30
	Atom	0.02	0.14	0.05	2.06	2.00		3.73			8
SR250	AI	0.18	1.31	0.52	37.48	39.19	n.a.	21.49	n.a.	n.a.	100.17
	Atom	0.02	0.12	0.05	2.00	1.96		3.86			8
SR250	AI	0.17	1.36	0.50	37.81	38.94	n.a.	21.46	n.a.	n.a.	100.24
	Atom	0.02	0.12	0.04	2.02	1.95		3.85			8
SR400	hc	7.48	3.32	0.28	41.56	0.00	23.59	24.31	n.a.	n.a.	100.55
	Atom	0.70	0.27	0.02	2.01	0.00	1.04	3.96			8
SR400	hc	7.33	2.69	0.42	41.22	0.14	23.44	23.92	n.a.	n.a.	99.15
	Atom	0.70	0.22	0.04	2.03	0.01	1.05	3.96			8
SR400	hc	8.17	2.22	0.49	41.53	0.00	23.93	23.92	n.a.	n.a.	100.26
	Atom	0.77	0.18	0.04	2.03	0.00	1.06	3.92			8
SR400	hc	7.34	3.20	0.39	41.43	0.01	24.06	24.07	n.a.	n.a.	100.49
	Atom	0.69	0.26	0.03	2.02	0.00	1.06	3.94			8
SR400	hc	7.68	2.99	0.40	42.09	0.03	23.35	23.44	n.a.	n.a.	99.99
	Atom	0.73	0.24	0.03	2.07	0.00	1.04	3.88			8
SR400	hc	7.72	2.84	0.41	41.99	0.04	23.68	23.29	n.a.	n.a.	99.96
	Atom	0.74	0.23	0.03	2.07	0.00	1.06	3.87			8
SR400	hc	7.72	2.84	0.41	41.99	0.04	23.68	23.29	n.a.	n.a.	99.96
	Atom	0.74	0.23	0.03	2.07	0.00	1.06	3.87			8
SR400	hc	7.93	3.13	0.38	41.13	0.06	23.01	23.81	0.40	0.44	100.29
	Atom	0.74	0.25	0.03	2.00	0.00	1.02	3.90	0.04	0.02	8
SR400	hc	8.02	2.30	0.52	40.88	0.01	23.23	23.52	0.28	0.46	99.22
	Atom	0.76	0.19	0.04	2.02	0.00	1.04	3.90	0.03	0.02	8
SR400	hc	7.61	2.74	0.54	40.83	0.11	23.10	23.33	0.38	0.43	99.06
	Atom	0.73	0.22	0.04	2.02	0.01	1.04	3.88	0.04	0.02	8
SR	pq*	1.19	8.95	1.84	40.33	n.a.	23.71	24.02	n.a.	n.a.	100.04
	Atom	0.11	0.72	0.15	1.98		1.06	3.97			8

* Kojima et al. (1979)

Rhodostannite and Toyohaite (Substage D):

Rhodostannite and toyohaite (Yajima et al., in press), the silver analogue of rhodostannite, occurs together at the lower levels, 300 to 500 mL, of the Sorachi vein (Sugaki and Hayashi, 1986; Ohta et al., 1987). These sulfides are found in massive pyrite-sphalerite ore of the substage B, and the ore appears to have been affected by the ore solution of the substage C and later (Figure 20). The appearance and occurrence mode of rhodostannite under microscope are similar to those of toyohaite. They generally occur in corrosion pits along grain margins of sphalerite, and are closely associated with kaolin minerals (mostly coarse-grained dickite; see Figure 20), herzenbergite and/or berndtite. Teallite, stannite, pirquitasite and hocartite are frequently observed in the same samples. In that case, rhodostannite and toyohaite appear to be replacement products after stannite and hocartite respectively. Each grain of toyohaite or rhodostannite is a porous aggregate of smaller crystals which are generally less than 30 microns in diameter. EPMA map images in Figure 21 also reveal this microcrystalline feature, and slight increase of Cu/Ag+Cu ratio in toyohaite at the margins of individual grains. Representative chemical compositions of these minerals are shown in Table 10. Both silver-rich rhodostannite and the unnamed sulfide from the Pirquitas deposit (Johan and Picot, 1982) show compositions between toyohaite and rhodostannite, and can be explained as solid solutions of them.

Table 10. Representative EPMA analyses of toyohaite (ty), rhodostannite (rs) and possibly their solid solution (rt) from the Pirquitas deposit, Argentina (Johan and Picot, 1982).

Abbreviations; Atom:atomic composition, SR:Sorachi, JTU2:Drill JTU2 (642 m from the start; see Figure 1c), PIRQ:Pirquitas, n.a.:not analyzed
Numerals after the vein name abbreviations indicate levels in meters below the mining office at Toyoha.

Loc.	Name	Fe	Zn	Cu	Ag	In	Sn	S	Mn	Cd	Total
SR400	ty	6.28	0.37	0.14	24.39	0.05	41.24	28.16	0.00	0.22	100.86
	Atom	1.00	0.05	0.02	2.01	0.00	3.09	7.81	0.00	0.02	14
SR400	ty	5.82	0.47	0.20	24.39	0.07	40.49	27.86	0.00	0.29	99.58
	Atom	0.94	0.06	0.03	2.04	0.01	3.07	7.83	0.00	0.02	14
SR400	ty	5.95	0.35	0.26	24.45	0.01	41.19	28.45	0.00	0.30	100.96
	Atom	0.94	0.05	0.04	2.01	0.00	3.08	7.86	0.00	0.02	14
SR400	ty	5.87	0.36	0.28	24.38	0.10	41.38	28.09	n.a.	n.a.	100.46
	Atom	0.94	0.05	0.04	2.02	0.01	3.12	7.83			14
SR400	ty	5.52	1.14	2.10	21.51	0.41	41.87	28.18	n.a.	n.a.	100.74
	Atom	0.87	0.15	0.29	1.76	0.03	3.12	7.77			14
SR400	ty	5.87	0.87	3.67	18.79	0.35	41.90	28.30	n.a.	n.a.	99.74
	Atom	0.93	0.12	0.51	1.53	0.03	3.11	7.78			14
SR400	ty	5.89	1.22	3.83	18.60	0.25	41.42	28.02	0.16	0.20	99.59
	Atom	0.93	0.17	0.53	1.52	0.02	3.08	7.71	0.03	0.02	14
SR400	ty	6.01	1.01	3.98	18.44	0.31	41.92	28.50	0.10	0.17	100.45
	Atom	0.94	0.14	0.55	1.49	0.02	3.08	7.75	0.01	0.01	14
SR400	ty	5.88	1.88	4.41	17.62	0.21	41.59	28.23	0.20	0.18	100.19
	Atom	0.92	0.25	0.60	1.43	0.02	3.06	7.68	0.03	0.01	14
SR400	ty	6.09	0.67	4.47	18.00	0.26	42.09	28.33	0.08	0.18	100.17
	Atom	0.95	0.09	0.61	1.46	0.02	3.10	7.73	0.01	0.01	14
SR400	ty	6.18	1.29	5.15	16.31	0.17	42.01	28.39	0.14	0.14	99.79
	Atom	0.96	0.17	0.71	1.32	0.01	3.08	7.71	0.02	0.01	14
SR450	rs	5.90	2.28	13.19	3.69	0.18	44.92	29.91	n.a.	n.a.	100.07
	Atom	0.87	0.29	1.71	0.28	0.01	3.13	7.70			14
SR450	rs	6.08	1.96	13.14	3.73	0.16	44.96	30.10	n.a.	n.a.	100.12
	Atom	0.90	0.25	1.70	0.28	0.01	3.12	7.74			14
JTU2	rs	6.68	0.02	14.96	1.18	0.05	46.07	31.48	n.a.	n.a.	100.44
	Atom	0.96	0.00	1.90	0.09	0.00	3.13	7.91			14
JTU2	rs	6.41	0.05	14.94	0.69	0.07	46.58	31.88	n.a.	n.a.	100.61
	Atom	0.92	0.01	1.89	0.05	0.01	3.15	7.98			14
JTU2	rs	6.52	0.04	15.01	0.82	0.03	46.36	31.85	n.a.	n.a.	100.63
	Atom	0.94	0.01	1.89	0.06	0.00	3.13	7.97			14
PIRQ	rs	6.79	0.17	13.42	4.34	n.a.	43.81	31.26	n.a.	n.a.	99.80
	Atom	0.99	0.02	1.72	0.33		3.00	7.94			14
PIRQ	rs	6.80	0.00	11.69	6.51	n.a.	44.21	31.47	n.a.	n.a.	100.66
	Atom	0.99	0.00	1.50	0.49		3.03	7.99			14
PIRQ	rt	6.27	0.00	8.37	12.32	n.a.	42.77	30.19	n.a.	n.a.	99.93
	Atom	0.95	0.00	1.11	0.96		3.04	7.94			14
PIRQ	rt	6.59	0.00	6.70	14.17	n.a.	42.20	29.82	n.a.	n.a.	99.47
	Atom	1.01	0.00	0.90	1.12		3.03	7.94			14

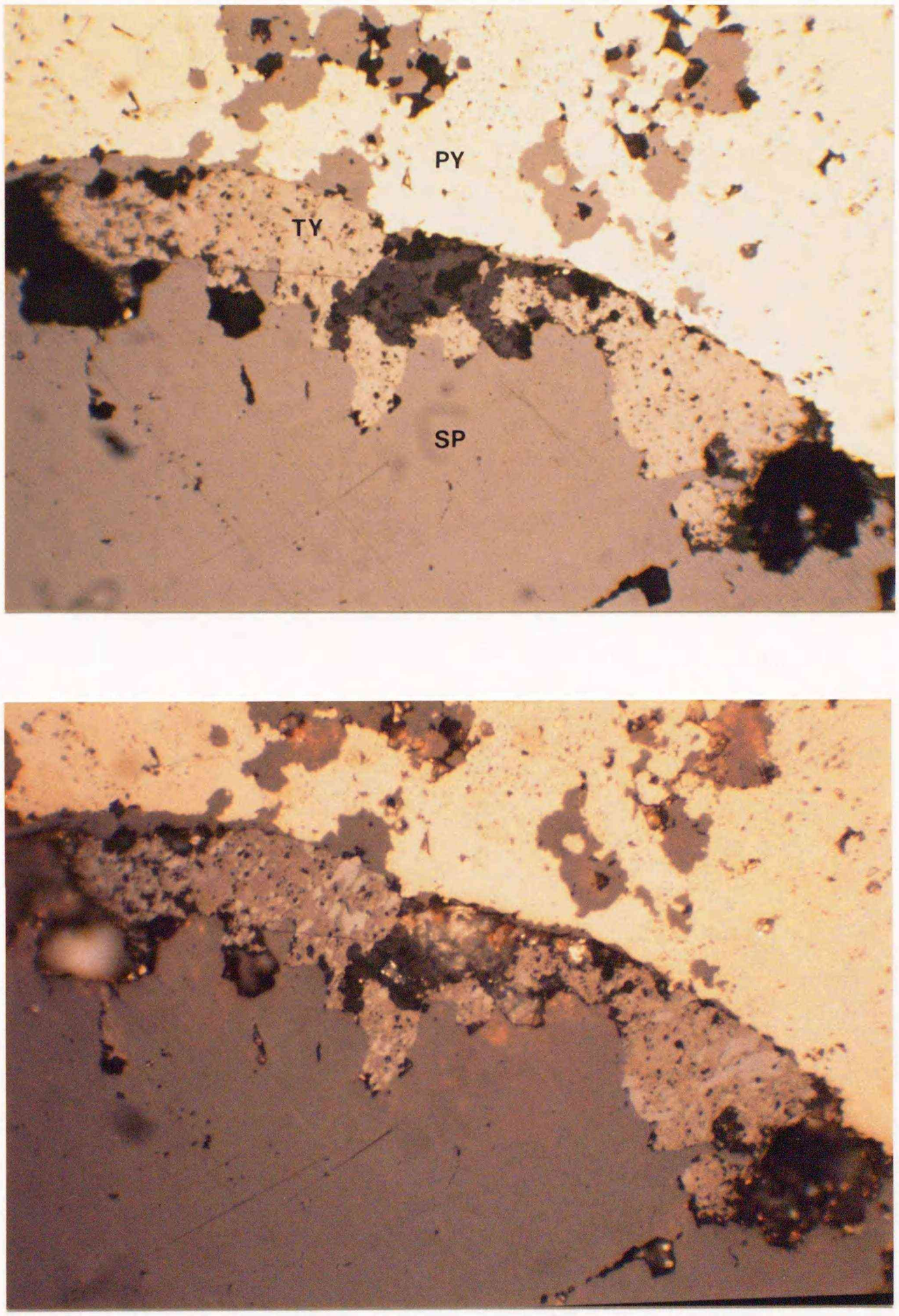

Figure 20. Photomicrographs of toyohaite (TY) in close association with stacked dickite (dark-gray grains at the center of the picture) along an eroded margin of sphalerite (SP) against pyrite in the same sample as shown in Figure 19.
The upper picture is under plane polarized light, and the lower is under crossed polars. Width of the pictured area is 0.6 mm.

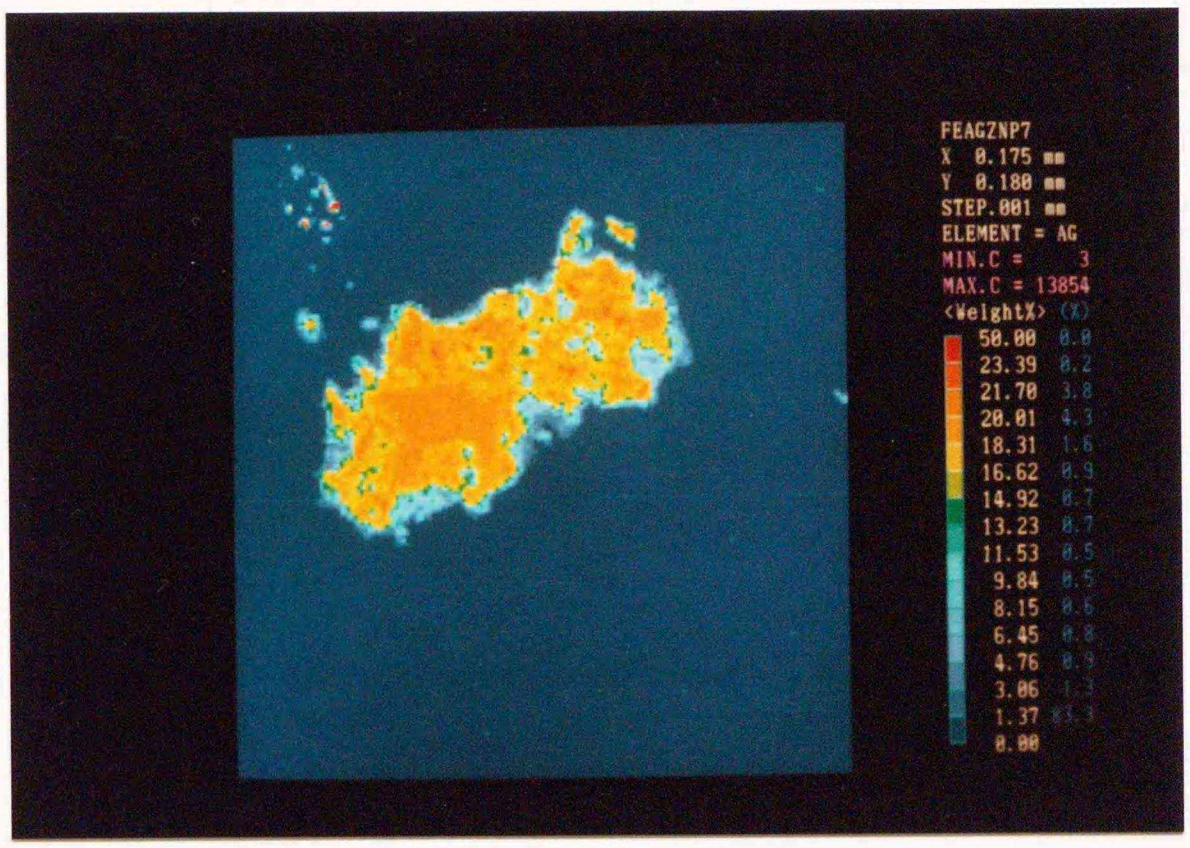

Figure 21. Silver and copper maps of toyohaite in the same sample as shown in Figure 19 and Figure 20.
The rhombic crystal in the lower left of the aggregate is one of the largest ever observed, and its dimensions are about 30 x 20 microns.

Canfieldite? (Substage C):

Occurrence of a canfieldite-like sulfide as reaction margins of cassiterite against argentite at the Tajima vein -200 mL (point 7 in Figure 1c) is reported by Ohta and Yajima (1977). Ohta (1980) described the same sulfide from the Sorachi vein, where it generally includes cassiterite, and is observed only in ore of the substage B affected by the silver mineralization of the substage C. Optical characters of this sulfide coincide with those of canfieldite described in Uytenbogaardt and Burke (1971), though the result of chemical analyses gives formulas close to Ag_7SnS_6, which is obviously not consistent with the ideal composition of canfieldite, Ag_8SnS_6. Discussing this problem, however, is out of scope of this study. Therefore, this should be left to a future study, and the author will tentatively describe the sulfide as "canfieldite?" hereafter in this paper. The formation process of canfieldite? is similar to those of hocartite, pirquitasite and the Ag-In mineral; reactions between tin- or indium-containing ore and the succeeding silver-containing ore solution. Moreover, the mode of occurrence of canfieldite? suggests that argentite mineralization in Tajima is later than the cassiterite deposition, hence provides one of the evidences that silver in the earlier veins is mostly due to the later-stage mineralization (Yajima and Ohta, 1979).

Teallite, Berndtite (Substage D) and Herzenbergite (Substages C and D):

Herzenbergite and berndtite are reported by Ohta et al. (1987), and teallite by Sugaki and Hayashi (1986). The former two generally occur in veinlets, ruses and eroded-out cavities of older ore minerals together with coarse-grained kaolin minerals, mostly dickite (Figure 22). Herzenbergite and berndtite replacing toyohaite, rhodostannite or

hocartite are frequently observed in corroded holes of sphalerite. Another typical occurrence mode of herzenbergite is as minute euhedral crystals included within hocartite. In the former case, herzenbergite is almost always associated with coarse-grained dickite, while there seems no direct genetic relation between the crystals of herzenbergite and any kind of kaolin minerals in the latter case. It appears that the herzenbergite inclusions in hocartite is a product of the substage C, and the others associated with kaolin minerals are obviously younger than hocartite, and may be put in the substage D. Representative analyses of these minerals are listed in Table 11.

Unnamed Cu-Zn-Fe Mineral (Substage B):

This unnamed sulfide is recognized in a polished sample from -550 meter level of the Soya vein (Ohta, 1989). This strongly anisotropic sulfide occurs as dendrites completely included within the anisotropic chalcopyrite (Figure 23) associated with roquesite, kesterite, sakuraiite, sphalerite and the Zn-In mineral. Its color is brownish gray with a violet tint, and pleochroism is not recognized. Chemical composition of this sulfide is plotted between chalcopyrite and sphalerite (Figure 13, Table 8). This phase can be recognized as "sphalerite star", if the size is too small to observe its actual anisotropy and to proceed EPMA analyses on it without the influence of copper and iron in the surrounding chalcopyrite. Hence this may become a clue to solve the "sphalerite star" problem.

Table 11. Representative EPMA analyses of teallite (tl), herzenbergite (hz), berndtite (bd), and canfieldite? (cf).

Abbreviations; Atom:atomic composition, SN:Shinano, SR:Sorachi, TA:Tajima, n.a.:not analyzed

Numerals after the vein name abbreviations indicate levels in meters below the mining office at Toyoha. Indium weight percent is less than 0.2 for all samples.

Loc. Name	Fe	Zn	Cu	Ag	Pb	Sn	S	Total
SR500 tl*	0.20	n.a.	n.a.	n.a.	58.60	25.50	15.90	100.20
Atom	0.01				1.13	0.86	1.99	4
SR400 hz	1.36	0.00	0.03	2.08	0.65	75.31	20.39	99.82
Atom	0.15	0.00	0.00	0.12	0.02	3.85	3.86	8
SR400 hz	0.55	0.09	0.00	0.58	0.00	78.98	20.17	100.38
Atom	0.06	0.01	0.00	0.03	0.00	4.06	3.84	8
SR400 bd	1.08	0.40	0.00	0.00	0.65	63.15	34.59	99.87
Atom	0.04	0.01	0.00	0.00	0.01	0.97	1.97	3
TA450 cf	n.a.	n.a.	0.17	70.12	n.a.	11.23	18.04	99.56
Atom			0.03	6.95		1.01	6.01	14
TA450 cf	n.a.	n.a.	0.23	70.34	n.a.	11.66	18.38	100.61
Atom			0.04	6.88		1.04	6.05	14
SN450 cf	n.a.	n.a.	0.39	70.85	n.a.	11.10	18.02	100.37
Atom			0.06	6.97		0.99	5.97	14

* Sugaki and Hayashi (1986)

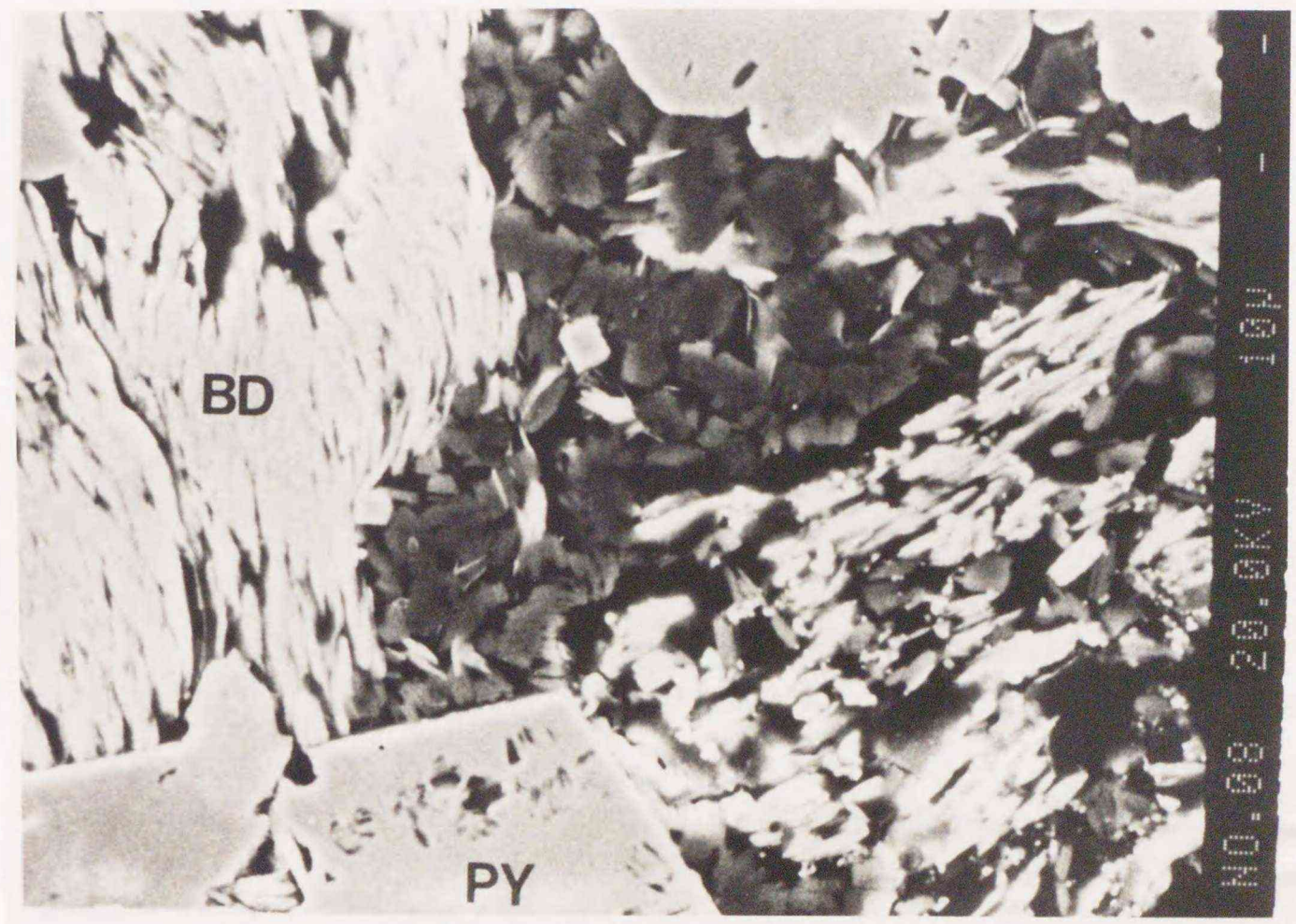

Figure 22. BSE image showing close association of berndtite (BD), stacked dickite (dark gray) and pyrite (PY) in a sample (formed in the substage B, and modified in the substages C and D) from the Sorachi vein -400 mL (about 50 m north of point 4 in Figure 1c).

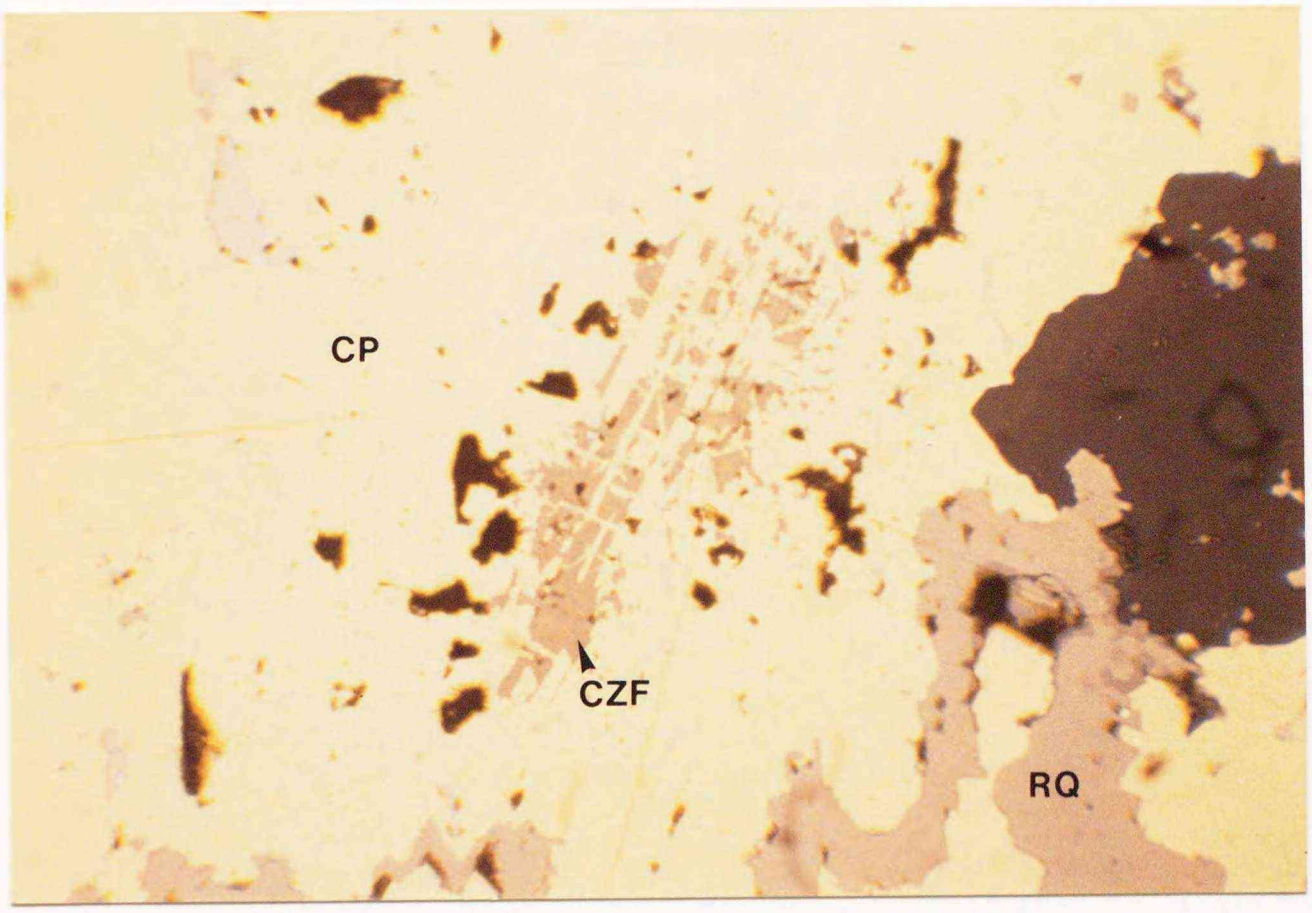

Figure 23. Photomicrograph of the dendritic Cu-Zn-Fe mineral (CZF) included within the anisotropic chalcopyrite (CP) in a chalcopyrite-rich sample of the substage B from -550 mL of the Soya vein (point 3 in Figure 1c).

Width of the pictured area is 0.2 mm.

RQ: aggregate of roquesite, the Zn-In mineral, kesterite, and the solid solutions between them.

4-3. Co-Ni-containing Sulfides

Arsenopyrite is one of main components of the substage B. It typically occurs as euhedral crystals grown over pyrrhotite of the substage A (Figure 24). Thus, the substage boundary between A and B is put at the beginning of arsenopyrite deposition, because detailed microscopic observations indicate that deposition of the rare elements which characterize the polymetallic mineralization at Toyoha started with the initial crystallization of arsenopyrite (Ohta, 1980). Though pyrrhotite is mostly replaced by marcasite and/or pyrite, microscopic observations reveal that arsenopyrite overgrew directly on pyrrhotite before the replacement. In some cases, pyrrhotite was almost completely eroded out after the overgrowth of arsenopyrite, and formed cavities which have been filled with other minerals, such as sphalerite (Ohta, 1980). Cobalt and nickel are detected in the cobaltite-arsenopyrite solid solution, which occurs as intergrowth bands within arsenopyrite (Table 13, Figure 25), and rarely as homogeneous minute crystals included in chalcopyrite or sphalerite. The cobaltite-arsenopyrite solid solution with Co/(Fe+Co) ratio between 0 and 0.76 seems to be complete (Figure 26) for samples from Toyoha. Minor amounts of nickel and antimony are also detected in this solid solution. Nickel is concentrated in the high-cobalt bands, and antimony in the low-cobalt bands (Figure 25, Figure 28). Thus, two types of compositional zonings are recognized in the cobaltite-arsenopyrite solid solution from Toyoha. One is attributed to the substitution of cobalt or nickel for iron (Figure 25), and another is due to the mutual substitutions among sulfur, arsenic and antimony (Figure 27, Figure 29, Figure 30). There appears to be no correlation between the amount of antimony and the

As/As+Sb+S ratio in arsenopyrite from Toyoha (Figure 31).

The arsenic-containing pyrite is generally accompanied by the cobaltite-arsenopyrite solid solution, and exhibits concentric growth bands which are attributed to a substitution of arsenic for sulfur (Figure 27, Table 13). This indicates that arsenic exists as FeAsS molecule in pyrite, or the arsenic-containing pyrite is a pyrite-arsenopyrite solid solution in chemical term. Observed maximum concentration of arsenic in pyrite is about 7 weight percent. This value corresponds to 12 mole percent of arsenopyrite in the solid solution. Minor amounts of cobalt and nickel also exist in the arsenic-containing pyrite (Table 13). These minor elements may be the cause of weak anisotropism commonly observed on pyrite from the later veins.

All observed As/(As+Sb) ratios in the Fe-Co-Ni-As-Sb sulfides in Toyoha are higher than 0.96. Co/(Co+Ni) atomic ratios in the minerals which contain more than 0.2 weight percent of Co+Ni are higher than 0.82. This indicates that the ratio in the whole ore of Toyoha may be more than 0.8. The distribution and occurrence mode of these minerals suggest that the cobalt-nickel mineralization is related to the tin-indium mineralization of the substage B in time and space. Pyrrhotite grains of the substage A in several samples are checked for cobalt and nickel contents by means of EPMA. The result indicates that concentrations of these elements in pyrrhotite are less than 0.05 weight percent. Hence, it is likely that Co and Ni are mostly in the cobaltite-arsenopyrite solid solution, and that the mineralization substage of these elements is essentially B only.

For estimation of formation temperatures of arsenopyrite based on the experimental data of Kretschmar and Scott (1976), cobalt, nickel and antimony are unfavorable elements. Therefore, the estimation was done for seven points whose chemical analysis data satisfy the following stipulation.

1: the totals are in the range of 100±1 wt%

2: antimony is less than 0.3 mol%

3: sum of cobalt and nickel is less than 0.3 mol%

Results obtained are listed in Table 14, and will be discussed in Chapter 5.

Table 12. Minerals of Fe-Co-As-S and Fe-Sb-S systems observed in Toyoha.

Fe-Co-As-S system			
pyrite	FeS_2	pyrrhotite	$Fe_{1-x}S$
native arsenic	As	arsenopyrite	FeAsS
löllingite	$FeAs_2$*1	cobaltite	CoAsS
cobaltite-arsenopyrite solid solution			
pyrite-arsenopyrite solid solution			

*1 Kase (personal communication)

Fe-Sb-S system			
native antimony	Sb*2	stibnite	Sb_2S_3
berthierite	$FeSb_2S_4$		

*2 Fujikawa et al. (1990)

Table 13. Representative EPMA analyses of the cobaltite-arsenopyrite solid solutions (co) and arsenic-containing pyrite (py) from Toyoha.

Abbreviations; SN:Shinano, SR:Sorachi, n.a.:not analyzed

Numerals after the vein name abbreviations indicate levels in meters below the mining office at Toyoha.

Loc.	Name	Fe	Cu	As	Sb	Co	Ni	S	total
SN350	co	12.51	n.a.	44.26	0.00	22.21	1.73	19.85	100.55
	Atom	0.36		0.96	0.00	0.61	0.05	1.01	3
SN450	co	10.96	n.a.	45.03	0.08	21.08	2.51	19.65	99.31
	Atom	0.33		1.00	0.00	0.59	0.07	1.01	3
SN450	co	12.38	0.24	46.75	0.10	18.25	3.16	19.23	100.10
	Atom	0.37	0.01	1.03	0.00	0.51	0.09	0.99	3
SN450	co	15.37	0.23	46.99	0.09	17.61	0.84	19.19	100.31
	Atom	0.45	0.01	1.03	0.00	0.49	0.02	0.99	3
SR500	co	21.02	n.a.	45.70	0.11	11.33	2.46	18.80	99.42
	Atom	0.62		1.01	0.00	0.32	0.07	0.97	3
SR500	co	26.04	n.a.	44.90	0.00	8.52	0.22	19.92	99.60
	Atom	0.76		0.98	0.00	0.24	0.01	1.02	3
SN450	co	30.44	n.a.	47.57	1.24	2.09	0.15	18.60	100.08
	Atom	0.90		1.05	0.02	0.06	0.00	0.96	3
SN450	co	33.18	n.a.	42.75	2.94	0.11	0.01	20.89	99.89
	Atom	0.97		0.93	0.04	0.00	0.00	1.06	3
SN450	co*	32.75	n.a.	47.84	1.41	0.09	0.00	17.37	99.46
	Atom	0.99		1.08	0.02	0.00	0.00	0.91	3
SR500	co	35.40	n.a.	44.09	0.64	0.04	0.07	20.36	100.61
	Atom	1.02		0.95	0.01	0.00	0.00	1.02	3
SR350	py	42.07	0.33	6.93	0.04	0.28	0.04	49.82	99.50
	Atom	0.94	0.01	0.12	0.00	0.01	0.00	1.93	3
SR350	py	43.71	0.48	5.10	0.09	0.27	0.01	50.43	100.10
	Atom	0.96	0.01	0.08	0.00	0.01	0.00	1.94	3
SN450	py	43.43	0.00	4.57	0.04	0.04	0.04	51.47	99.58
	Atom	0.95	0.00	0.07	0.00	0.00	0.00	1.97	3
SN450	py	45.03	0.00	4.42	0.03	0.02	0.04	50.93	100.48
	Atom	0.98	0.00	0.07	0.00	0.00	0.00	1.94	3
SN450	py	43.03	0.59	3.49	0.10	0.73	0.08	52.31	100.33
	Atom	0.94	0.01	0.06	0.00	0.01	0.00	1.98	3
SN450	py	42.74	0.15	2.60	0.06	1.87	0.15	52.45	100.03
	Atom	0.93	0.00	0.04	0.00	0.04	0.00	1.99	3
SN450	py	43.84	0.07	2.31	0.04	0.12	0.01	53.18	99.55
	Atom	0.95	0.00	0.04	0.00	0.00	0.00	2.01	3
SR350	py	44.74	0.14	1.28	0.07	0.11	0.05	53.38	99.78
	Atom	0.96	0.00	0.02	0.00	0.00	0.00	2.01	3
SN450	py	44.67	n.a.	0.67	0.01	0.04	0.05	54.25	99.69
	Atom	0.96		0.01	0.00	0.00	0.00	2.03	3
SN350	py	44.83	n.a.	0.43	0.00	0.06	0.03	54.63	99.98
	Atom	0.96		0.01	0.00	0.00	0.00	2.03	3

* data used in Figure 30

Table 14. EPMA analyses of arsenopyrite and its formation temperatures estimated from the data of Kretschmar and Scott (1976).

T1: Calculated temperature for sulfur fugacity at the upper limit of löllingite.

T2: Calculated temperature for sulfur fugacity at the pyrrhotite - pyrite boundary.

T3: Calculated temperature for sulfur fugacity at the arsenopyrite - pyrite+arsenic (T < 363°C), and arsenopyrite - pyrite+liquid (T is 363°C or higher) boundary.

Loc.	Fe	As	Sb	Co	Ni	S	Total	T1	T2	T3
SR500	34.61	44.70	0.00	0.08	0.11	20.03	99.52			
Mol%	33.61	32.35	0.00	0.07	0.10	33.87	100	356	450	461
SN450	33.05	44.75	0.27	0.15	0.03	21.08	99.34			
Mol%	31.96	32.25	0.12	0.14	0.03	35.51	100	350	443	457
SN450	33.23	44.46	0.29	0.08	0.08	21.45	99.59			
Mol%	31.94	31.86	0.13	0.08	0.07	35.93	100	329	418	434
SN450*	33.97	44.33	0.41	0.11	0.05	21.31	100.17			
Mol%	32.51	31.62	0.18	0.10	0.04	35.54	100	316	403	428
SR500	35.40	44.09	0.64	0.04	0.07	20.36	100.61			
Mol%	33.99	31.56	0.28	0.04	0.07	34.05	100	313	399	425
SN450*	35.68	42.16	0.36	0.11	0.01	22.61	100.93			
Mol%	33.42	29.44	0.16	0.10	0.01	36.89	100	198	264	319
SN450	33.25	41.01	0.44	0.22	0.10	24.49	99.51			
Mol%	31.08	28.58	0.19	0.19	0.09	39.87	100	151	210	270

* data used in Figure 30

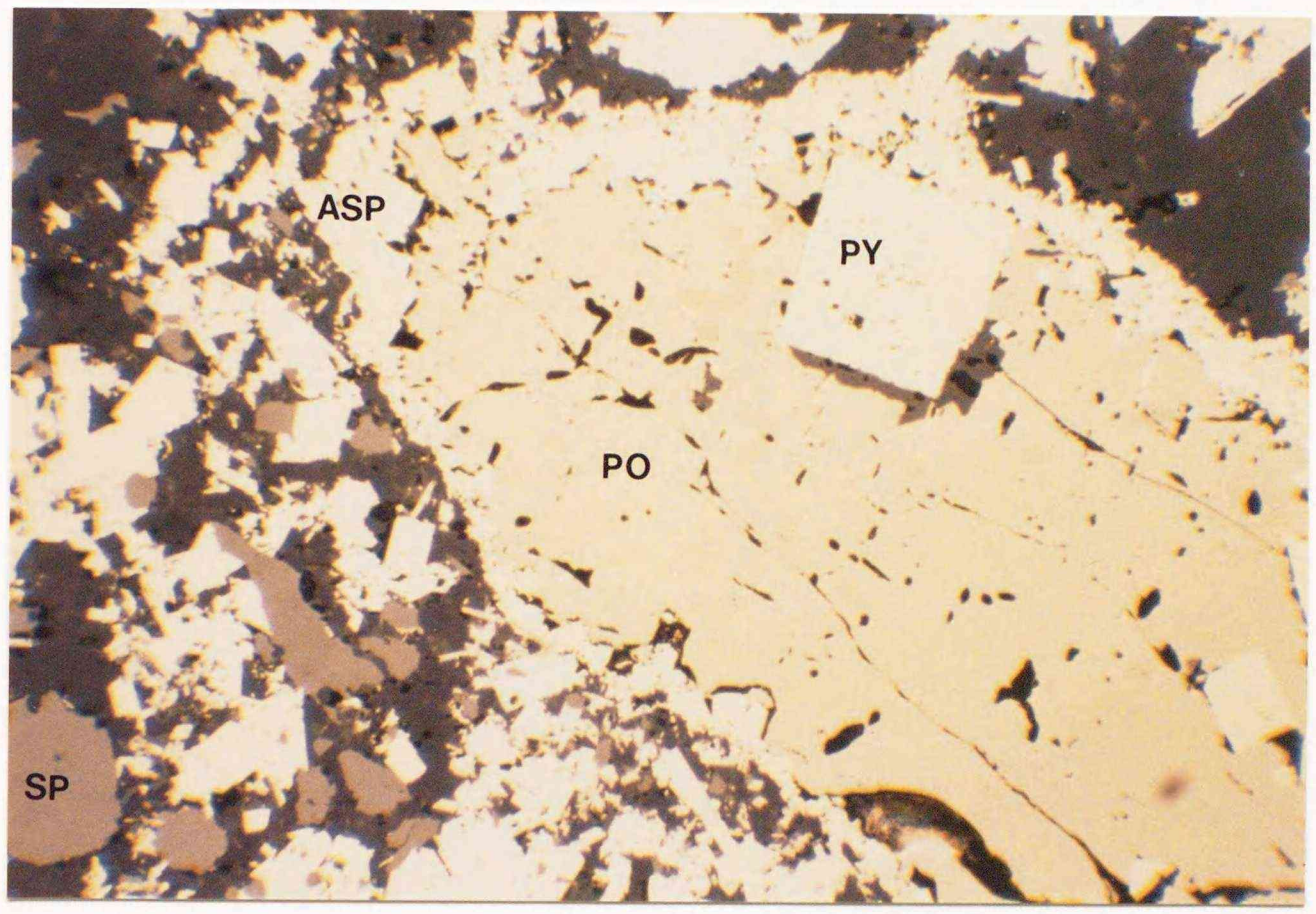

Figure 24. Photomicrograph of arsenopyrite (ASP; substage B) overgrew pyrrhotite (PO; substage A) in a black-sphalerite-rich sample from the Sorachi vein -400 mL (point 5 in Figure 1c).
Width of the pictured area is 0.6 mm. The pyrite cubes (PY) are replacement products of the substage B.
PY:pyrite (substage B), SP:sphalerite (substage B).

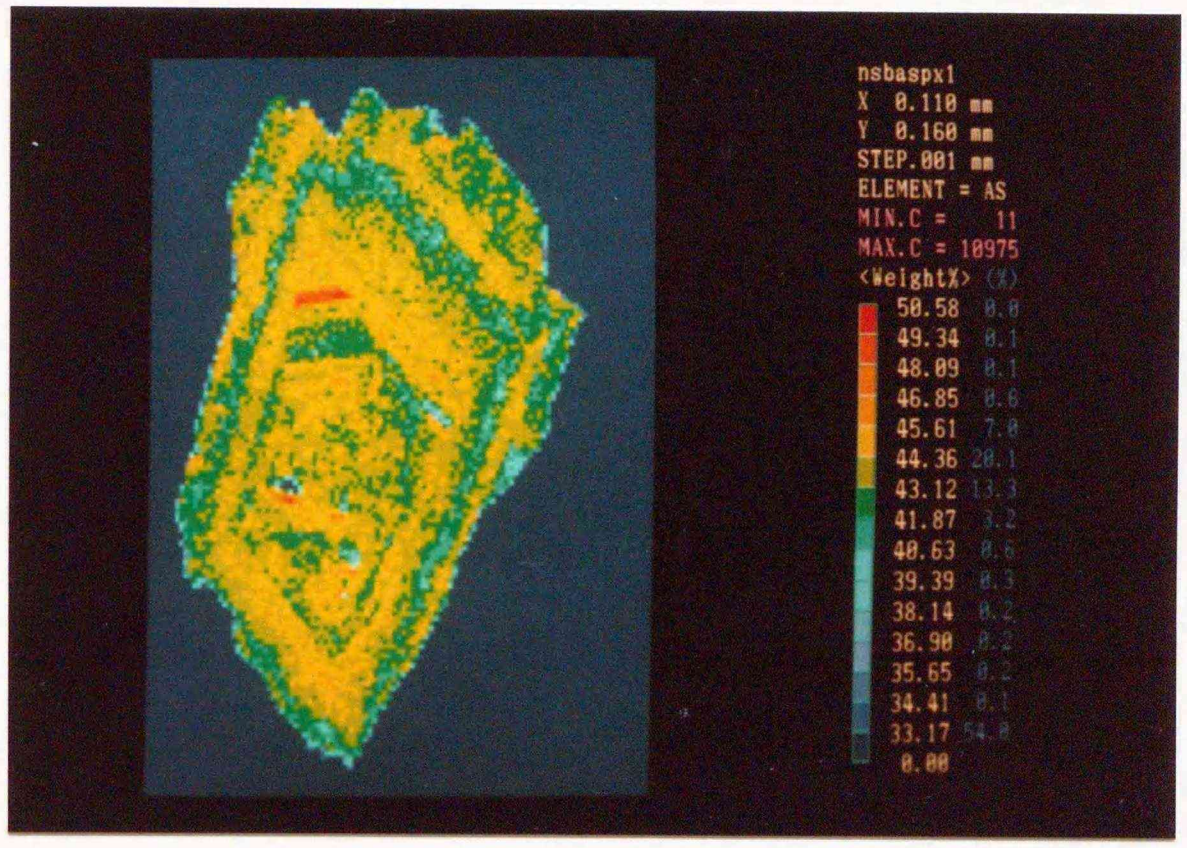

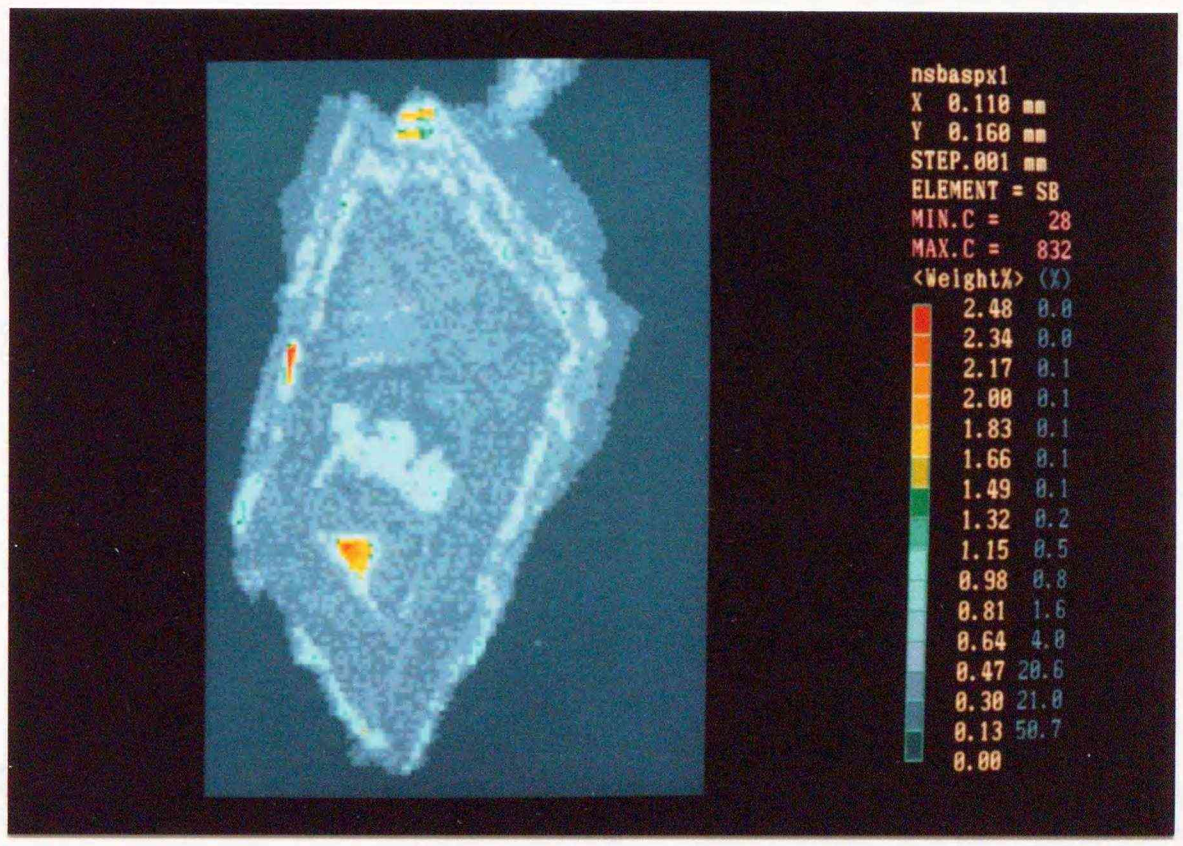

Figure 25a. Arsenic and antimony maps showing growth banding due to substitutions among sulfur, arsenic and antimony in an arsenopyrite single crystal intergrown by bands of the cobaltite-arsenopyrite solid solution in a chalcopyrite-pyrite-rich ore from the Shinano vein -450 mL (point 2 in Figure 1c).

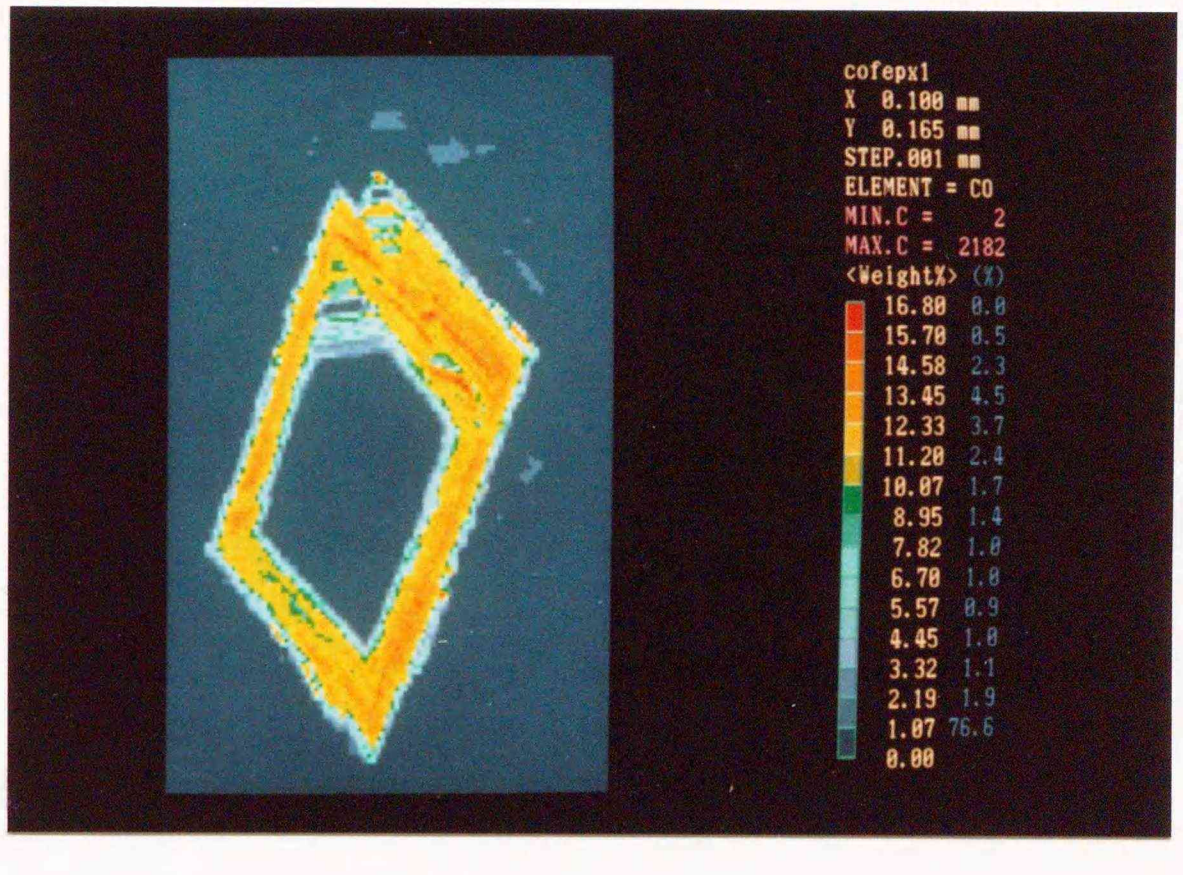

Figure 25b. Cobalt and nickel maps showing growth banding due to substitution of iron with cobalt and nickel in the cobaltite-arsenopyrite solid solution included in the same grain with that in Figure 25a. Note the positive correlation between the concentrations of cobalt and nickel.

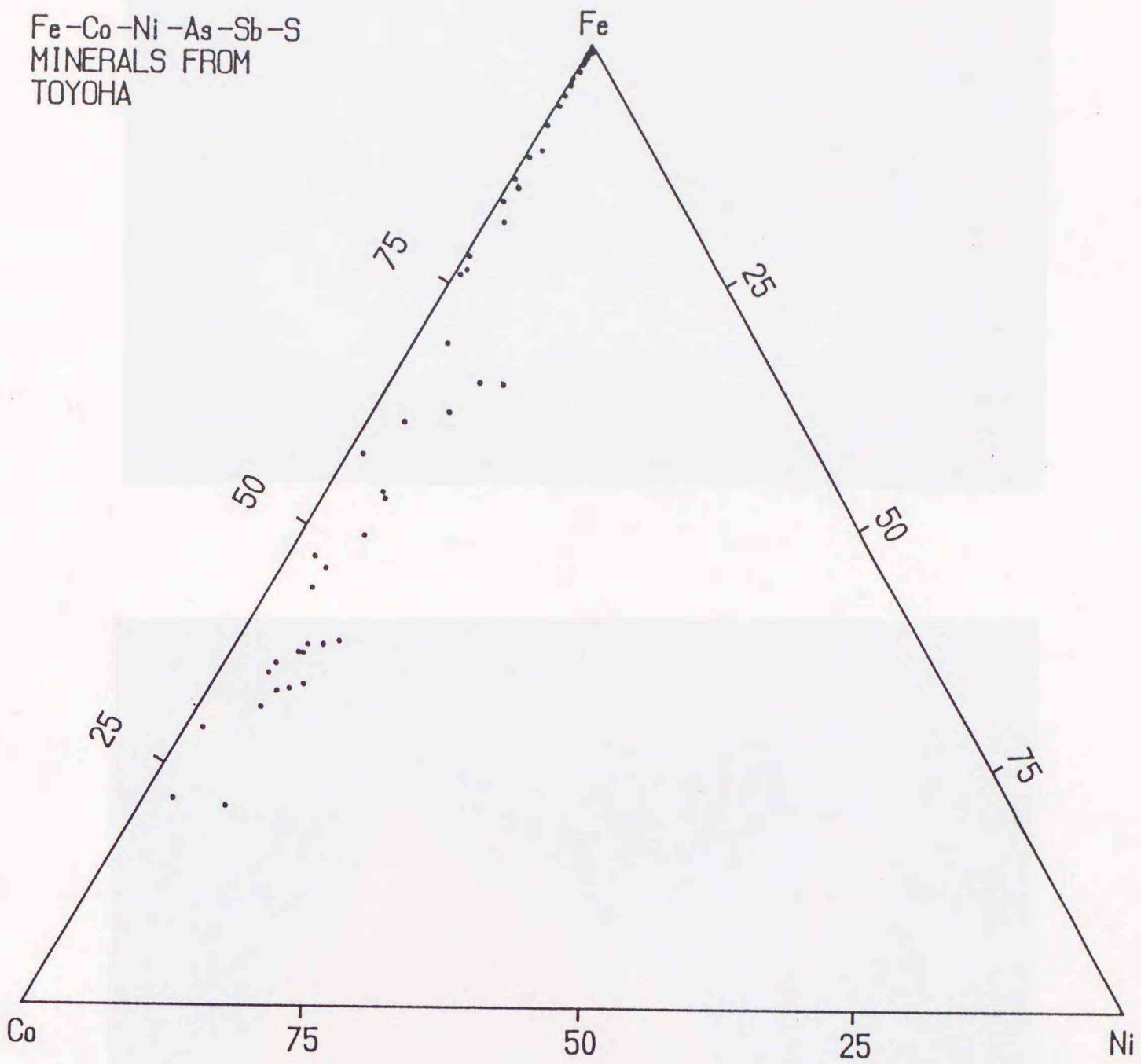

Figure 26. Fe-Co-Ni (mol) diagram of Fe-Co-Ni-As-Sb sulfides (the solid solutions between cobaltite and arsenopyrite, and between pyrite and arsenopyrite) from Toyoha.
All data of the pyrite-arsenopyrite solid solution are plotted in the vicinity of top (Fe) of the diagram.

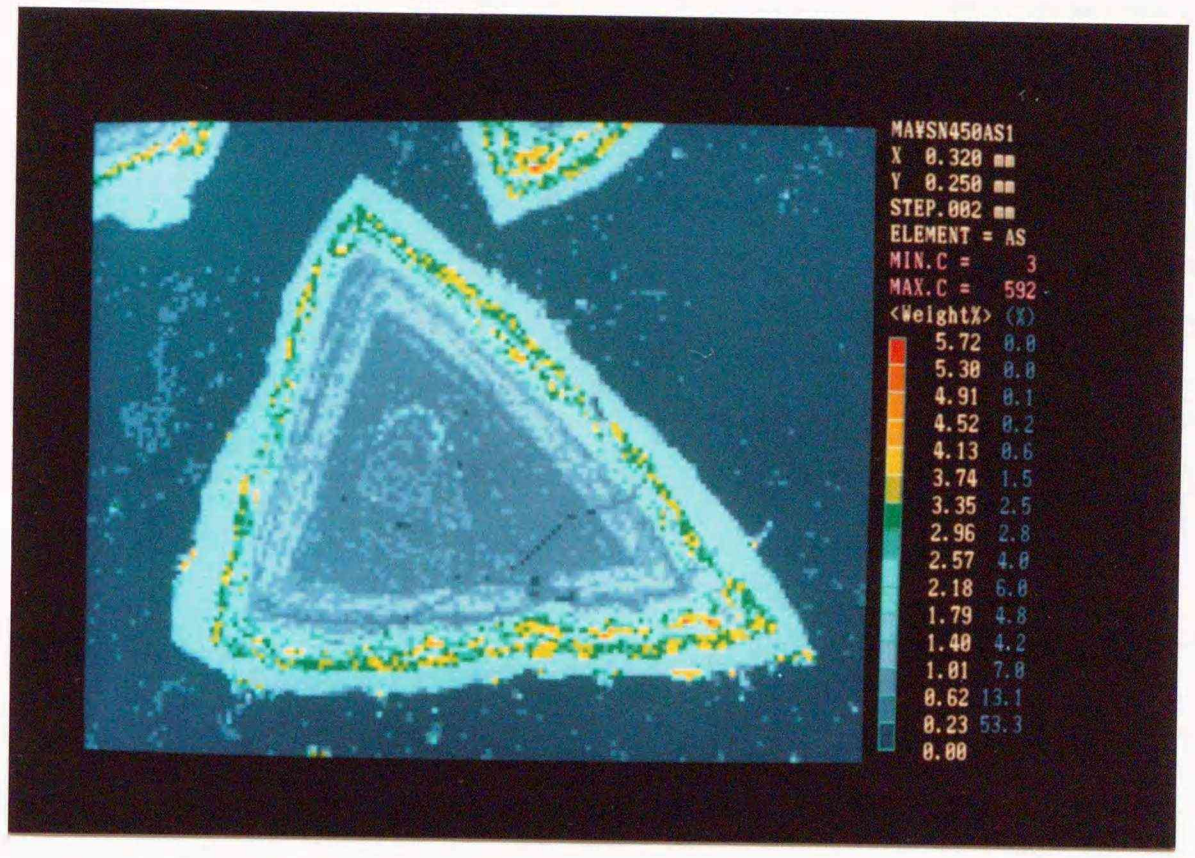

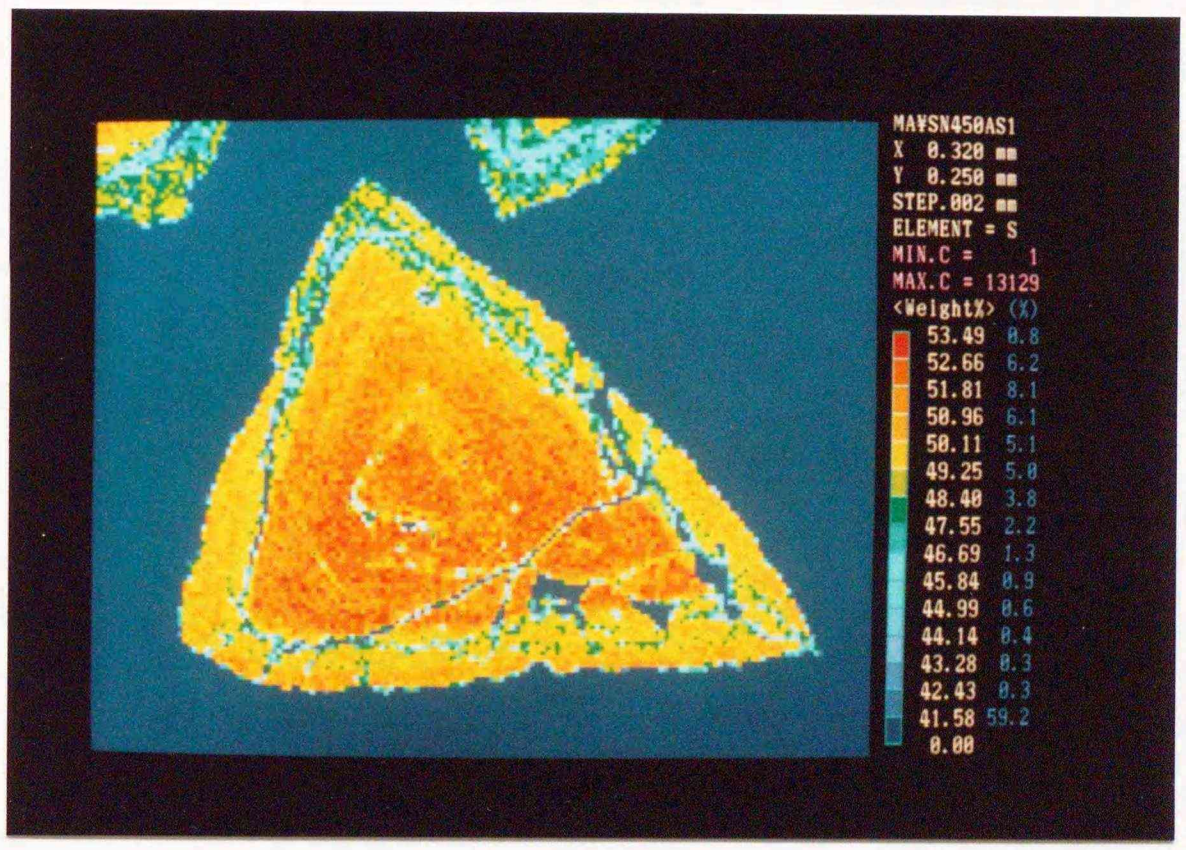

Figure 27. Arsenic and sulfur maps showing growth zoning of arsenic-containing pyrite (the pyrite-arsenopyrite solid solution) in a chalcopyrite-pyrite-rich ore from the Shinano vein -450 mL (point 2 in Figure 1c). All pyrite grains in the vicinity exhibit similar arsenic-rich margins.

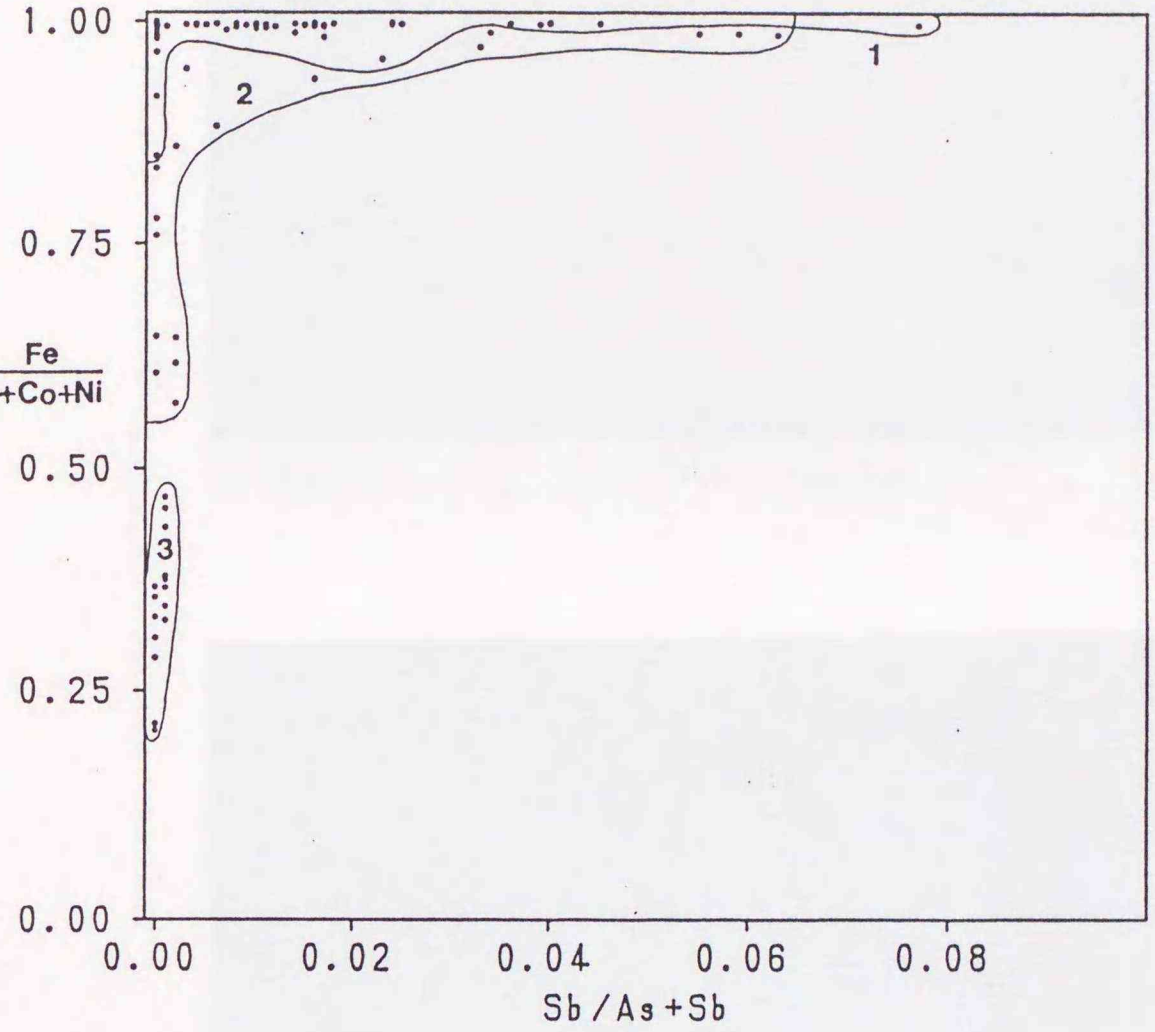

Figure 28. Sb/As+Sb vs. Fe/Fe+Co+Ni (mol) diagram of Fe-Co-Ni-As-Sb sulfides from Toyoha.
The cobaltite-arsenopyrite solid solution with iron mol fraction less than 0.5 is expressed as cobaltite on the diagram.

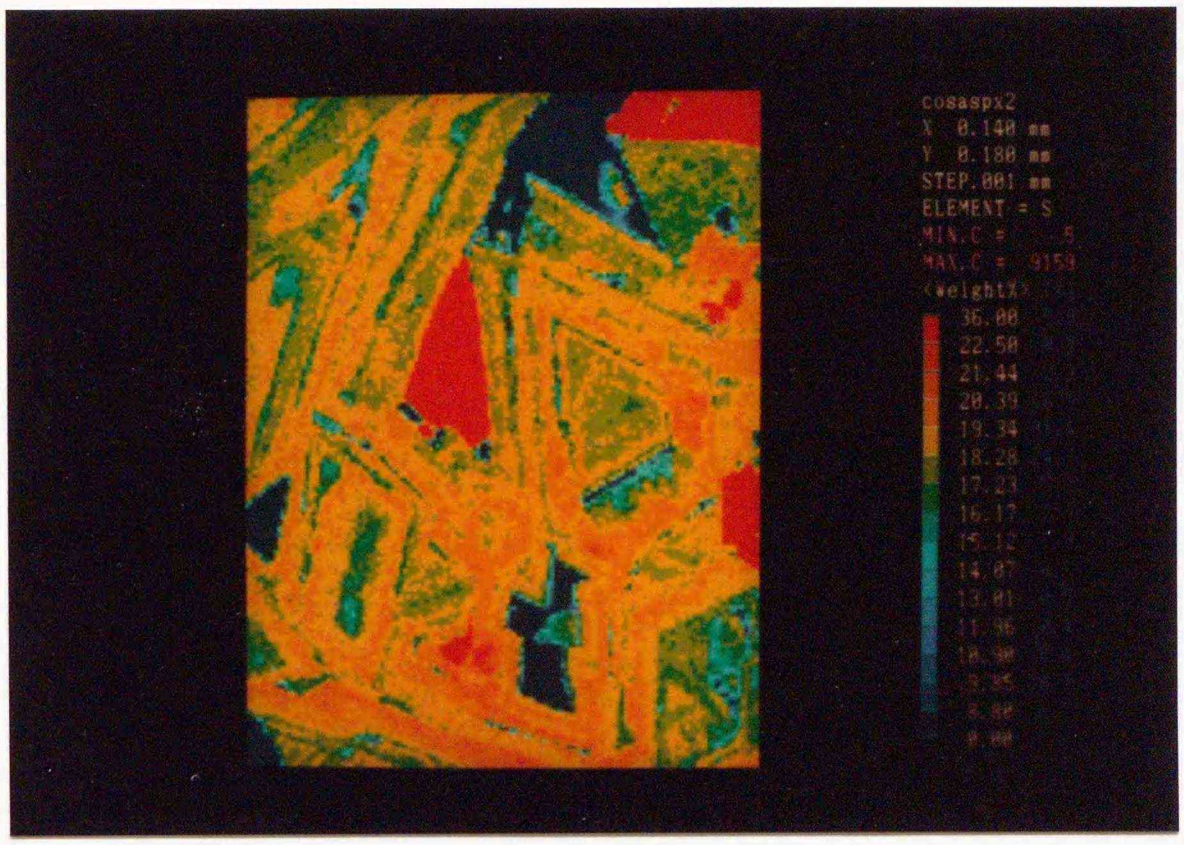

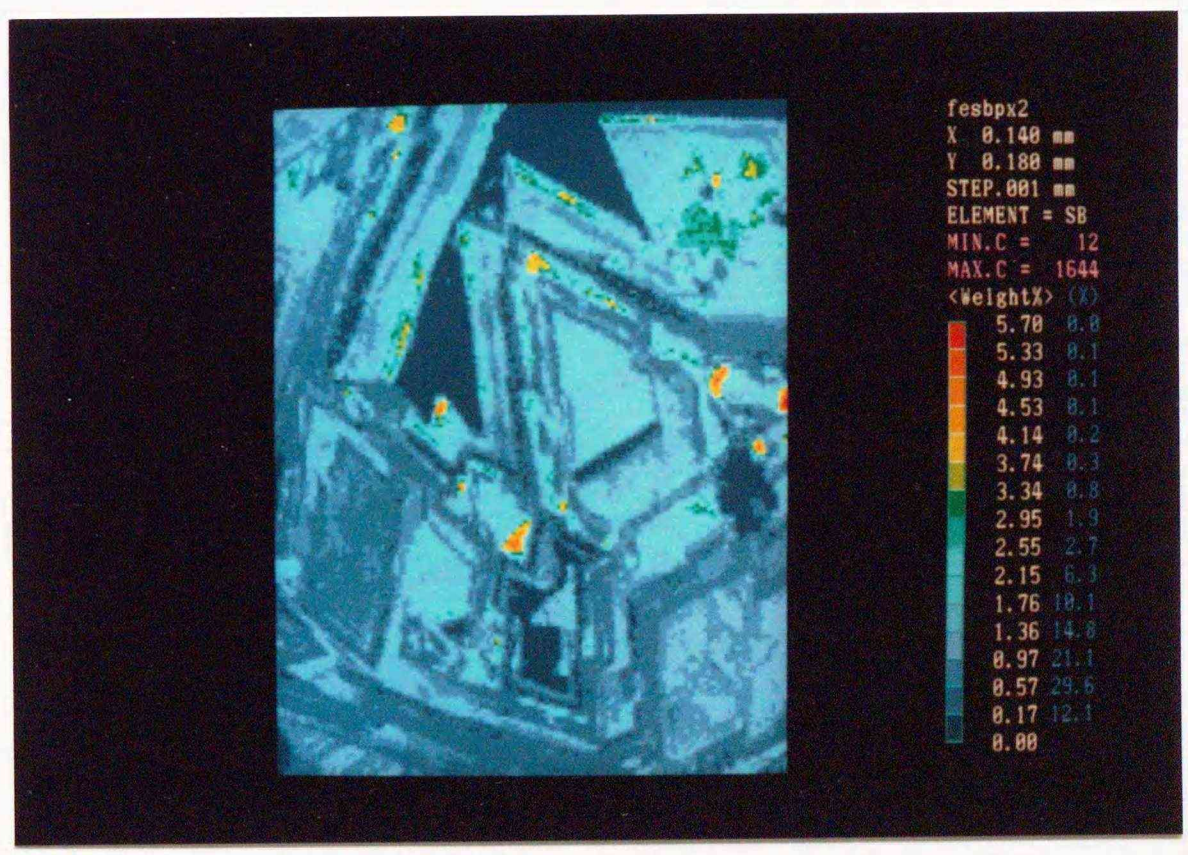

Figure 29. Sulfur and antimony maps showing growth zoning due to substitutions among S, As and Sb in arsenopyrite in the same sample as shown in Figure 25.

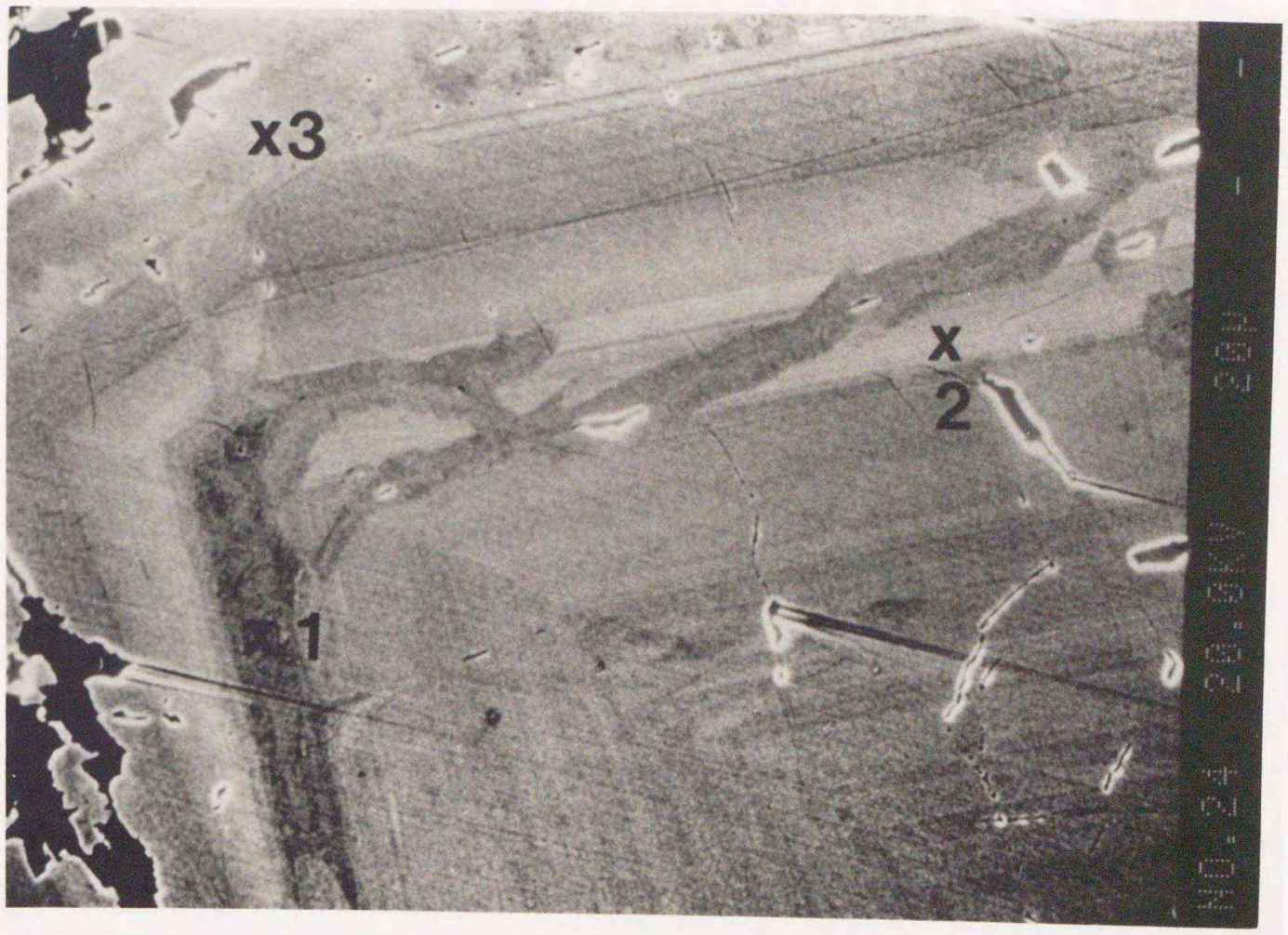

Figure 30. BSE image showing growth zoning and later modification of composition along a crack (dark band cutting the rhythmic growth bands) of arsenopyrite in a brown-sphalerite-rich sample from the Shinano vein -450 mL (point 2 in Figure 1c).

The zoning within this grain is attributed to substitutions among S, As and Sb. The brighter zones contain more heavy elements (As, Sb) than the darker.

Weight percents of S, As and Sb at points 1, 2 and 3 are as follows:

	S	As	Sb	
1:	22.61	42.16	0.36	(Table 14)
2:	17.37	47.84	1.41	(Table 13)
3:	21.31	44.33	0.41	(Table 14)

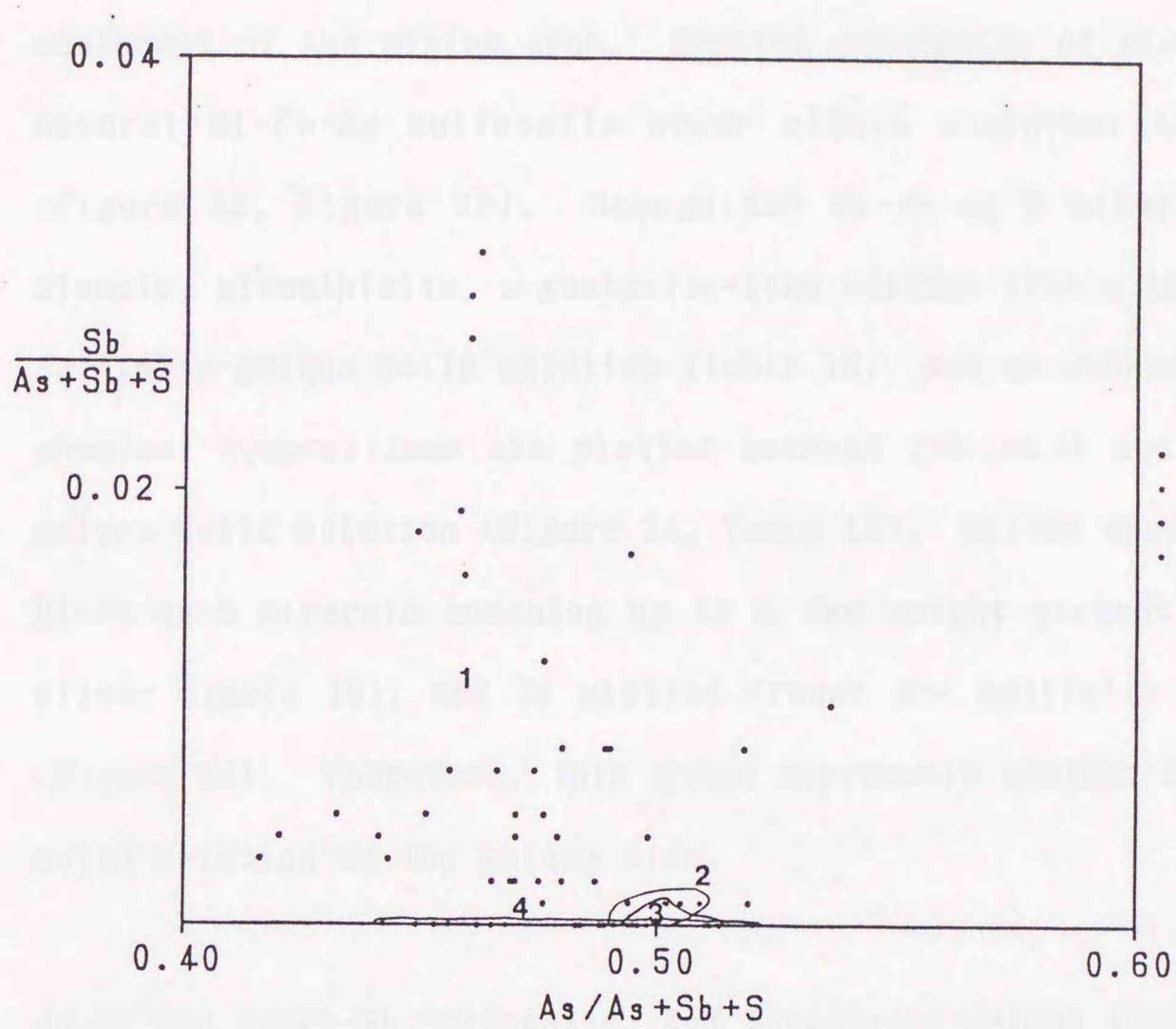

Figure 31. As/As+Sb+S vs. Sb/As+Sb+S (mol) diagram of the cobaltite-arsenopyrite solid solution from Toyoha.

4-4. Sulfosalts

Bi-Pb-Ag Sulfosalts (Substage B):

Bismuth is one of the common elements in copper-rich ore of the substage B from deep levels of the later veins distributed in the southeast of the mining area. Complex aggregates of minute crystals of several Bi-Pb-Ag sulfosalts occur within chalcopyrite in most case (Figure 32, Figure 33). Recognized Bi-Pb-Ag-S minerals are native bismuth, bismuthinite, a gustavite-like sulfide (Table 15), matildite, a matildite-galena solid solution (Table 16), and an unknown sulfide whose chemical compositions are plotted between gustavite and the matildite-galena solid solution (Figure 34, Table 15). Galena associated with the Bi-Pb-Ag-S minerals contains up to a few weight percent of bismuth and silver (Table 16), and is plotted around the matildite-galena tie-line (Figure 34). Therefore, this phase represents another matildite-galena solid solution on the galena side.

Ag-Sb and Ag-Pb-Sb Sulfosalts, and Associated Galena (Substage C):

Many kinds of silver sulfosalts are observed in the later veins. This is in contrast with the occurrence of argentite in the earlier veins. Galena of the substage C frequently includes grains of the silver sulfosalts and silver-rich tetrahedrite or freibergite*. Large

---

* In this report, the term "freibergite" is used for tetrahedrite with Ag/Ag+Cu atomic ratio higher than 0.25 when its chemical composition is known. The ratio approximately corresponds to 15 wt% Ag, and may be reasonable to define the term (see Figure 37). When composition is not known, the term is used just for "silver-rich tetrahedrite".

irregular-shaped grains are possibly products of replacement or intergrowth, but small euhedral or subhedral grains appear to have exsolved from galena after precipitation. Wherever these grains are observed, galena apparently contains a few weight percent of silver and antimony. Careful observation on back-scattered electron images, however, reveals that the high concentrations are due to minute grains of the silver sulfosalts (Figure 35), and that actual maximum concentration of silver in galena of the substage C is around 0.25 weight percent as is shown in Table 17. Although the concentrations are too low to make accurate comparison, Ag/Sb+As atomic ratios are approximately unity, and bismuth is not detected in galena of the substage C (Table 17). This implies a substitution of Sb+Ag or As+Ag for Pb+Pb in galena.

Pb-Sb Sulfosalts (Substage D or E):

In the later veins, lead-antimony sulfosalts postdate the silver sulfosalts, and always occur in cracks of galena or as replacement products after galena and the silver sulfosalts. Therefore the lead-antimony sulfosalts are obviously younger than the latter two. Though the relation of the lead-antimony sulfosalts to other minerals from Toyoha is not known, they may belong to the substage D or E as is discussed later in the text. Table 17 shows representative analyses of some of the lead-antimony sulfosalts.

Table 15. Representative EPMA analyses of native bismuth (nb), bismuthinite (bi), a gustavite-like sulfide (gs), and an unknown sulfide of Bi-Ag-Pb-S system (uk) from Toyoha.

Abbreviations; Atom:atomic composition, SN:Shinano, SR:Sorachi, JTU2:Drill JTU2 (642 m from the start), n.a.:not analyzed

Numerals after the vein name abbreviations indicate levels in meters below the mining office at Toyoha.

Loc.	Name	Cu	Ag	Pb	Bi	As	Sb	S	Se	Total
JTU2	nb	0.36	0.06	2.65	96.19	0.16	0.34	0.02	0.14	99.91
Atom		1.16	0.10	2.63	94.62	0.45	0.58	0.11	0.36	100
JTU2	bi	0.30	0.03	1.83	79.32	0.12	0.31	18.17	0.26	100.34
Atom		0.49	0.03	0.91	39.23	0.16	0.27	58.56	0.34	100
JTU2	bi	0.31	0.04	1.58	78.99	0.15	0.48	18.30	0.25	100.09
Atom		0.50	0.03	0.79	38.94	0.20	0.41	58.80	0.33	100
JTU2	bi	0.34	0.05	1.67	79.89	0.14	0.37	18.07	0.29	100.81
Atom		0.55	0.05	0.83	39.48	0.19	0.31	58.22	0.38	100
JTU2	bi	0.37	0.00	1.89	79.26	0.16	0.38	17.77	0.35	100.18
Atom		0.61	0.00	0.95	39.58	0.22	0.33	57.86	0.46	100
JTU2	bi	0.38	0.00	1.84	79.73	0.13	0.44	18.11	0.36	100.99
Atom		0.62	0.00	0.92	39.28	0.18	0.37	58.17	0.47	100
JTU2	bi	0.41	0.05	2.10	78.94	0.17	0.42	18.07	0.41	100.56
Atom		0.66	0.04	1.04	38.97	0.23	0.36	58.15	0.54	100
SN300	bi	2.76	0.08	3.78	73.88	n.a.	3.00	17.94	0.00	101.43
Atom		4.33	0.08	1.83	35.33		2.46	55.96	0.00	100
SR500	uk	0.17	16.88	23.73	40.56	n.a.	1.63	15.87	n.a.	98.84
Atom		0.27	16.03	11.73	19.89		1.37	50.70		100
SR500	uk	0.10	16.18	21.00	45.19	n.a.	1.50	16.29	n.a.	100.26
Atom		0.17	15.16	10.24	21.85		1.24	51.33		100
SR500	uk	0.51	13.92	25.53	41.76	n.a.	1.60	16.10	n.a.	99.41
Atom		0.82	13.23	12.63	20.49		1.35	51.48		100
SN450	uk	0.51	10.65	28.13	43.58	n.a.	0.99	16.49	n.a.	100.35
Atom		0.83	10.14	13.95	21.42		0.83	52.83		100
SN450	uk	0.24	13.88	35.62	33.64	n.a.	0.40	15.65	n.a.	99.43
Atom		0.40	13.45	17.97	16.83		0.34	51.02		100
SN450	gs	0.54	8.38	20.94	51.72	n.a.	2.16	16.10	n.a.	99.83
Atom		0.89	8.14	10.59	25.93		1.86	52.60		100
SN450	gs	0.44	8.34	20.73	52.71	n.a.	1.79	15.63	n.a.	99.63
Atom		0.74	8.23	10.65	26.86		1.56	51.94		100
SR500	gs	1.23	10.00	19.36	51.01	n.a.	2.34	16.48	n.a.	100.42
Atom		1.97	9.43	9.51	24.83		1.96	52.30		100

Table 16. Representative EPMA analyses of the matildite-galena ss. (ma) and bismuth-containing galena (gn) from Toyoha.

Abbreviations; Atom:atomic composition, SN:Shinano, SR:Sorachi, JTU1:Drill JTU1 (541 m from the start)

Numerals after the vein name abbreviations indicate levels in meters below the mining office at Toyoha.

Loc.	Name	Cu	Ag	Pb	Bi	As	Sb	S	Total
JTU1	ma	0.28	26.56	0.31	56.84	0.17	0.07	16.08	100.30
Atom		0.42	23.95	0.15	26.45	0.23	0.05	48.76	100
JTU1	ma	0.14	26.20	0.82	55.64	0.19	0.00	16.22	99.24
Atom		0.22	23.72	0.39	26.00	0.25	0.00	49.41	100
JTU1	ma	0.10	26.22	1.06	55.30	0.11	0.08	16.14	99.01
Atom		0.15	23.83	0.50	25.94	0.14	0.07	49.37	100
JTU1	ma	0.32	25.44	2.90	53.82	0.05	0.11	16.05	98.69
Atom		0.50	23.25	1.38	25.38	0.07	0.09	49.34	100
SR500	ma	0.95	26.60	3.83	53.01	0.00	0.35	15.99	100.72
Atom		1.44	23.82	1.78	24.50	0.00	0.28	48.19	100
SR500	ma	0.17	17.70	11.30	53.18	0.00	1.55	16.91	100.81
Atom		0.26	16.15	5.37	25.05	0.00	1.25	51.92	100
JTU1	ma	0.30	22.80	11.86	48.32	0.01	0.13	15.74	99.16
Atom		0.48	21.21	5.74	23.20	0.01	0.11	49.25	100
SR500	ma	0.57	23.84	12.76	46.99	0.00	0.72	16.31	101.19
Atom		0.87	21.44	5.97	21.81	0.00	0.57	49.34	100
JTU1	ma	0.33	22.15	15.79	45.43	0.03	0.14	15.85	99.72
Atom		0.52	20.54	7.62	21.74	0.04	0.12	49.43	100
SR400	ma	0.27	21.49	16.94	44.40	0.00	0.65	15.80	99.56
Atom		0.43	20.00	8.21	21.33	0.00	0.54	49.49	100
JTU1	ma	0.11	19.50	26.21	38.73	0.15	0.12	15.38	100.21
Atom		0.17	18.50	12.95	18.97	0.21	0.10	49.10	100
JTU1	gn	0.15	1.38	81.97	2.80	0.05	0.14	13.56	100.04
Atom		0.02	0.12	3.73	0.13	0.01	0.01	3.99	8
JTU1	gn	0.07	1.93	81.37	2.63	0.09	0.25	13.51	99.85
Atom		0.01	0.17	3.70	0.12	0.01	0.02	3.97	8
SN350	gn	0.17	0.09	86.81	0.34	0.00	0.09	13.19	100.70
Atom		0.03	0.01	4.01	0.02	0.00	0.01	3.94	8
SR500	gn	0.11	0.16	85.86	0.27	0.00	0.42	13.10	99.93
Atom		0.02	0.01	3.99	0.01	0.00	0.03	3.93	8
SN350	gn	0.06	0.07	86.82	0.18	0.00	0.13	12.92	100.18
Atom		0.01	0.01	4.06	0.01	0.00	0.01	3.91	8

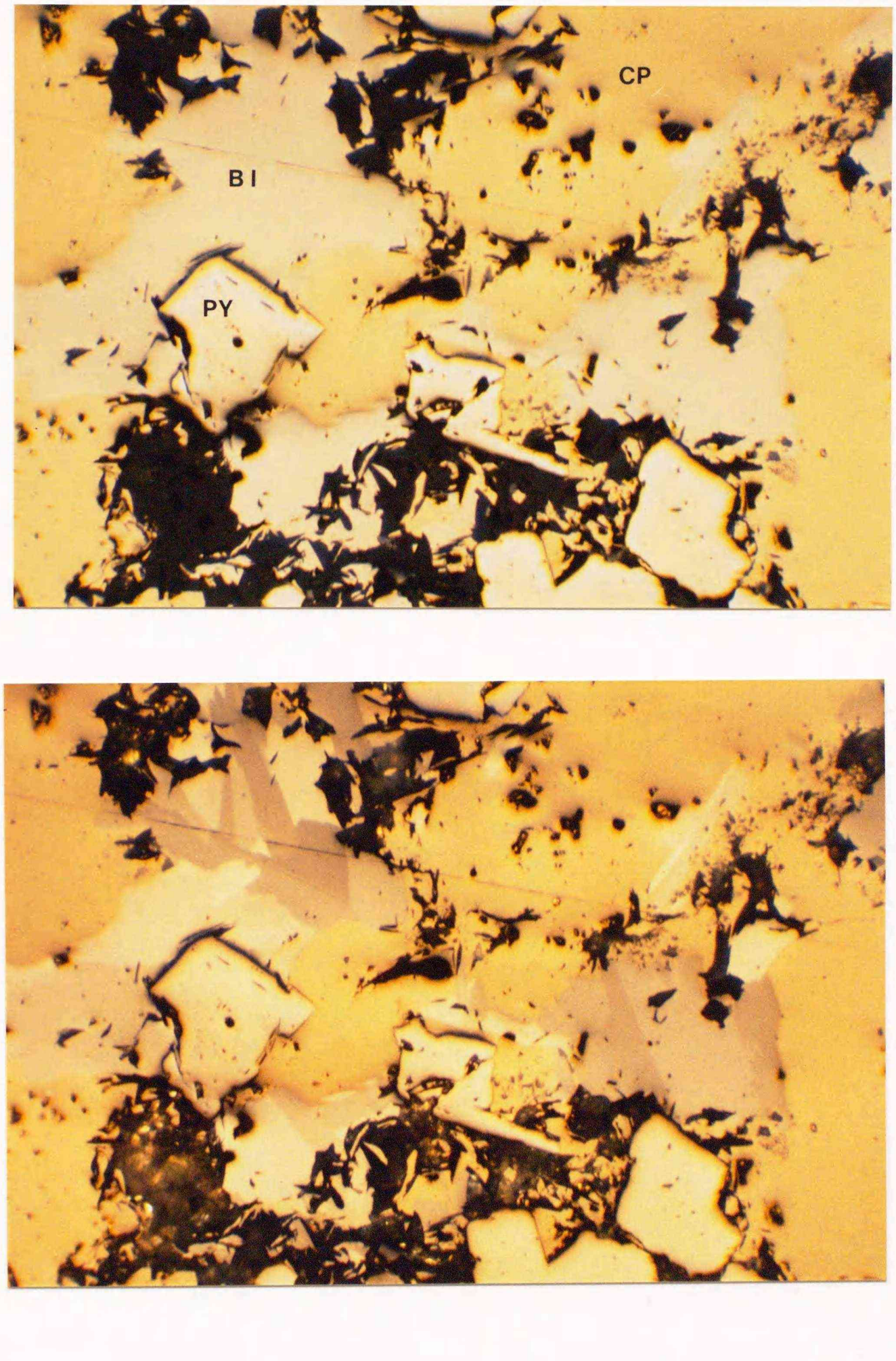

Figure 32. Photomicrograph showing typical occurrence of Bi-Pb-Ag sulfosalts (BI) within chalcopyrite (CP) in a chalcopyrite-rich sample from the Sorachi vein -500 mL (point 4 in Figure 1c).
Major part of the bismuth minerals shown on the pictures is the matildite-galena solid solution. The upper picture is under plane polarized light, and the lower is under crossed polars.
PY:pyrite. Width of the pictured area is 0.6 mm.

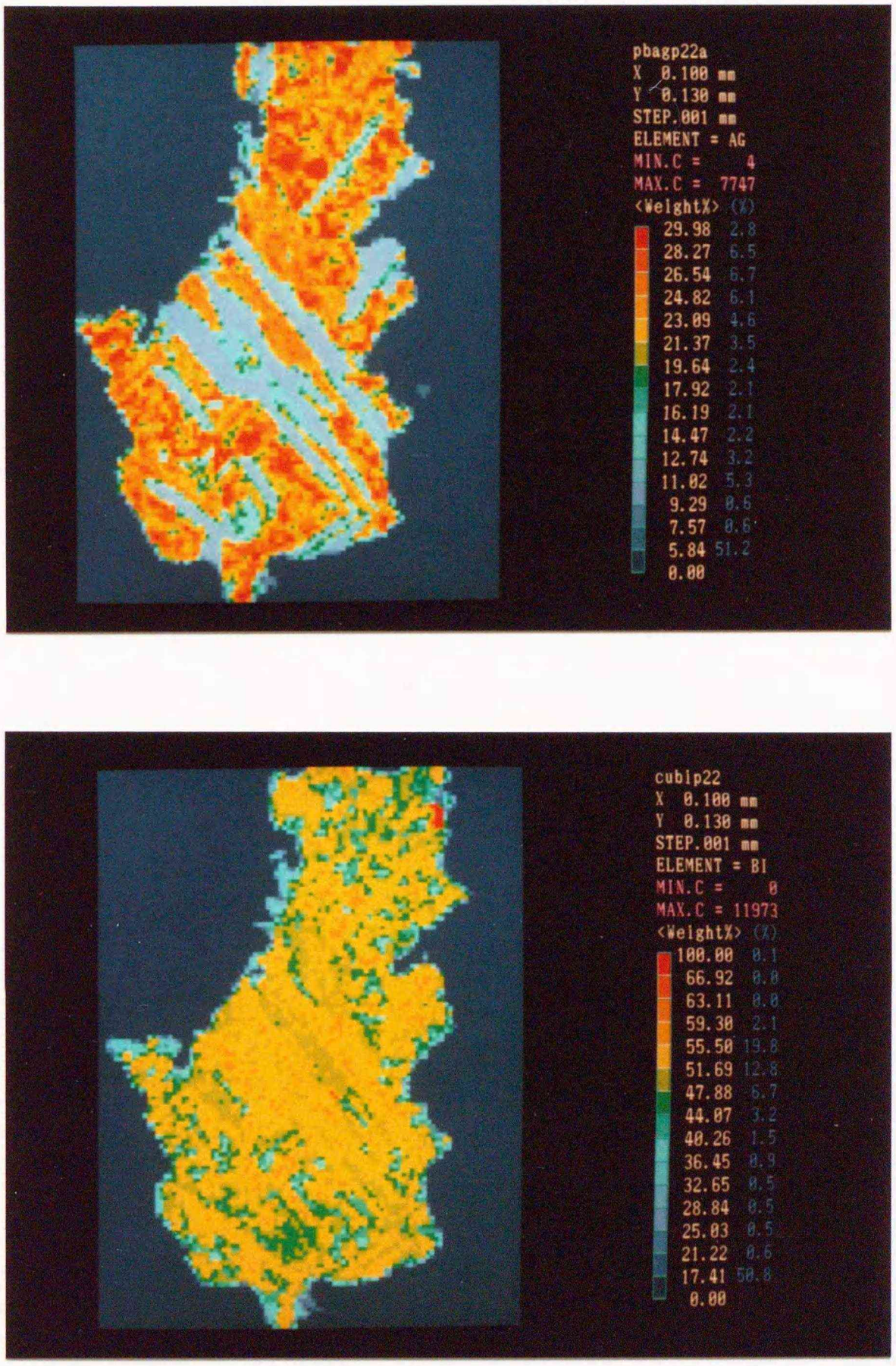

Figure 33. Silver and bismuth maps showing intergrowth of bismuth minerals in a chalcopyrite-rich sample from the Sorachi vein -500 mL (point 4 in Figure 1c).

The light blue parts on the Ag map correspond to the gustavite solid solution, and the yellow to red parts to the matildite-galena solid solution. A small piece of native bismuth is observed at the upper right margin of the grain (red point seen in the Bi map).

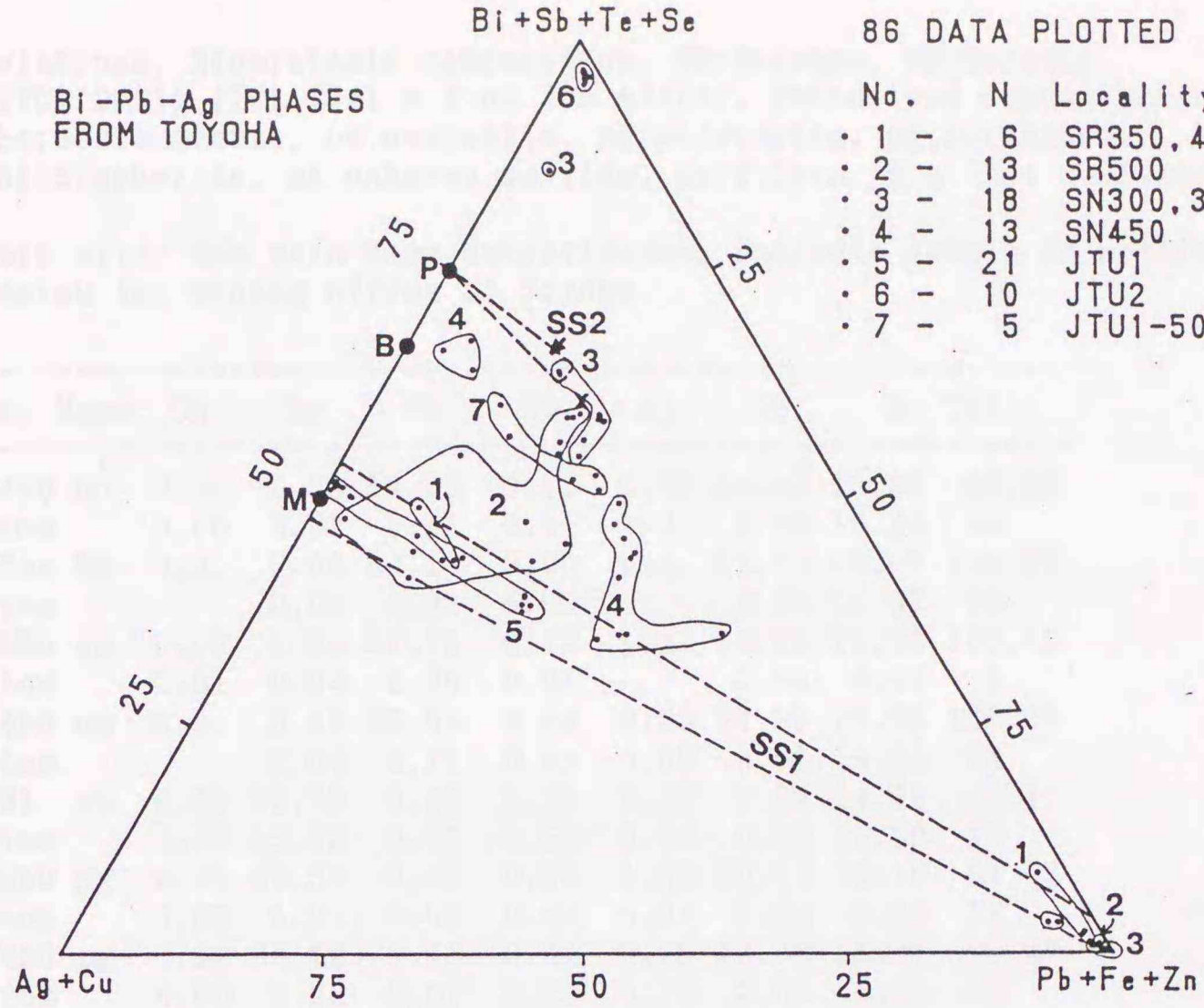

Figure 34. Mol composition diagram of Bi-Pb-Ag sulfides from Toyoha. The area delimited by broken line, and marked with P and SS2 represents the pavonite solid solution, B represents the benjaminite solid solution, and the area delimited by broken line and marked with SS1 is the matildite-galena solid solution at 500°C (Chang et al., 1988). M is the ideal composition of matildite. X marks $AgPbBi_3S_6$ composition which may be an end member of the gustavite solid solution (Karup-Møller, 1970). The amounts of Sb, Te and Se compared to Bi, of Fe and Zn compared to Pb are small and negligible on the diagram. Also, Ag predominates over Cu in the Bi-Ag-Pb sulfides.

SRxxx: -xxx mL of the Sorachi vein, SNxxx: the Shinano vein.

Table 17. Representative EPMA analyses of Ag-Sb, Ag-Pb-Sb and Pb-Sb sulfosalts, and associated galena from Toyoha.

Abbreviations; Atom:atomic composition, SN:Shinano, SR:Sorachi, JTU1:Drill JTU1 (541 m from the start), PbCon:lead concentration, bo:boulangerite, ow:owyheeite, pb:polybasite, pg:pyrargyrite, di:diaphorite, uk:unknown sulfide, gn:galena, n.a.:not analyzed

Numerals after the vein name abbreviations indicate levels in meters below the mining office at Toyoha.

Loc.	Name	Cu	Ag	Pb	Bi	As	Sb	S	Total
SN450	bo	0.00	0.38	56.53	0.11	0.31	24.43	16.85	98.62
Atom		0.00	0.07	5.42	0.01	0.08	3.98	10.44	20
PbCon	bo	n.a.	0.00	54.19	0.00	n.a.	27.73	19.07	100.99
Atom			0.00	4.82	0.00		4.20	10.97	20
SR350	uk	0.09	0.54	67.72	0.12	n.a.	14.28	17.55	100.28
Atom		0.01	0.04	2.95	0.01		1.06	4.93	9
SN450	ow	n.a.	8.90	39.64	0.24	0.28	32.21	18.98	100.25
Atom			2.04	4.72	0.03	0.09	6.52	14.60	28
JTU1	pb	9.61	62.75	0.17	5.33	3.07	3.04	14.14	98.11
Atom		3.46	13.33	0.02	0.58	0.94	0.57	10.10	29
SN450	pg	0.00	60.32	0.02	0.50	1.63	20.14	16.40	99.02
Atom		0.00	6.21	0.00	0.03	0.24	1.84	5.68	14
SN450	pg	0.00	60.52	0.15	0.00	0.45	22.33	16.02	99.47
Atom		0.00	6.28	0.01	0.00	0.07	2.05	5.59	14
SN450	pg	0.00	60.63	0.27	0.31	1.33	21.79	15.78	100.11
Atom		0.00	6.28	0.01	0.02	0.20	2.00	5.50	14
SN450	pg	0.00	60.82	0.38	0.17	1.98	20.65	16.23	100.24
Atom		0.00	6.22	0.02	0.01	0.29	1.87	5.59	14
SN450	di	0.00	24.59	29.54	0.42	0.41	27.57	17.31	99.84
Atom		0.00	6.37	3.99	0.05	0.15	6.33	15.10	32
SN450	di	0.00	24.91	30.07	0.20	0.22	26.98	17.43	99.81
Atom		0.00	6.45	4.05	0.03	0.08	6.19	15.19	32
SN450	di	0.00	25.26	29.17	0.47	0.40	27.48	17.43	100.20
Atom		0.00	6.51	3.91	0.06	0.15	6.27	15.10	32
SN450	di	0.00	25.76	28.68	0.59	0.42	27.31	17.19	99.94
Atom		0.00	6.67	3.87	0.08	0.16	6.27	14.97	32
SN450	di	0.49	25.00	29.88	0.00	0.45	26.59	17.74	100.14
Atom		0.21	6.36	3.96	0.00	0.17	5.99	15.18	32
SR350	gn	n.a.	0.25	85.92	n.a.	0.00	0.29	13.46	99.93
Atom			0.02	3.95		0.00	0.02	4.00	8
SR350	gn	n.a.	0.24	85.69	n.a.	0.01	0.28	13.39	99.60
Atom			0.02	3.96		0.00	0.02	4.00	8
SR350	gn	n.a.	0.19	86.16	n.a.	0.00	0.21	13.41	99.97
Atom			0.02	3.97		0.00	0.02	4.00	8
SR350	gn	n.a.	0.18	86.03	n.a.	0.00	0.19	13.45	99.85
Atom			0.02	3.96		0.00	0.01	4.00	8
SR350	gn	n.a.	0.18	85.73	n.a.	0.11	0.09	13.39	99.50
Atom			0.02	3.96		0.01	0.01	4.00	8

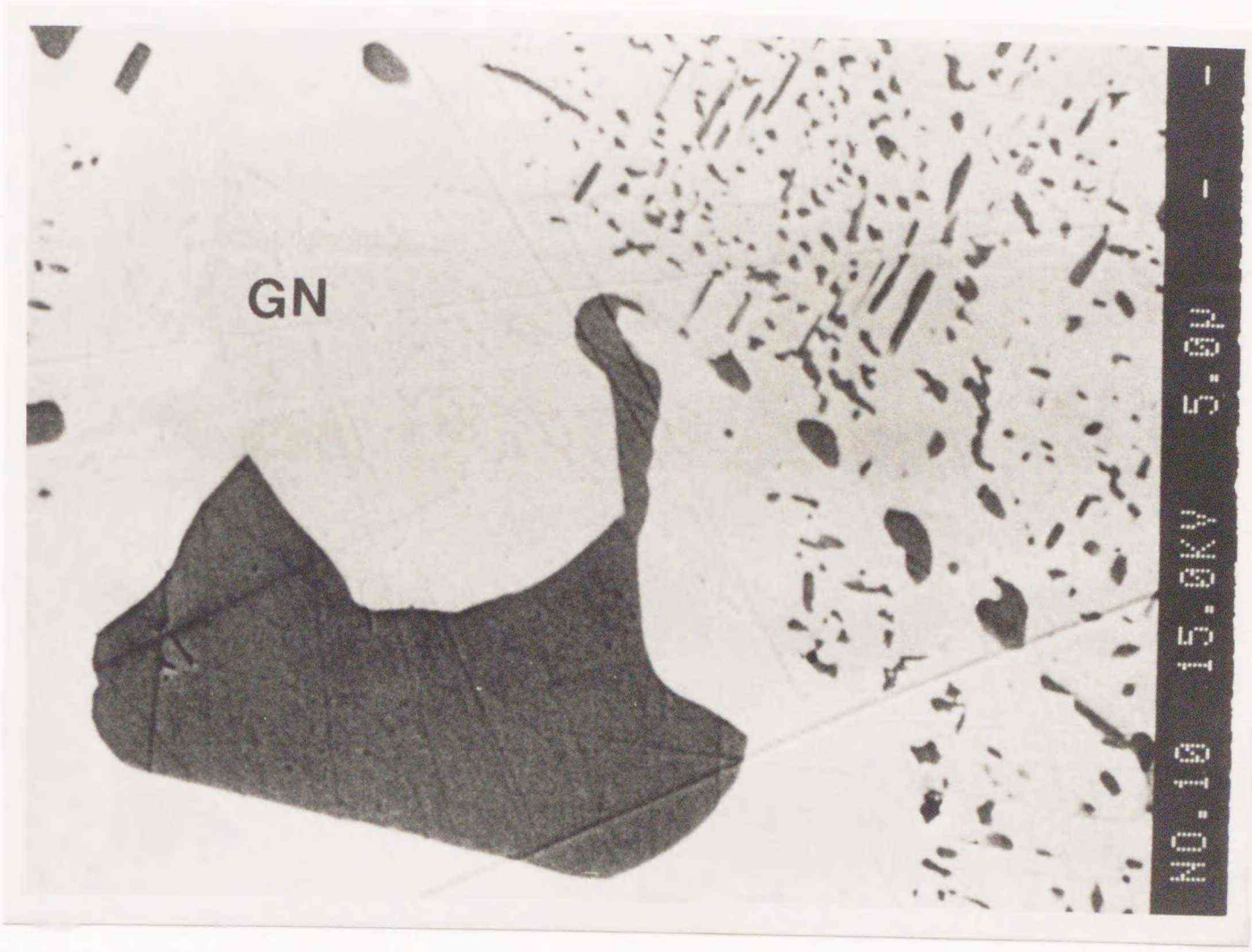

Figure 35. BSE image of diaphorite in galena (GN) in a galena-rich sample from the Shinano vein -450 mL (point 2 in Figure 1c).
Dark gray grains are mostly of diaphorite. Some of the minute grains, however, can possibly be of other Ag-Sb and Ag-Pb-Sb sulfosalts because freibergite and pyrargyrite are identified by quantitative analysis within the same grain of galena.

4-5. Other Characteristic Minerals

Tetrahedrite-Tennantite Solid Solution (Substages B and C):

This system commonly occurs in ores of the substages B and C. Up to 4.35 weight percent of bismuth is detected in this solid solution when it is associated with the Bi-Pb-Ag-S minerals(Table 18). As Figure 37 shows, a wide range of Sb/Sb+As+Bi ratio in this solid solution from Toyoha is observed. As a whole, maximum silver contents increase as Sb/Sb+As+Bi ratios increase (Figure 37, Table 18). This is likely a common feature of this solid solution from many ore deposits in the world (e.g. Wu and Petersen, 1977; Yoneda, 1987; Sato and Ono, 1988). Each trend on Figure 37, however, is not on a common line. Moreover, the positions of points plotted in a trend are not necessarily in time order, that is, the Sb/Sb+As+Bi ratio changes rhythmically or rather randomly (Figure 38) from the growth center to the rim of a grain. Therefore the positive correlation of the Ag/Ag+Cu and Sb/Sb+As+Bi ratios in a trend is probably due to structural control as is indicated by Wu and Petersen (1977). The average Ag/Cu+Ag of a trend presumably reflect the activity ratio aAg^{+}/aCu^{+} at its locality during the crystallization of the solid solution. In general, antimony-rich phases of the tetrahedrite-tennantite solid solution are dominant in the substage C, while As-rich ones were deposited in the substage B as is pointed out by Kanbara et al. (1989). Figure 36 shows maximum concentration of bismuth in the solid solution is at around 0.5 of Sb/Sb+As, and that correlation between Bi/Sb+As+Bi and Sb/Sb+As+Bi is negative for some of the individual trends. These compositional relations are consistent with the result of observations that arsenopyrite and bismuth-containing minerals are constituents of the substage B, and that

the silver-antimony and silver-lead-antimony sulfosalts were deposited only in the substage C.

Table 18. Representative analyses of the tetrahedrite-tennantite solid solution from Toyoha.

Abbreviations; Atom:atomic composition, SN:Shinano, SR:Sorachi
ten: tennantite or the solid solution with more As mol% than Sb
tet: tetrahedrite or the solid solution with more Sb mol% than As, and Ag/Ag+Cu atomic ratio equal to or less than 0.25
fre: tetrahedrite with the Ag/Ag+Cu ratio more than 0.25

Numerals after the vein name abbreviations indicate levels in meters below the mining office at Toyoha. Mn is less than 0.1, and Cd is less than 0.15 weight percent for all points analyzed.

Loc.	Name	Fe	Zn	Cu	Ag	Bi	As	Sb	S	Total
SR350	ten	4.81	2.50	37.17	8.20	1.41	17.31	3.78	25.33	100.52
Atom		1.35	0.60	9.20	1.20	0.11	3.63	0.49	12.42	29.00
SR350	ten	5.65	2.46	36.28	8.03	1.98	16.60	4.19	25.18	100.36
Atom		1.60	0.60	9.02	1.18	0.15	3.50	0.54	12.41	29.00
SR350	ten	4.69	2.36	36.05	9.28	1.32	15.26	6.69	24.62	100.27
Atom		1.35	0.58	9.11	1.38	0.10	3.27	0.88	12.33	29.00
SN450	ten	3.58	3.59	37.42	3.89	0.97	14.04	9.86	26.47	99.82
Atom		1.01	0.86	9.27	0.57	0.07	2.95	1.27	12.99	29.00
SN450	ten	3.51	3.63	37.29	4.02	1.22	13.74	10.25	26.48	100.13
Atom		0.99	0.87	9.24	0.59	0.09	2.89	1.32	13.01	29.00
SR350	ten	4.38	3.43	34.75	9.83	0.08	13.01	10.68	23.87	100.03
Atom		1.28	0.86	8.94	1.49	0.01	2.84	1.43	12.16	29.00
SN450	ten	3.39	3.56	36.45	4.19	2.53	12.86	10.32	25.46	98.75
Atom		0.98	0.88	9.29	0.63	0.20	2.78	1.37	12.86	29.00
SN450	tet	3.39	3.89	39.12	2.11	0.55	9.45	16.32	24.63	99.45
Atom		0.98	0.97	9.99	0.32	0.04	2.05	2.18	12.47	29.00
SN450	tet	3.77	3.72	38.65	2.57	0.64	9.06	17.52	25.07	100.99
Atom		1.08	0.91	9.77	0.38	0.05	1.94	2.31	12.55	29.00
SR350	tet	4.09	3.28	32.11	12.34	0.23	8.37	16.42	23.75	100.59
Atom		1.23	0.84	8.46	1.92	0.02	1.87	2.26	12.41	29.00
SN450	tet	3.86	3.62	37.76	2.80	0.53	7.09	20.07	24.28	100.01
Atom		1.14	0.91	9.77	0.43	0.04	1.56	2.71	12.45	29.00
SN450	tet	2.89	4.11	33.52	6.55	4.35	7.06	17.48	24.56	100.54
Atom		0.87	1.05	8.86	1.02	0.35	1.58	2.41	12.86	29.00
SN350	tet	2.24	4.69	34.17	5.74	1.08	3.12	25.95	22.44	99.42
Atom		0.70	1.25	9.38	0.93	0.09	0.73	3.72	12.21	29.00
SN350	tet	2.37	4.81	34.30	5.89	0.80	3.12	26.05	22.83	100.16
Atom		0.73	1.27	9.31	0.94	0.07	0.72	3.69	12.28	29.00
SN350	tet	2.62	4.35	33.20	6.86	1.78	2.08	26.51	22.72	100.12
Atom		0.82	1.16	9.12	1.11	0.15	0.48	3.80	12.36	29.00
SN350	tet	2.50	4.23	32.85	7.13	1.90	1.94	26.88	22.52	99.95
Atom		0.79	1.14	9.08	1.16	0.16	0.45	3.88	12.34	29.00
SN450	fre	4.38	0.00	19.07	26.60	0.23	0.71	27.68	22.07	100.76
Atom		1.47	0.00	5.61	4.61	0.02	0.18	4.25	12.87	29.00

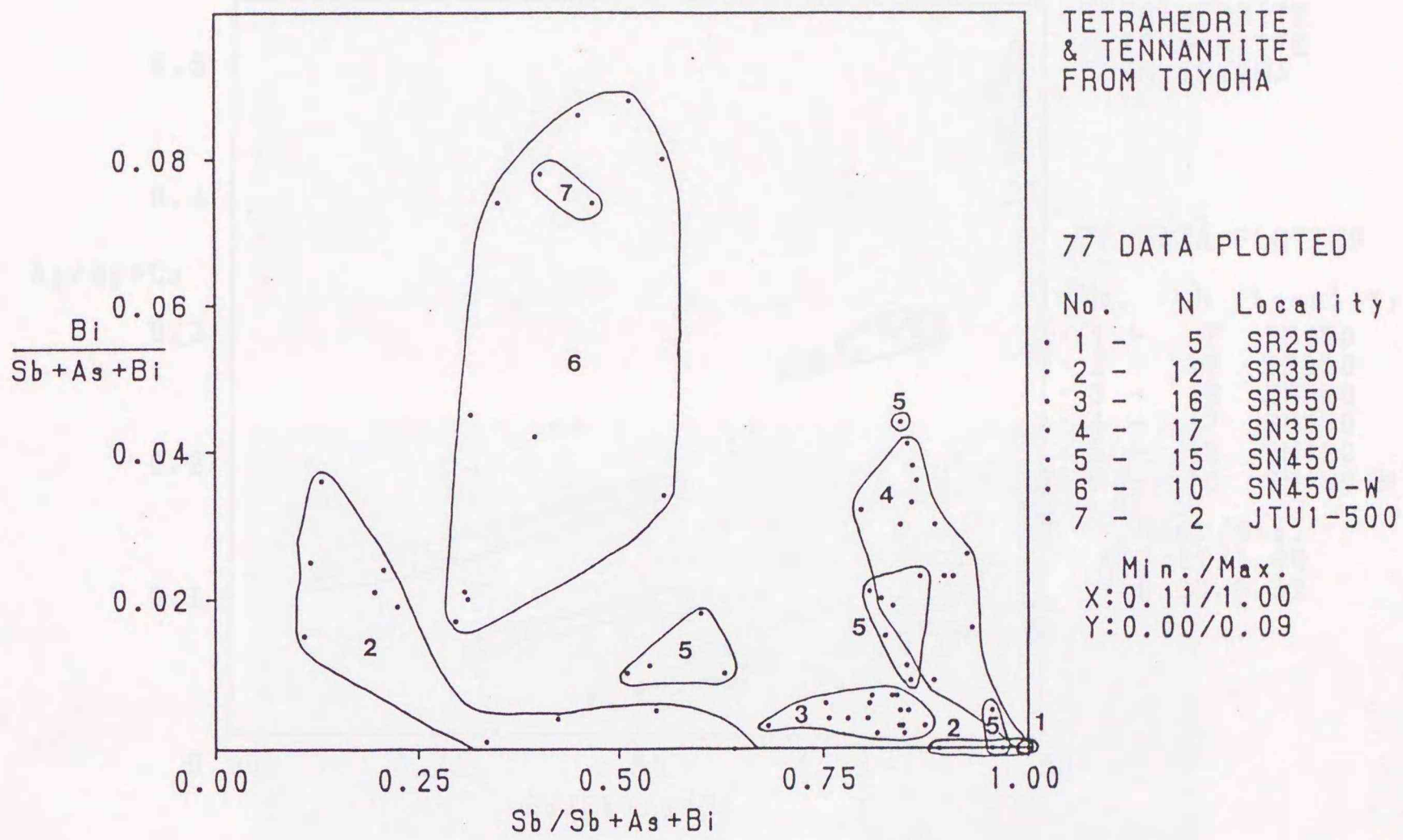

Figure 36. Sb/Sb+As+Bi vs. Bi/Sb+As+Bi (mol) diagram of the tetrahedrite-tennantite solid solution from Toyoha.
SRxxx: -xxx mL of the Sorachi vein, SNxxx: the Shinano vein.

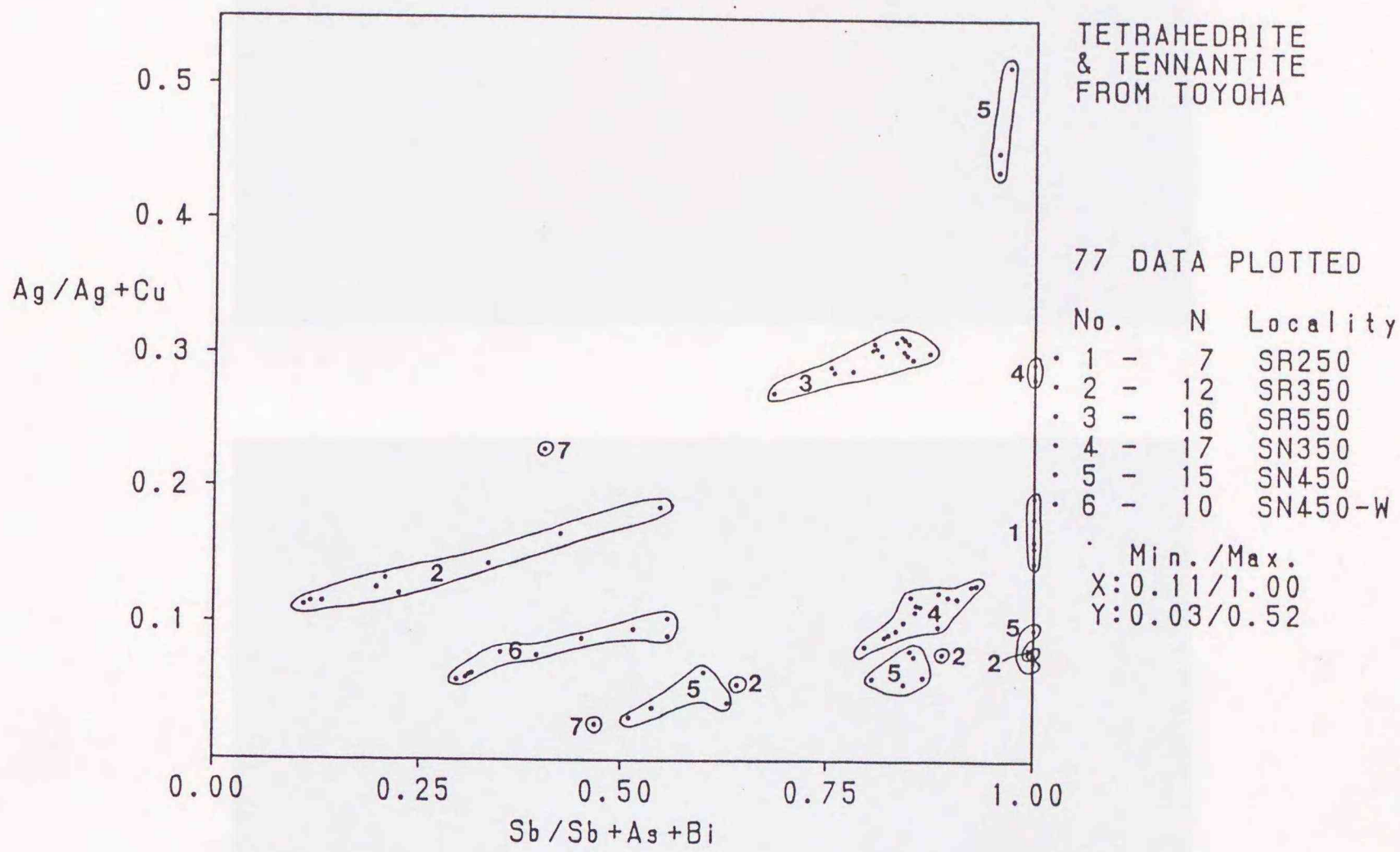

Figure 37. Sb/Sb+As+Bi vs. Ag/Ag+Cu (mol) diagram of the tetrahedrite-tennantite solid solution from Toyoha.
SRxxx: -xxx mL of the Sorachi vein, SNxxx: the Shinano vein.
Data marked with 7 are of samples from the drill JTU1.

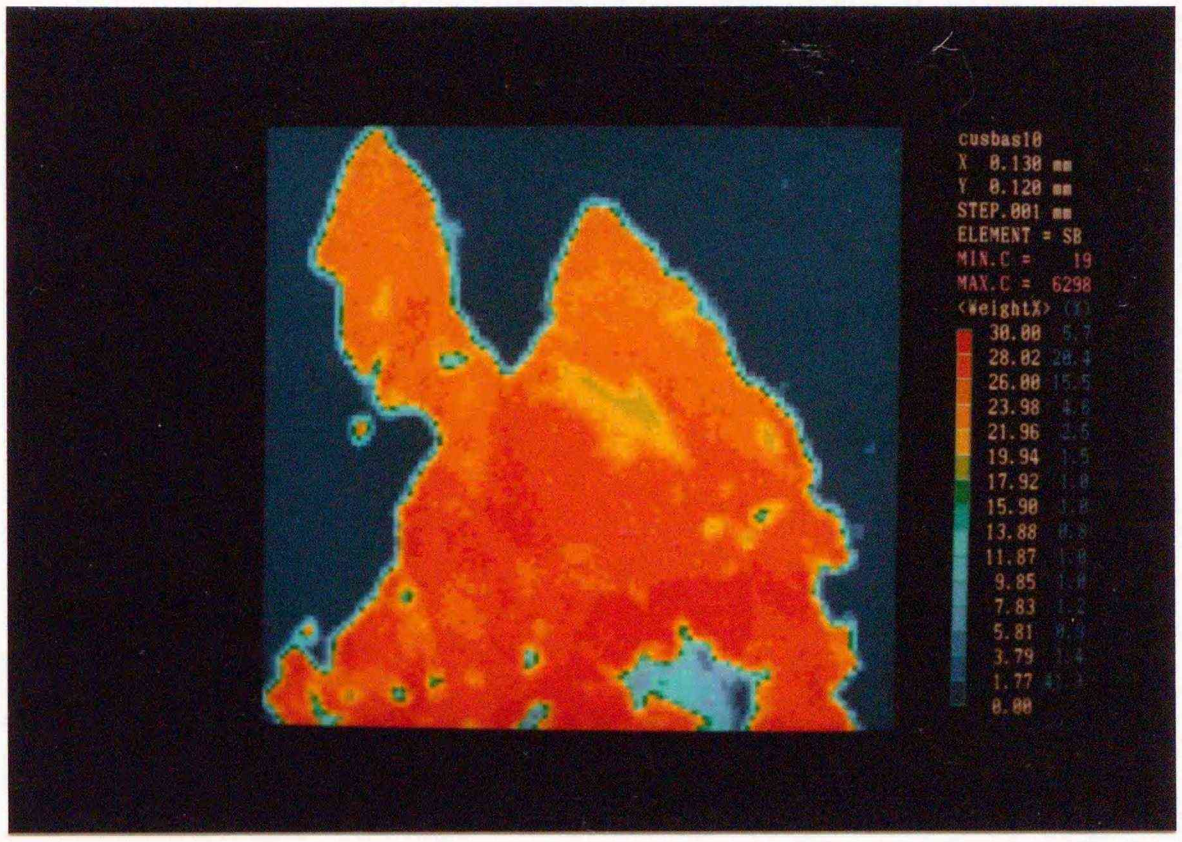

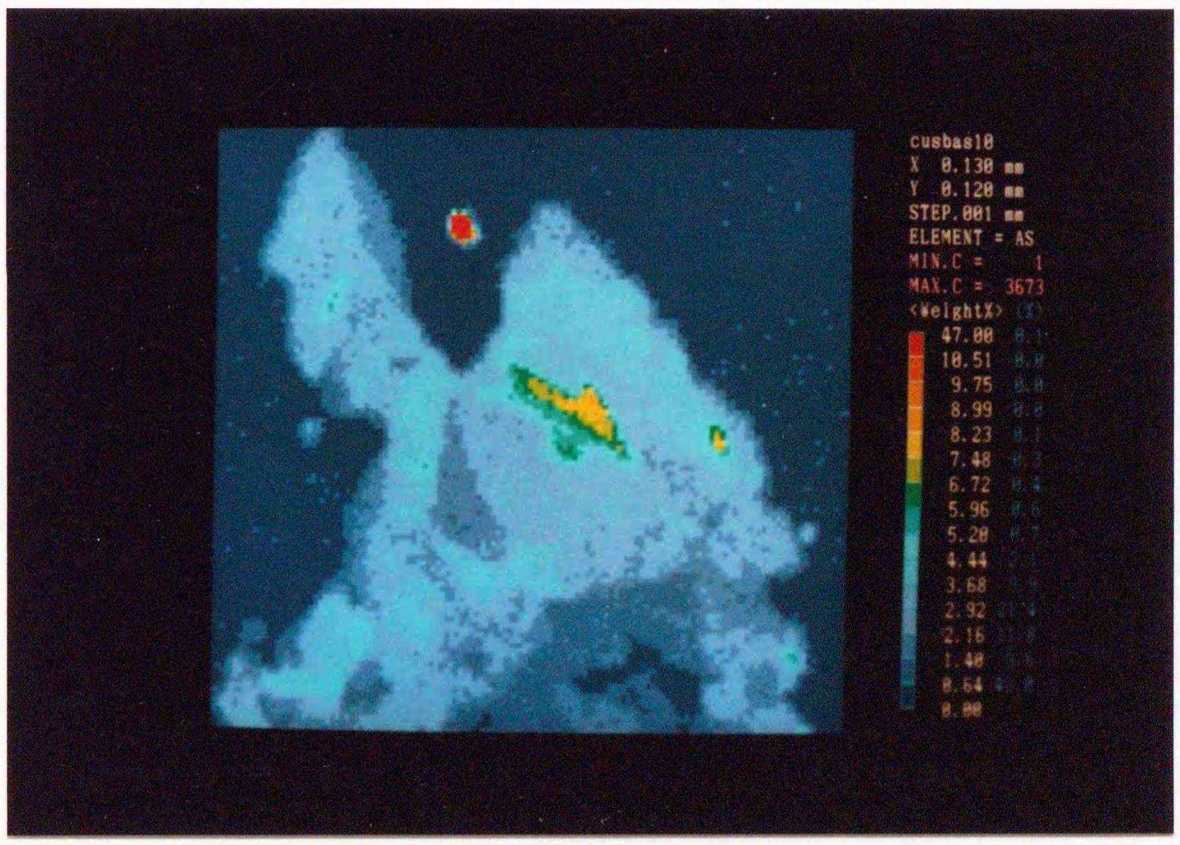

Figure 38. Antimony and arsenic maps showing heterogeneity of the tetrahedrite-tennantite solid solution in a chalcopyrite-rich sample (formed in the substage B and modified in the substage C) from the Shinano vein -450 mL (point 2 in Figure 1c).
The red grain in the arsenic map is of arsenopyrite.

Mo-Pb-Sb Sulfides (Substage B):

Two types of Mo-Pb-Sb sulfides occur in the Shinano vein at -300 mL (Type I; Ohta et al., 1987) and -450 mL (Type I and II). Type I occurs as feathery aggregates, and II as aggregates of small acicular crystals (Figure 39). EPMA analyses in Table 19 reveal that Pb/Mo mole ratio of type I is about 1, and that of II is about 2.6. Moreover type II contains around 2 weight percent tin, and 4 weight percent zinc, while tin is not detected and zinc is less than 0.5 weight percent in type I. In either type, arsenic weight percent is less than 0.2. The chemical composition of type II is rather close to that of an unnamed sulfide (hereafter expressed as type J) found in the Jokoku Mine, southwest Hokkaido (Ishiyama and Matsueda, 1988; see Table 19). Based on the chemical data and charge balance calculation assuming that the valence of sulfur is -2, valences of metals in, and chemical formulas of these sulfides are estimated as follows:

Type I: Cu is +1; Zn, Pb and minor part of Fe are +2; Sb, As and major part of Fe are +3; Mo is +4

Formula: $Cu_x(Pb,Fe,Zn)_5(Mo,Sb,As)_{5-x}S_{15}$

Type II: Fe, Zn, Pb and major part of Mo are +2; Sb, As and Sn are +3; minor part of Mo are either +3 or +4

Formula: $(Pb,Fe,Zn)_8Mo_2^{+2}(Sb,Sn,Mo^{+3})_2S_{13}$

Type J: Fe and Pb are +2; Sb and As are +3; Mo is +4

Formula: $(Pb,Fe)_{14}(Sb,As)_4Mo_3S_{26}$

The type II included in a growth band of sphalerite from -450 mL of the

Shinano vein appears to have grown on the surface of iron-poor sphalerite, and then overgrown by iron-rich sphalerite (Figure 40). Galena and arsenopyrite exist in the same polished sample contain no detectable amount of bismuth nor cobalt. Thus the Mo-Pb-Sb sulfides might have precipitated in the substage B, but later than the precipitation of bismuth- and cobalt-containing minerals. The sudden change in iron concentration in sphalerite after the deposition of the type II (Figure 40) indicates increase in temperature and/or decrease in sulfur fugacity on the molybdenum deposition.

Fe-Sb-S Minerals (Substage C or later):

Minerals of this system detected in Toyoha are listed in Table 12. A mineralization sequence, pyrrhotite+arsenopyrite -→ native arsenic -→ berthierite, is observed in one of the veinlets cutting the Tajima vein at lower levels (Ohta and Yajima, 1977; Ohta, 1979; Yajima and Ohta, 1979). The native arsenic contains a few weight percent of antimony, and 0.47 weight percent of arsenic is detected in the berthierite (Ohta, 1979). A piece of galena with rim of a lead-antimony sulfosalt was found in one of the veinlets. Ohta (1979) concluded that the former is an accidental fragment fallen into the veinlet from the surrounding ore of the earlier stage, and that the latter is due to a reaction between the former and the ore solution which deposited berthierite. Though native antimony from the Shinano vein is described by Fujikawa et al. (1990), no piece of stibnite nor berthierite has ever been observed in the southeastern later veins.

Table 19. Representative EPMA analyses of Mo-Pb-Sb sulfides from Toyoha.

Abbreviations; Atom:atomic composition, SN:Shinano,
I:type I, II:type II,
J:unknown sulfide from Jokoku Mine (type J) in Ishiyama and Matsueda (1988)
n.a.:not analyzed

Numerals after the vein name abbreviations indicate levels in meters below the mining office at Toyoha.

Loc. Name	Fe	Zn	Cu	Pb	Sn	Mo	As	Sb	S	Total
SN450 I	3.66	0.18	0.00	43.01	n.a.	20.45	0.17	6.15	26.02	99.64
Atom	4.84	0.20	0.00	15.34		15.75	0.17	3.73	59.97	100
SN450 I	5.78	0.38	2.31	39.68	n.a.	18.30	0.00	5.88	26.20	98.53
Atom	7.42	0.41	2.60	13.74		13.69	0.00	3.47	58.66	100
SN450 I	4.19	n.a.	1.40	40.98	n.a.	22.49	n.a.	5.25	25.77	100.08
Atom	5.45	n.a.	1.60	14.37		17.03		3.13	58.41	100
SN300 II	1.81	4.36	n.a.	53.83	1.88	9.35	n.a.	8.84	18.72	98.78
Atom	2.87	5.91		23.02	1.40	8.63		6.43	51.74	100
SN300 II	2.02	3.64	n.a.	54.96	1.87	9.73	n.a.	8.99	19.08	100.30
Atom	3.17	4.87		23.20	1.38	8.87		6.46	52.05	100
Jokoku J	2.20	n.a.	n.a.	60.00	n.a.	7.30	0.10	11.00	19.90	100.50
Atom	3.52	n.a.		25.91		6.81	0.12	8.09	55.55	100
Jokoku J	2.00	n.a.	n.a.	59.70	n.a.	7.00	0.10	11.00	19.90	99.70
Atom	3.23	n.a.		25.97		6.58	0.12	8.14	55.95	100

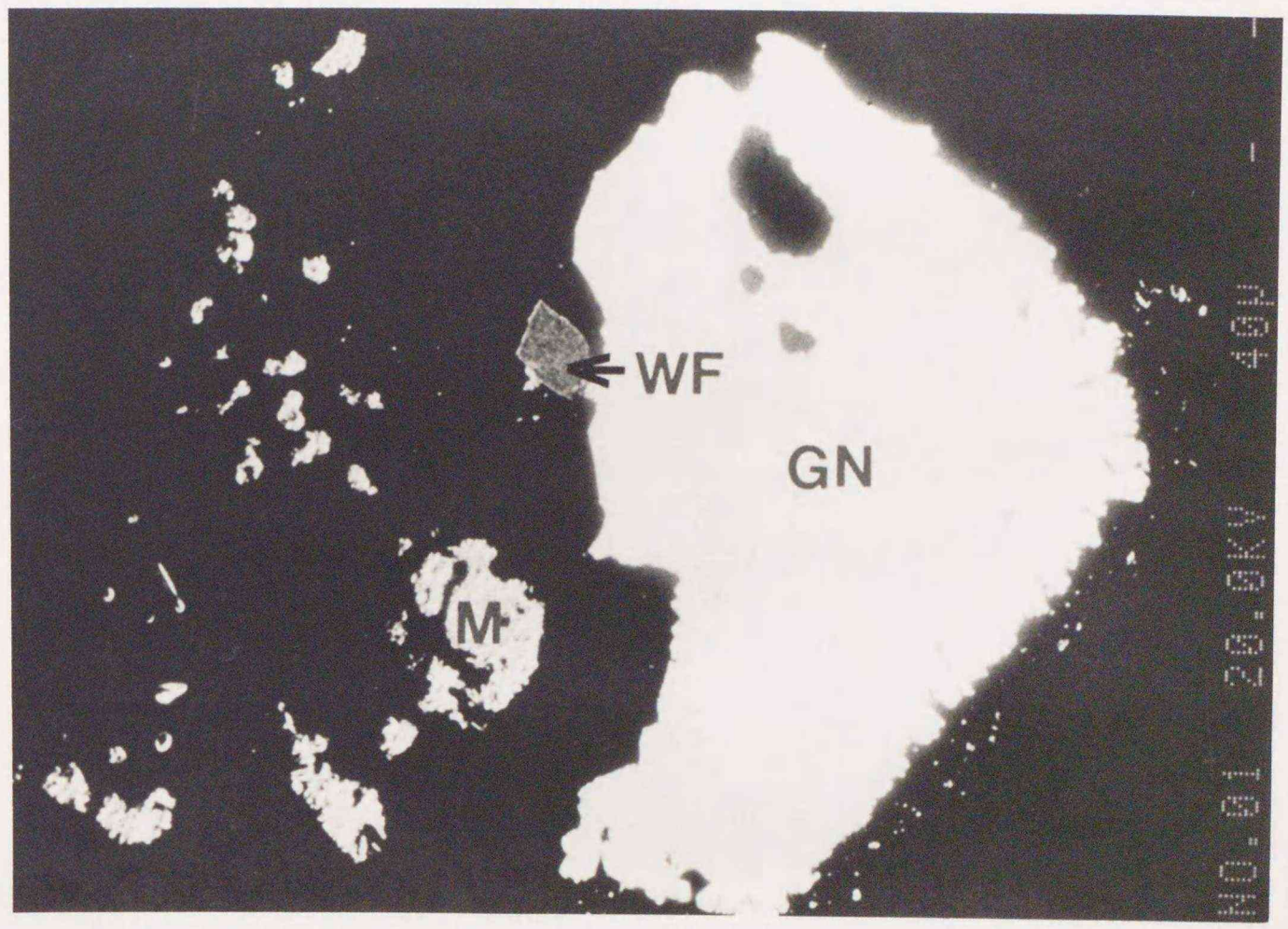

Figure 39. BSE image showing association of the Mo-Pb-Sb sulfide II (M), wolframite (WF) and galena (GN) in a sphalerite-rich sample of the substage B from the Shinano vein -450 mL.
Black background is sphalerite (point 2 in Figure 1c).

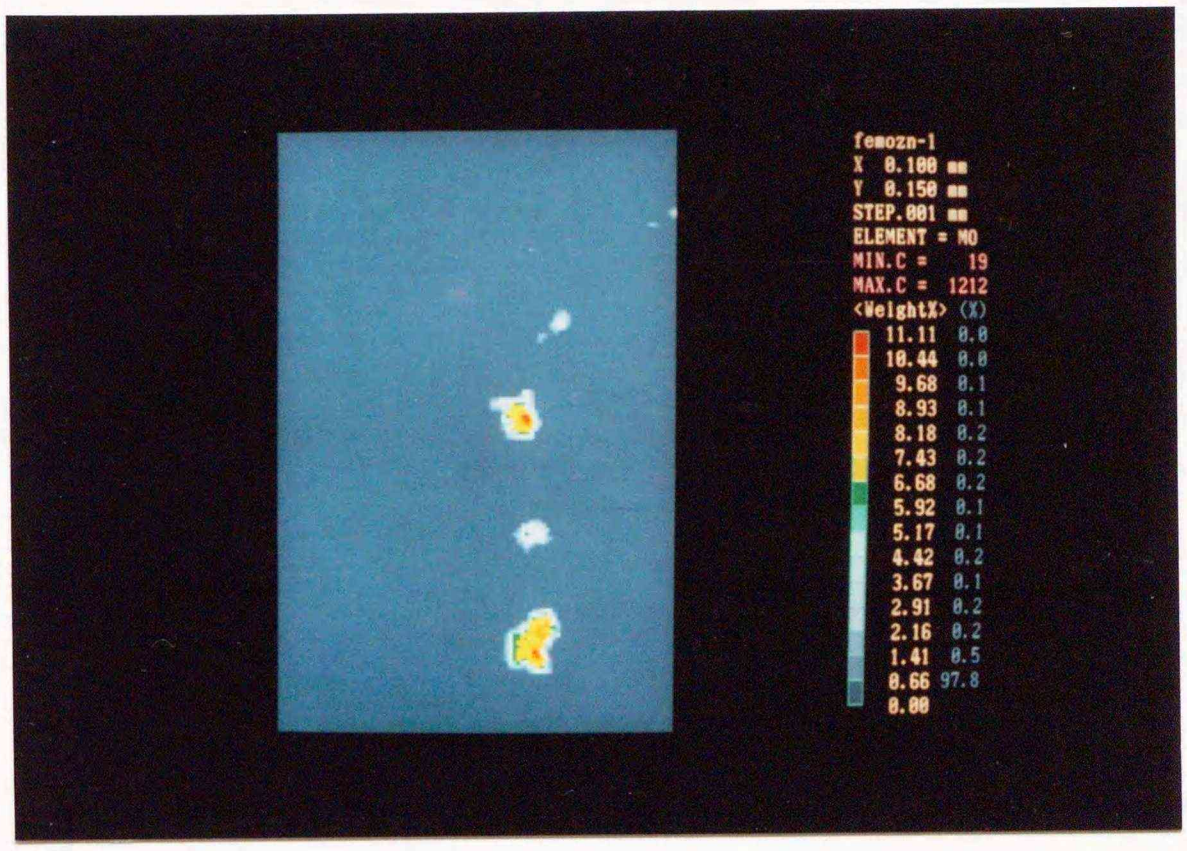

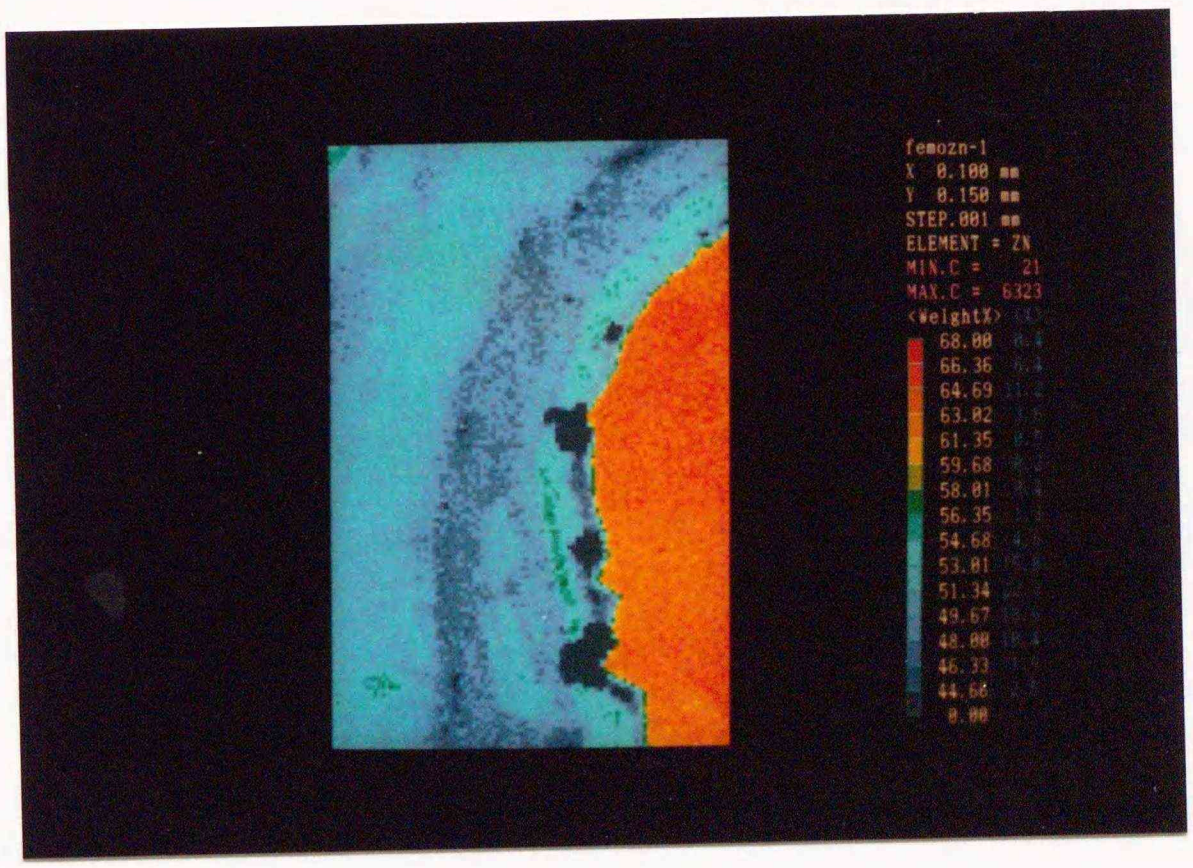

Figure 40. Molybdenum and zinc maps of the Mo-Pb-Sb sulfide II (upper image) grew on iron-poor sphalerite and overgrown by iron-rich sphalerite (lower image) in the same sample as shown in Figure 39.

Cassiterite (Substage B):

Cassiterite occurs mostly as aggregate of fine grains (Narita et al., 1977, Yajima , 1977), and each grain is generally less than 10 microns in diameter. The microtextures of cassiterite indicates that its main precipitation mechanism was not direct crystallization from the ore solution but deposition of small grains like sedimentation of sand (Ohta, 1980). This implies rapid flow of the ore solution and supersaturation of cassiterite at the deposition site. Cassiterite is commonly observed in sphalerite and fine-grained aggregate quartz whose precipitation mechanism is the same as cassiterite. This sedimentary texture of fine-grained quartz and cassiterite is common in the tin-producing veins of the Toyoha deposit. Microscopic observations reveal that cassiterite precipitation started after the initial precipitation of arsenopyrite at the beginning of the substage B. It appears that the replacement of pyrrhotite with pyrite and/or marcasite started mostly at this time, and that cassiterite was deposited only in the substage B. Frequent remnants of cassiterite within tin sulfides such as stannite, canfieldite? and hocartite, however, indicate that cassiterite fed the later ore solution with tin to form these sulfides. Representative analyses of cassiterite are listed in Table 20. The FeO mol percent in cassiterite is in a range between 0.64 and 5.42. The range is low compared with that of cassiterite from Potosi, Bolivia, though similar to those of other Bolivian tin-bearing sulfide veins (Sugaki and Kitakaze, 1988). The WO_3 mol percent is positively correlated with, but always lower than the FeO mol percent. This probably indicates substitution of 2Sn with FeW, and that WO3 exists as ferberite ($FeWO_4$) molecule in cassiterite.

Wolframite (Substage B):

Wolframite is rare as compared with cassiterite. This mineral generally occurs as euhedral lath-shaped crystals in sphalerite and in gangue quartz, and frequently exhibits sector structures which are clarified by BSE images or element maps (Figure 41), but not visible under normal optical microscope. Therefore it is evident that, in contrast to cassiterite, wolframite crystallized directly from the ore solution. Microscopic observations reveal that wolframite was deposited in the latter half of the substage B, and are commonly associated with cassiterite, quartz, sphalerite, arsenopyrite and pyrite. The sector structures are attributed to the wide-range solid solution between huebnerite and ferberite (Table 21). Observed range in ferberite mol percent is between 72 and 26.

Table 20. Representative EPMA analyses of cassiterite from the Tajima vein -450 mL.

Mol: mol percent

No.	SnO2	TiO2	Al2O3	WO3	FeO	Total
1	98.50	0.21	0.09	0.77	0.30	99.88
Mol	98.33	0.40	0.14	0.50	0.64	100.00
2	98.26	0.27	0.07	0.68	0.44	99.73
Mol	98.02	0.52	0.11	0.44	0.91	100.00
3	96.86	0.25	0.12	0.89	1.56	99.68
Mol	95.57	0.47	0.17	0.57	3.22	100.00
4	96.78	0.28	0.09	0.68	0.90	98.72
Mol	97.01	0.53	0.14	0.44	1.88	100.00
5	95.28	0.19	0.11	1.01	2.64	99.23
Mol	93.43	0.35	0.16	0.64	5.42	100.00
6	94.28	0.07	0.14	2.28	2.60	99.36
Mol	92.84	0.12	0.21	1.46	5.37	100.00

Table 21. Representative EPMA analyses of wolframite from the Shinano vein -350 mL.

Mol: mol percent

No.	FeO	MnO	CaO	WO3	MoO3	Total
1	17.13	6.66	0.07	76.08	0.00	99.94
Mol	35.97	14.15	0.37	49.51	0.00	100.00
2	14.18	9.10	0.08	76.09	0.15	99.60
Mol	30.01	19.51	0.41	49.90	0.16	100.00
3	13.79	9.54	0.03	75.65	0.10	99.09
Mol	29.33	20.55	0.14	49.88	0.10	100.00
4	13.41	10.64	0.03	75.01	0.00	99.08
Mol	28.23	22.70	0.14	48.94	0.00	100.00
5	12.74	11.25	0.03	74.97	0.00	98.98
Mol	26.85	24.02	0.16	48.97	0.00	100.00
6	10.50	13.47	0.06	75.18	0.00	99.21
Mol	22.07	28.68	0.31	48.95	0.00	100.00
7	10.14	13.86	0.02	75.28	0.00	99.30
Mol	21.32	29.52	0.10	49.06	0.00	100.00
8	9.46	14.31	0.05	75.09	0.00	98.92
Mol	19.97	30.61	0.29	49.13	0.00	100.00
9	6.38	17.66	0.06	74.77	0.00	98.87
Mol	13.42	37.58	0.32	48.69	0.00	100.00

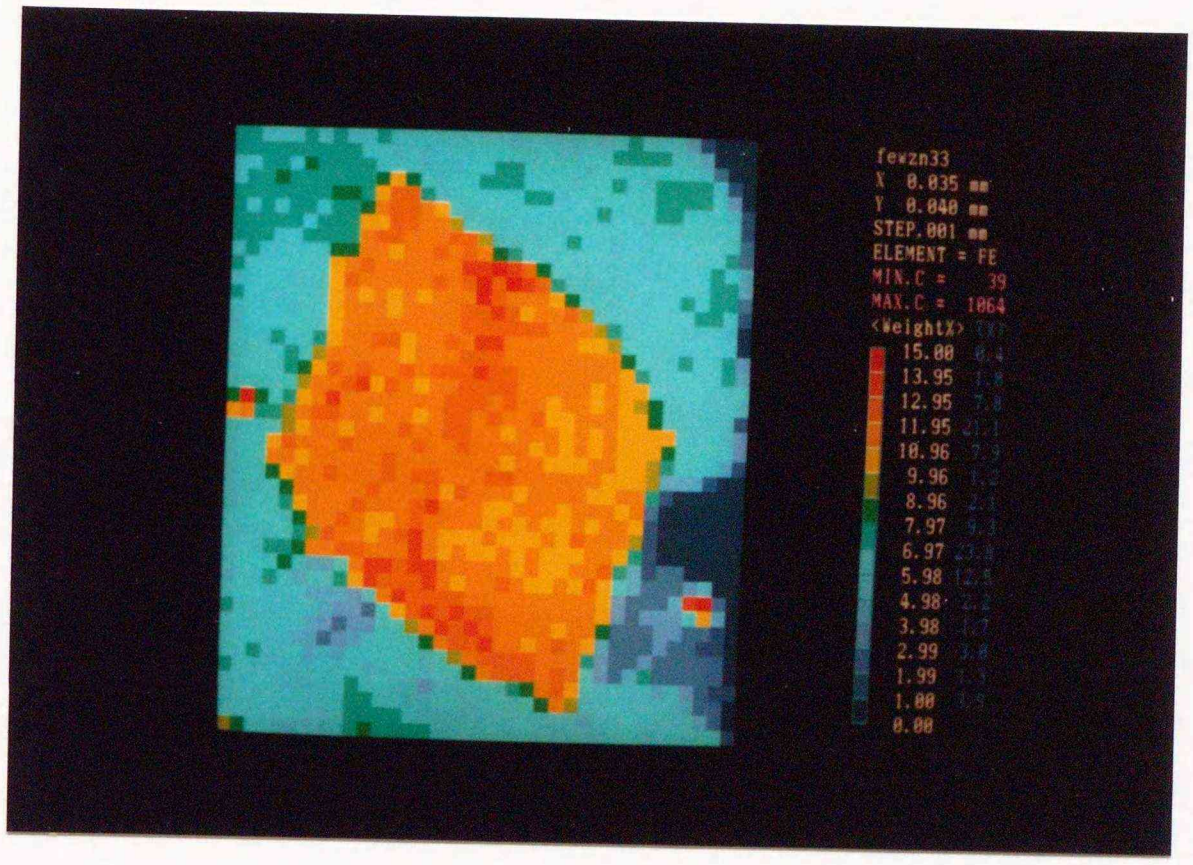

Figure 41. Iron map showing a pinwheel-like sector structure of a single crystal of wolframite shown in Figure 39. The structure have been formed probably by the same mechanism as the hour-glass structure observed in silicate crystals such as augite.

4-6. Summary of Rare-metal Partitioning in Minerals

The results of the EPMA analyses figured out minerals in which rare metals are concentrated. Tin and indium are detected in the minerals listed in Table 3. Bismuth is in the minerals of Bi-Pb-Ag-S system, namely matildite, bismuthinite, a gustavite-like sulfide, native bismuth, galena and solid solutions among these minerals, and in tetrahedrite of the substage B. Cobalt and nickel are detected in antimony-poor parts of the iron-arsenic sulfides. Arsenic and antimony occur in cobalt-poor parts of the iron-arsenic sulfides, the tetrahedrite-tennantite solid solution, native arsenic, native antimony, berthierite and stibnite. Silver occurs as native silver and argentite in the earlier veins (Yajima and Ohta, 1979; Kojima et al., 1979), while it constitutes the sulfosalts with lead and antimony, the tetrahedrite-tennantite solid solutions, silver-containing minerals in Table 3, and Bi-Pb-Ag sulfides in the later veins. Silver is detected also in electrum from both the earlier and the later veins (Kanbara and Kumita, 1990). One remarkable feature of silver minerals from Toyoha is that arsenic does not make a sulfosalt with silver as main component in the Toyoha deposit, though the silver-antimony and silver-lead-antimony sulfosalts are common ore minerals in the substage C. Gold is detected only in electrum, and wolfram only in wolframite. Gallium is detected as a minor component in sphalerite, though no germanium is found to date.

CHAPTER 5

DISCUSSIONS

5-1. Distribution of Minerals and Inclusions

Underground observations followed by detailed microscopic and EPMA-analysis work have revealed that the minerals containing tin, indium, wolfram, bismuth, cobalt and nickel are mostly distributed in the southeastern later veins, namely Shinano, Izumo, Sorachi, and southern half of Soya. Distribution of silver minerals at Toyoha mapped by Yoshie et al. (1986) also indicates that the center of silver mineralization is at the southeast of the mining area (Figure 42). Actually the silver sulfosalts are common in not only the silver sulfosalt zones but also the freibergite zones in Figure 42. Both the silver sulfosalts and tetrahedrite or freibergite, however, are rare in the argentite-native silver zones, and argentite and native silver are observed only in the argentite-native silver zones. In addition, Kanbara and Kumita (1990) revealed that compositions of electrum systematically changes from the Izumo and Sorachi veins (gold rich) to the Chikugo I, II, and III veins (silver rich) via the Soya vein (intermediate). Zonation of gangue minerals (graphite, rutile, kaolin minerals, pyrophyllite, sericite, chlorite, apatite and carbonates) revealed by Ohta and Marumo (1985), and grade patterns of each metals in the later veins (Kuwahara et al., 1983; Yoshie et al., 1986; Kanbara et al., 1989) are consistent with the distribution pattern of ore-mineral assemblages.

It is well known that alteration halos above the veins in the southeast of the mining area is not recognized on the surface, while those in the north and northwest are widely developed. Moreover, both the upper and lower limits of mineable levels of the veins get deeper southeastwards (Yajima and Ohta, 1979; Kuwahara et al., 1983; Takeyama, personal communication). Both the filling temperatures and salinities of fluid inclusions increase downward in the Izumo vein, while those in the Tajima vein show their maximums at the levels between -250 mL and -300 mL, and decrease downwards as well as upwards (Figure 43). Although the fluid inclusion data of the Harima vein are limited only for -300 mL and the shallower levels, the data of the Harima and Tajima veins are plotted on the same trend in Figure 44, and both the overall filling temperatures and salinities of fluid inclusions from the Harima vein are higher than those from the Tajima vein. On the other hand, the trend of fluid inclusions from the Izumo vein is shifted to the higher temperature side by about 40°C. All these observations and data reconfirm that the ore solution of the earlier-stage mineralization flew almost laterally from the Harima vein to the earlier veins in the northwest of the vein swarm through the Tajima vein, and that the later-stage ore solution came up from the depth at around the junction of the Izumo and Shinano veins, and flew to the north and northwest of the Toyoha vein swarm through the Sorachi and Soya veins as major path (Yajima and Ohta, 1979).

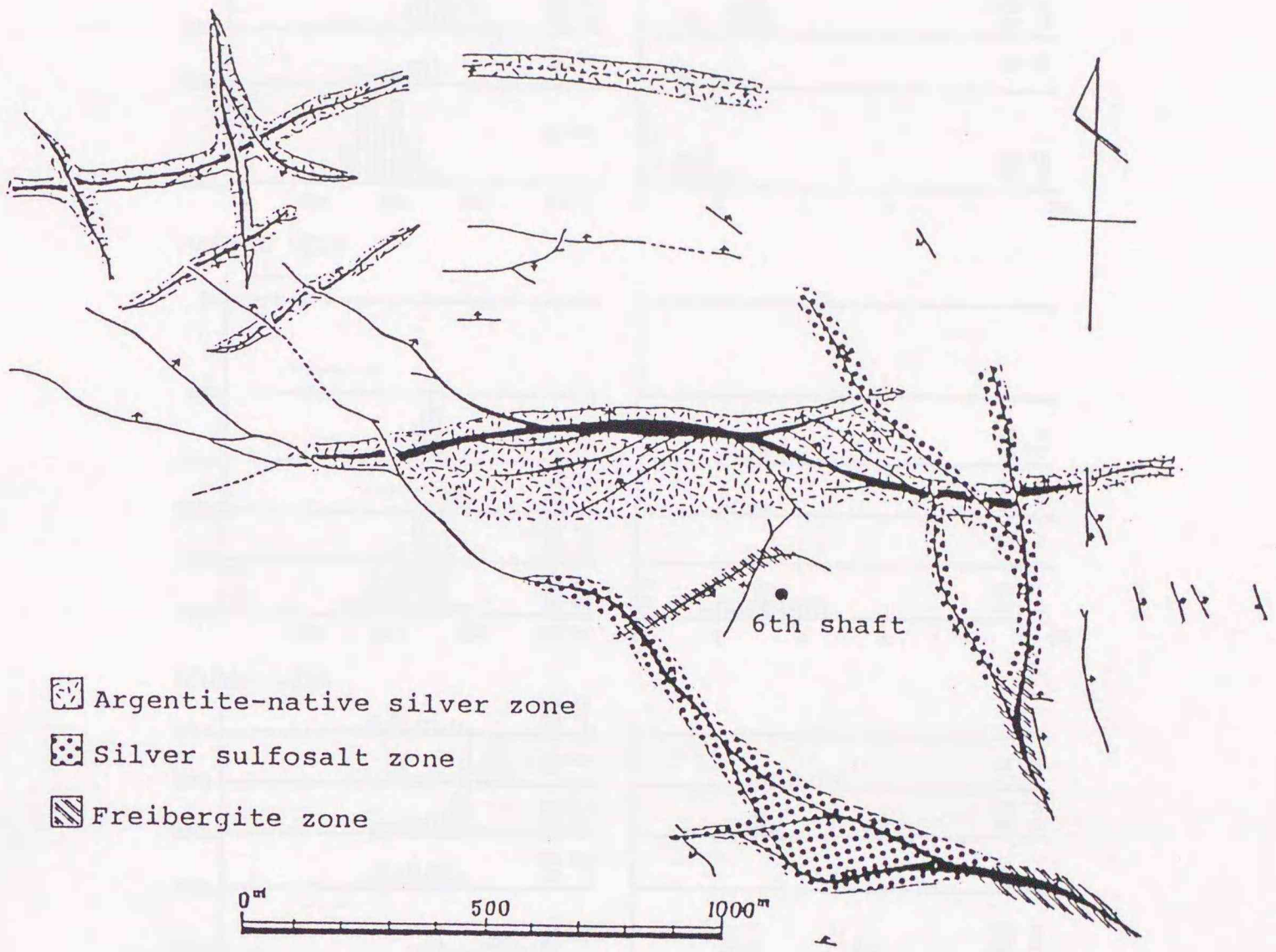

Figure 42. Distribution of silver minerals at Toyoha (simplified after Yoshie et al., 1986).

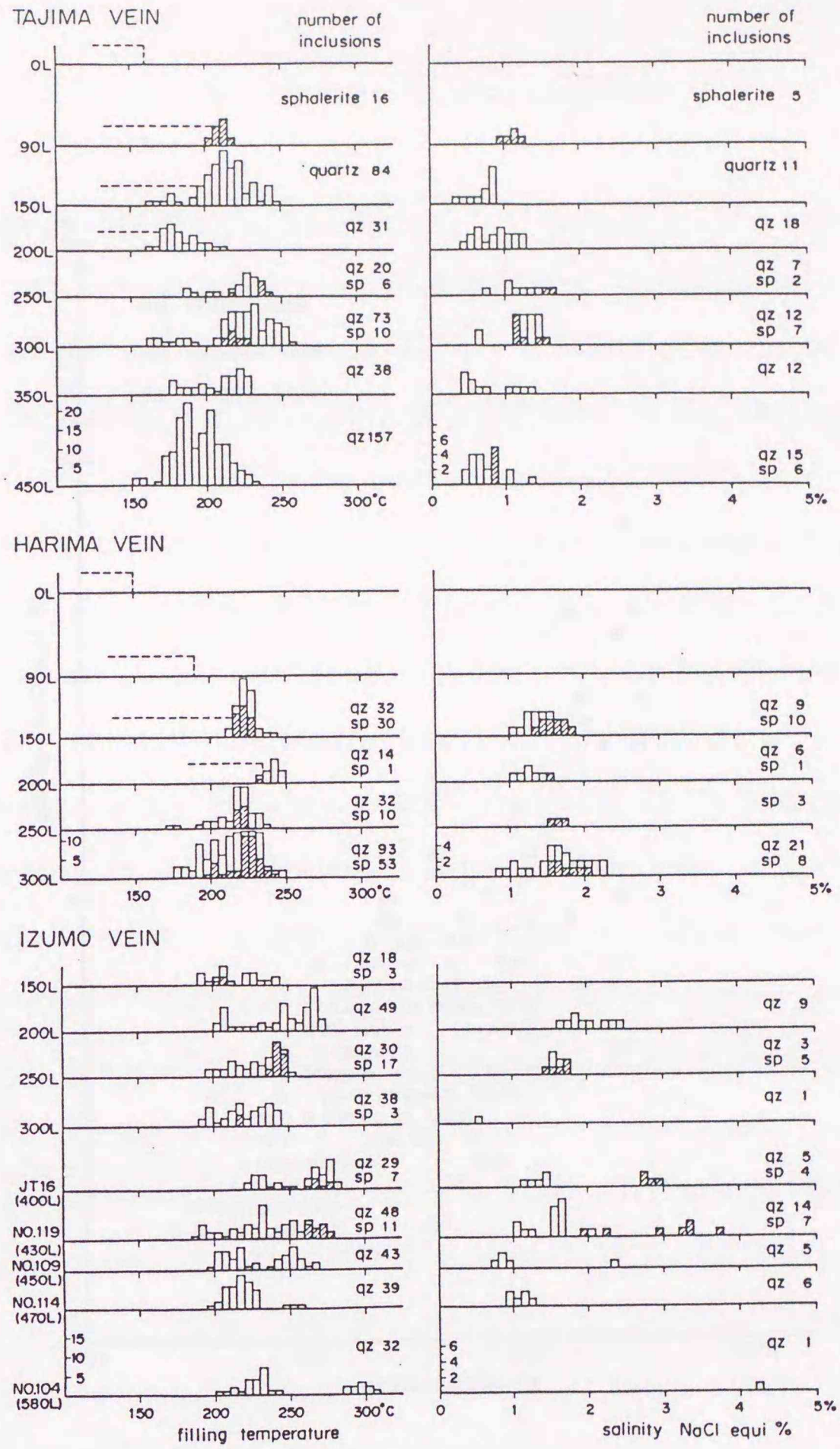

Figure 43. Histogram of filling temperature and NaCl equivalent wt% of fluid inclusions for each level of the Tajima, Harima and Izumo veins at Toyoha (after Yajima and Ohta, 1979).

The filling temperatures were measured in Leitz Heating Stage 1350, and the NaCl equivalent wt% were obtained by cooling method using Nikon Freezing Stage NE-1.

Open rectangular represent quartz, shaded ones sphalerite.

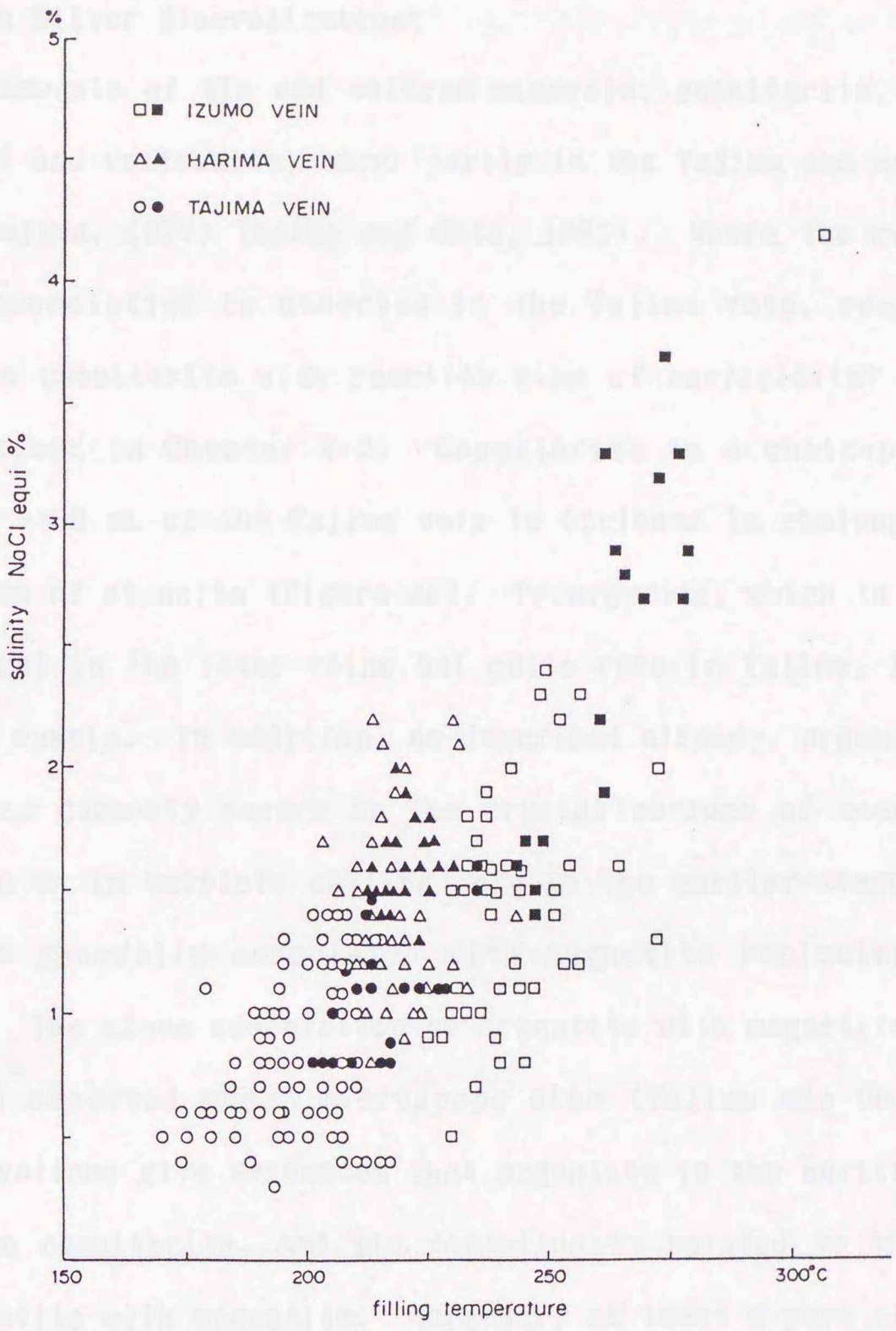

Figure 44. Filling temperature vs. NaCl equivalent wt% diagram of fluid inclusions from Toyoha (after Yajima and Ohta, 1979).
Open marks indicate inclusions in quartz, solid ones sphalerite.

5-2. Mineralization Stages

Stage of the Silver Mineralization:

Small amounts of tin and wolfram minerals; cassiterite, stannite, canfieldite? and wolframite; occur partly in the Tajima and Harima veins (Ohta and Yajima, 1977; Yajima and Ohta, 1979). Where the cassiterite-argentite association is observed in the Tajima vein, overgrowth of argentite on cassiterite with reaction rims of canfieldite? is evident as is described in Chapter 4-2. Cassiterite in a chalcopyrite-rich sample from -450 mL of the Tajima vein is included in chalcopyrite with reaction rims of stannite (Figure 45). Pyrargyrite, which is a dominant silver mineral in the later veins but quite rare in Tajima, is observed in the same sample. In addition, as described already, argentite in the earlier veins commonly occurs on the crystal surface of coarse-grained geode quartz or in veinlets cutting through the earlier-stage lead-zinc ore, and is generally associated with magnetite replacing hematite (Figure 3). The close association of argentite with magnetite replacing hematite is observed under microscope also (Yajima and Ohta, 1979). These observations give evidences that argentite in the earlier veins is younger than cassiterite, and its formation is related to the replacement of hematite with magnetite. Moreover, at least a part of chalcopyrite-rich zones which are sporadically distributed in the Harima and Tajima veins (Yajima and Ohta, 1979) is younger than cassiterite from Tajima, and was formed simultaneously with pyrargyrite. In addition, Figure 46 reveals that the Tajima vein is intersected not only by major later veins but also numerous veinlets of NW-SE and N-S trends. These veinlets, including those with berthierite or stibnite, are composed mostly of quartz, rhodochrosite and manganocalcite, and hold geodes

which indicate that the veinlets were formed in open fractures.

All these observations suggest that the later-stage ore solution permeated all over the earlier veins, and significantly modified the earlier-stage ore while it deposited lead, zinc, copper, manganese and antimony along its main pass (open fractures) to have formed the later veins and veinlets. Thus it is likely that the silver and copper in the earlier veins have mostly derived from the later-stage ore solution. Figure 42 shows, however, that even at around the crossing of the earlier (Tajima and Harima) and the later (Soya and Sorachi) veins, argentite is observed within the earlier veins and the silver sulfosalts within the later. This inconsistent occurrence modes of silver must be explained by the single-ore-solution model in order to conclude that major part of the silver production from Toyoha is attributed to the later-stage mineralization. Possibly only one explanation is that the silver deposition in the earlier veins is related to the reduction of hematite to form magnetite, in other word, oxidation of the ore solution by the reaction with hematite.

Mineral assemblages imply that both oxygen and sulfur fugacities in terms of mineral assemblages were lower during the later-stage mineralization than those in the earlier stage (Yajima and Ohta, 1979; Ohta, 1980). The mineral assemblages and FeS mol% in sphalerite suggest that oxygen fugacity, fo_2, was lower than or at around the upper limit of pyrrhotite (Figure 49), and sulfur fugacity, fs_2, was at around the arsenopyrite - pyrite+arsenic boundary during the substage C of the later-stage mineralization (described later in the text; see Figure 48). Whether the silver sulfosalts precipitate or argentite does, depends on

the activity of Sb_2S_3 as indicated by the equation

$$2Ag_3SbS_3(\text{pyrargyrite}) = 3Ag_2S(\text{argentite}) + Sb_2S_3 \quad (1)$$

Stibnite is found only in some of the later veins and veinlets which cut through the Tajima and Harima veins, and is not associated with any silver mineral. It is obvious, however, activity of Sb_2S_3 was high enough to form the silver sulfosalts in the major later veins. Moreover, the fs_2 for the reaction

$$2Ag_3SbS_3 + 1/2O_2 = 3Ag_2S + Sb_2S_2O + 1/2S_2 \quad (2)$$

is a function of temperature, fo_2 and the activity of Sb_2S_2O (aSb_2S_2O). Equation (2) suggests that the stability field of pyrargyrite against argentite reaches at its maximum when aSb_2S_2O equals one, that is, if solid Sb_2S_2O (kermesite) exists. It suggests also that decrease in the common logarithm of aSb_2S_2O by one will increase the logarithm of fs_2 by two. From this consideration, it is deduced that the pyrargyrite-stable field (Figure 47) was wide enough to cover the estimated fs_2 range during the substage C within the later veins even when aSb_2S_2O were as low as 0.2. This is consistent with the occurrence of the silver sulfosalts in the later veins. On the other hand, Figure 47 evidently shows that pyrargyrite is not stable if fs_2 and fo_2 in the ore solution are buffered by the hematite+magnetite+pyrite assemblage which is commonly observed in the earlier veins. Consequently, it is likely that the reaction of the later-stage ore solution with hematite formed argentite together with magnetite in the earlier veins, and silver precipitated mainly as sulfosalts in the later veins where little iron

oxides exist.

Crerar et al. (1985) deduced that silver exists mainly as chloride complexes in high-chloride hydrothermal solutions, while silver-sulfide complexes such as $AgHS^\circ$, $HAg(HS)_2^\circ$ or $Ag(HS)_2^-$ are predominant in low-chloride solutions. As Barnes (1979) pointed out, oxidation of the ore solution increases solubility of chloride complexes, but decrease that of sulfide complexes. Salinity of the later-stage ore solution permeated into the earlier veins was probably around the lower end of the Izumo trend (less than 1 equivalent wt% NaCl; see Figure 44). This implies that, in the earlier veins during the substage C, majority of silver was carried as sulfide complexes, and was deposited by oxidation reactions like

$$2AgHS^\circ(aq) + 3Fe_2O_3 \rightarrow Ag_2S(\text{argentite}) + 2Fe_3O_4 + H_2O + 1/2S_2 \qquad (3)$$

While, in the later veins where salinity of the ore solution was higher and little hematite was available, the silver may have precipitated by a reaction such as

$$2AgCl^\circ(aq) + H_2S(aq) \rightarrow Ag_2S(\text{in sulfosalts or freibergite}) + 2H^+ + 2Cl^- \qquad (4)$$

or as

$$2AgCl^\circ(aq) + Cu_2S(\text{in stannite}) \rightarrow 2CuCl^\circ(aq) + Ag_2S(\text{in hocartite}) \qquad (5)$$

The freibergite zones in Figure 42 correspond to copper-rich zones, and chalcopyrite being replaced by freibergite is frequently observed.

These facts suggest that, wherever in the southeastern later veins, the reaction (4) formed freibergite where copper was available, and the silver sulfosalts where silver and antimony dominate over copper.

As is described in Chapter 3, the difference between the sequence of ore minerals observed in the veinlets cutting the Tajima vein, and the sequence commonly observed in the later veins is the existence of berthierite instead of silver-antimony sulfosalts in the former, and the position of the carbonate minerals. The difference is interpreted in two ways:

1: The mineralization of the substages C and D was not proceeded in these veinlets, and native arsenic and berthierite precipitated at the end of the substage E.

2: The mineralization of the substage C formed native arsenic, berthierite and manganocalcite in the veinlet while native arsenic and silver-antimony sulfosalts were precipitating in the major later veins.

As already mentioned in Chapter 3, the latter interpretation is likely. In either case, however, the reason might be that the silver-chloride concentration was too low to deposit a silver sulfosalt because these veinlets are far from the major later veins, and that there was no hematite to react with silver-sulfide complexes in the ore solution to form argentite. Otherwise, berthierite may not have precipitated because the assemblage pyrargyrite+pyrrhotite (or pyrite) is more stable than the assemblage argentite+berthierite.

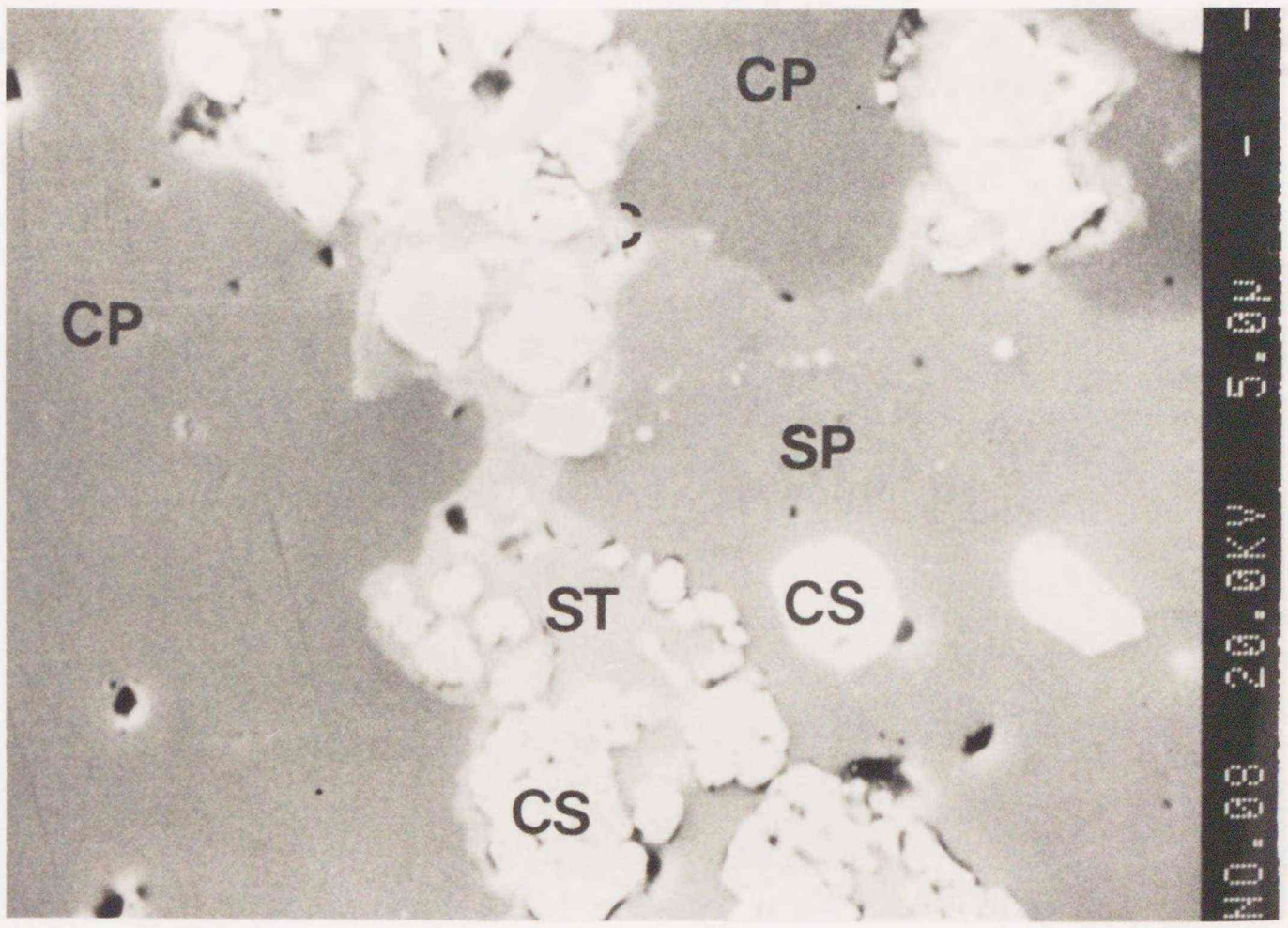

Figure 45. BSE image of cassiterite (CS) and chalcopyrite (CP) with reaction margin of stannite (ST) in a chalcopyrite-sphalerite-rich ore from the Tajima vein -450 mL (point 6 in Figure 1c).
Note that cassiterite included in sphalerite (SP) does not have stannite rim.

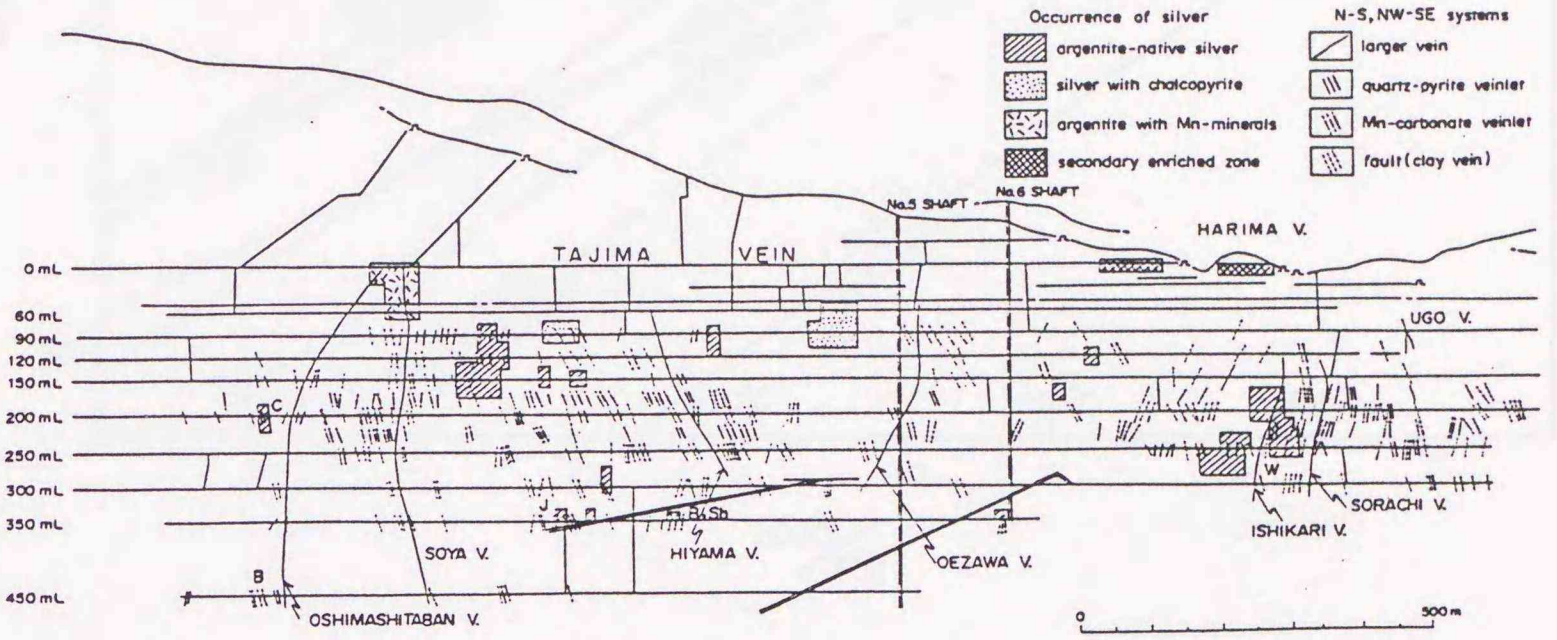

Figure 46. Section map showing the later veins and veinlets of NW-SE and N-S trends cutting the Tajima and Harima veins with occurrence of silver-rich zones and minerals presumably formed in the later-stage mineralization (after Yajima and Ohta, 1979).

Abbreviations for localities of the minerals; B:berthierite, C:cassiterite, J:jamesonite, Sb:stibnite, W:wolframite.

The Oshimashitaban, Hiyama, Oezawa, Ishikari and Ugo veins are the later veins not discussed in the text.

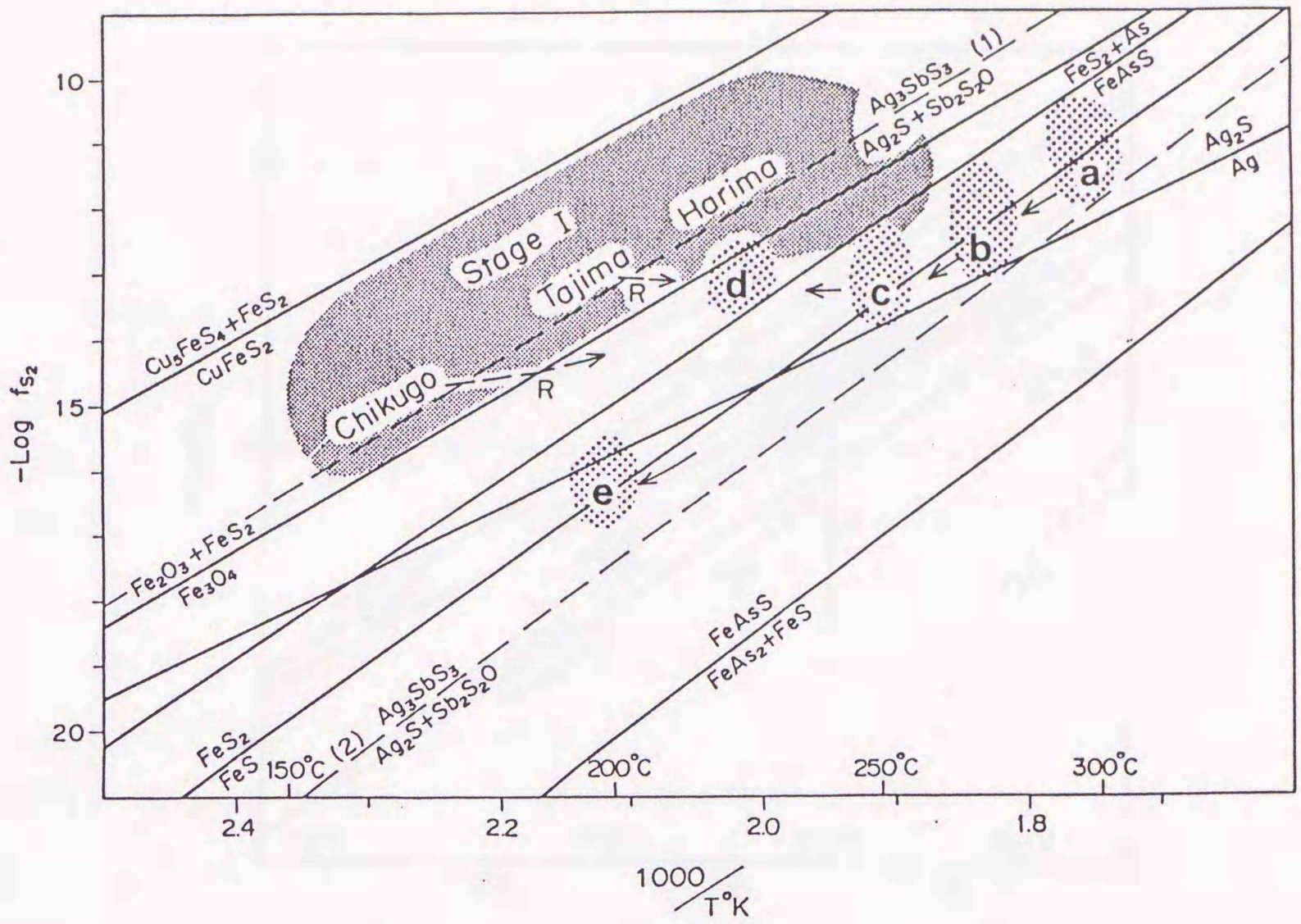

Figure 47. Diagram showing the temperature(T)-sulfur fugacity(fs_2) conditions of ore formation at Toyoha (modified after Yajima and Ohta, 1979)

Stage I: Formation conditions of hematite-pyrite ore in the earlier-stage mineralization at the Chikugo, Tajima and Harima veins. fs_2 for the formation of Zn-Pb ore of the earlier stage may be slightly lower than shown in this diagram (Figure 50).

a to e: Conditions during the substages B and C at the Izumo vein -580 mL(a) and -430 to -400 mL(b), the Sorachi vein -300 mL(c), argentite-quartz veinlets in the Tajima vein -200 mL(d), and calcite-quartz-berthierite veinlets crossing the Tajima vein -450 mL(e). fs_2 at the end of the substage C was slightly higher than shown here (see Figure 48 and the text). Solid arrows show a flow path of the ore solution, and broken arrows marked with R indicate reduction of the early-stage ore by the later-stage ore solution.

Line (1) is pyrargyrite - argentite+kermesite boundary under fo_2 at the hematite-magnetite boundary, which corresponds to the fo_2 when magnetite was replacing hematite in the earlier veins.

Line (2) is the same boundary under fo_2 at the upper limit of pyrrhotite, which corresponds to the fo_2 in the later veins when the silver sulfosalts were precipitating.

The diagram is based on data in Holland (1959), Barton (1969), Craig and Barton (1973), and Ripley and Ohmoto (1977).

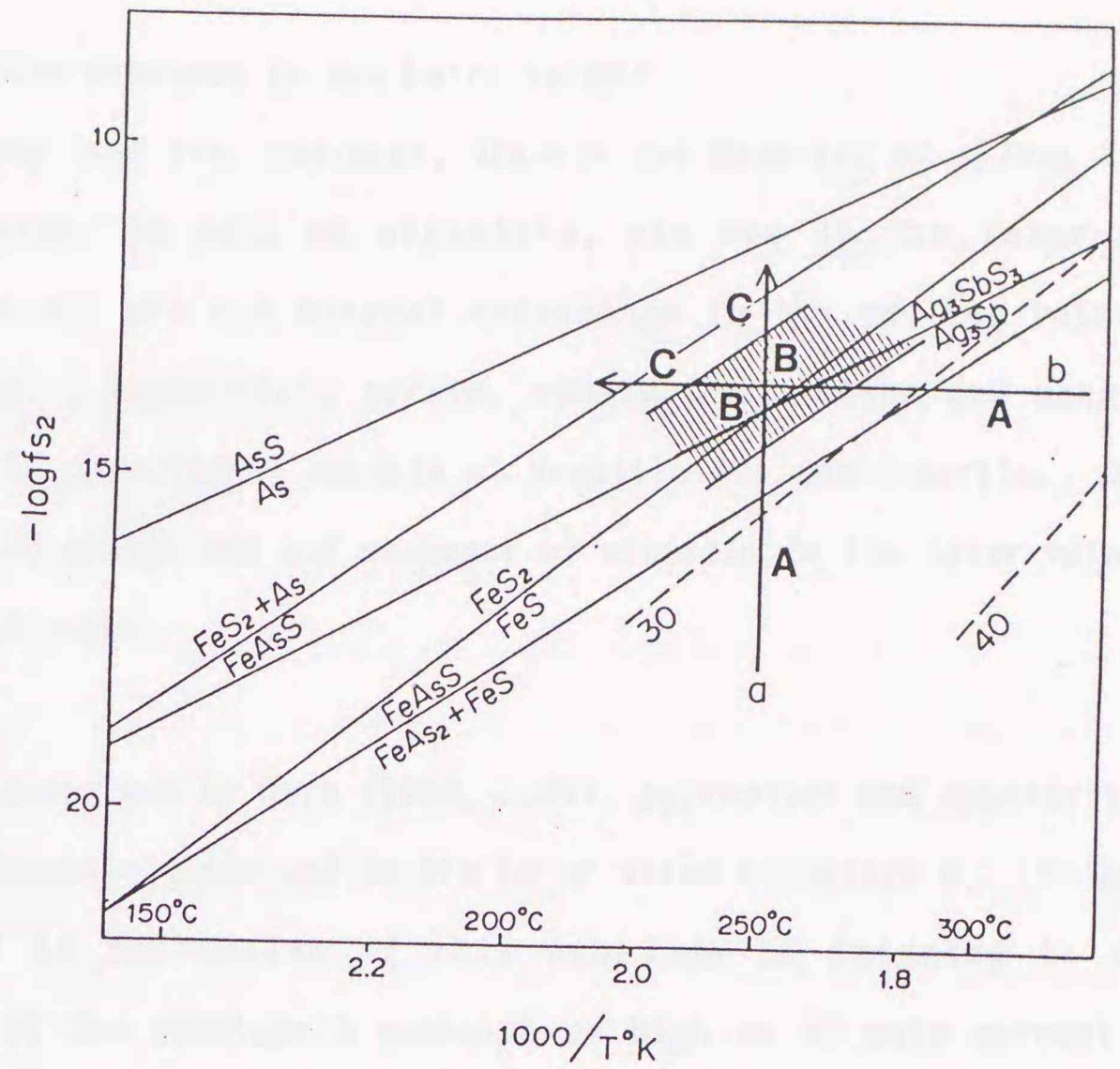

Figure 48. Typical transition of temperature and sulfur fugacity in the later veins based on successive change of mineral assemblages modified after Ohta (1980).

a: transition vector due to increase of sulfur fugacity
b: transition vector due to decrease of temperature

The zones A, B and C along the arrows correspond the substages A, B and C. Actual trend may be a composite of the vectors a and b, though the vector b (decreasing temperature) was presumably the main factor. Note that absolute values of temperature and sulfur fugacity depend on the location in the vein system. Broken lines with numerals are isopleths of FeS mol% in sphalerite.

The boundary between the substages A and B in the figure corresponds to the upper limit of löllingite. The thermochemical data are after Barton (1968), Craig and Barton (1973) and Scott and Barnes (1971).

Mineralization Sequence in the Later Veins:

Provided that tin, antimony, arsenic and majority of silver in the earlier veins, as well as magnetite, are due to the later-stage mineralization, the ore mineral assemblage in the earlier veins are rather simple; essentially pyrite, sphalerite, galena and manganese minerals with subordinate amounts of hematite and chalcopyrite. On the contrary, the assemblage and sequence of minerals in the later veins are rather complicated.

As is described by Ohta (1980, 1989), pyrrhotite and sphalerite are the first minerals deposited in the later veins (substage A). No cobalt nor nickel in pyrrhotite of this substage is detected to date. Sphalerite of the substage A contains as high as 40 mole percent FeS, but little amounts of copper and indium. Major part of ore formed in the substage A are modified or eroded out by the later ore solutions as already mentioned. The substage B started with deposition of arsenopyrite over pyrrhotite and sphalerite of the substage A. Successive deposition of cassiterite, wolframite, cobaltite, chalcopyrite, stannite, Bi-Pb-Ag-S minerals, tennantite or arsenic-rich tetrahedrite, indium-containing sphalerite and the Zn-In mineral characterize the substage B. The substage C is marked by precipitation of the silver sulfosalts and replacement of copper in tin and indium minerals of the substage B with silver as is denoted in Chapter 4. This replacement formed hocartite, pirquitasite and the Ag-In mineral. The tetrahedrite-tennantite solid solution deposited in this substage contains more antimony and silver than that in the substage B. Canfieldite also is a product of the substage C.

Tin sulfides of the substages B and C are partly replaced by rhodostannite and toyohaite. Moreover, herzenbergite and berndtite replacing rhodostannite and/or toyohaite are frequently observed as is described already. The former two, therefore, seem to be slightly younger than the latter two. All of these four minerals are closely related to the formation of the kaolin minerals, or the argillic assemblage commonly recognized in the tin-bearing later veins, and exhibit the same occurrence mode. The argillic alteration shows many evidences of erosion of preexisting ore minerals such as sphalerite and galena. In addition, the porous appearance of rhodostannite and toyohaite suggests loss of volume. Thus the formation of these minerals is attributed to partial decomposition of preexisting tin sulfides such as:

$$3Me_2FeSnS_4 + 4H^+ \rightarrow Me_2FeSn_3S_8 + 2FeS_2 + 4Me^+ + 2H_2 \quad (6)$$

$$Me_2FeSn_3S_8 + 2H^+ \rightarrow 3SnS_2 + FeS_2 + 2Me^+ + H_2 \quad (7)$$

$$Me_2FeSnS_4 + 2H^+ \rightarrow SnS_2 + FeS_2 + 2Me^+ + H_2 \quad (8)$$

where Me represents Cu or Ag, Me_2FeSnS_4 stannite or hocartite, and $Me_2FeSn_3S_8$ rhodostannite or toyohaite. FeS_2 is pyrite, and SnS_2 is berndtite. All these reactions, even (6) for the formation of toyohaite or rhodostannite, remove silver or copper from ore, and it is evident that the mineralization which formed the assemblage, herzenbergite + berndtite + kaolin minerals, postdates the silver sulfosalt mineralization of the substage C. Thus the formation of these minerals, as well as of rhodostannite and toyohaite, is not directly related to the

silver-rich ore solution of the substage C, and is eventually attributed to the ore solution of the substage D which have formed the kaolin minerals within the later veins. Some of the lead-antimony sulfosalts observed in the later veins in Toyoha may also have formed in similar mechanism in the substage D or E. For example, a reaction to form a lead-antimony sulfosalt from a silver-lead-antimony sulfosalt and galena is expressed like as:

$$\underset{\text{(diaphorite)}}{2Ag_6Pb_4Sb_6S_{16}} + \underset{\text{(galena)}}{7PbS} + 12H^+ \rightarrow \underset{\text{(polybasite)}}{3Pb_5Sb_4S_{11}} + 12Ag^+ + \underset{\text{(aq)}}{6H_2S} \qquad (9)$$

No time gap between the substages A and B is indicated by micro- nor macro-textures of the ore, and the only reason to put a substage boundary between them is the extreme difference of mineral and element assemblages, while a tectonic boundary is recognized as cutting relation of ores between the substages B and C (Yoshie et al., 1986; Kanbara et al., 1989). Neither bismuth nor cobalt minerals are observed in ore samples of the substages C, D and E. In addition, occurrences of minerals show no evidence that tin and indium were derived directly from the ore solution in the substages C, D or E. Based on these observations, the mineralization sequence at the Toyoha deposit is summarized in Table 22. A common sequence recognized in both Toyoha and the Bolivian type tin deposits (Sugaki and Kitakaze, 1988) is

1: pyrrhotite+arsenopyrite+pyrite+cassiterite+wolframite

2: stannite+chalcopyrite+marcasite

3: silver sulfosalts+hocartite+canfieldite+rhodostannite+teallite

where 1 and 2 correspond to the substages A and B, and 3 to the substage C and later. It is noteworthy that the similarity is only for the later-stage mineralization, and none that corresponds to the earlier stage of the Toyoha deposit is recognized in Bolivian tin deposits. Therefore, the overlapping of the earlier- and the later-stages at Toyoha have occurred presumably by chance, while the sequence recognized through the substages A, B and C might be essential to the tin-bearing polymetallic veins.

Table 22. Mineralization sequence of ore in the Toyoha deposit.

	Earlier stage		Later stage				Notes (see text)
		A	B	C	D	E	
E	sp	========--	-----:	-----:	-----:		
a V	gn	========-		-----:	--:		
r e	py	==========	-?-	-?-	-----:	-----:--	
l i	hm	=== =====		****:	*****:	**:	* hm -> mg
i n	mn	--=			-:--1--:	--1==:==1==:	-=1 in northwestern
e s	cp	-?--			--:	-----:	veins
r	cs			--	:***	:	* cs -> cf
	ag				--:	=====: *?*:	* ag -> ns
	po		=====:	***--:	*****:	**	* po -> mc, py
S L	sp		=====:	=*=*:	=*=*:	=====:	* highFe -> lowFe
o a	gn				---:	=====: ---	
u t	py			=====:	=====:	=====:--	
t e	cp			--==:	-- ==:		
h r	asp			=====:	-		
e	cs			=*=*:	***		* cs -> Sn sulfides
a V	wf			---			
s e	st			-===:	**1**:	**2**:	*1 Cu,Ag substitution
t i	co			==			*2 to hz,bd,ty,rs
e n	bi			====:			
r s	tn			===-:	-		
n	tt			-==:	=====:		
	ssf				=====:	****:	* ssf -> pss
	pss					----:---	
	mn					-----:	
B V	asp		-----:	-			
e l	ber			--?-:	----		
r s	mn			--?--:	-----:	-?-	

== deposition (major amount) -- deposition (minor amount)
** modification A -> B change from A to B
Substage positions marked with ? are questionable.

Ber Vls:Quartz-manganocalcite-berthierite (or stibnite) veinlets cutting the Tajima vein.

ag:argentite asp:arsenopyrite bd:berndtite
ber:berthierite or stibnite bi:Bi minerals cf:canfieldite
co:Co-minerals cp:chalcopyrite cs:cassiterite gn:galena
hm:hematite hz:herzenbergite mc:marcasite mg:magnetite
mn:Mn-minerals ns:native silver po:pyrrhotite pss:Pb-Sb sulfosalts
py:pyrite rs:rhodostannite ssf:Ag sulfosalts sp:sphalerite
st:stannite tn:tennantite tt:tetrahedrite ty:toyohaite
wf:wolframite highFe:high-iron sphalerite lowFe:low-iron sphalerite

5-3. Formation Conditions and History

Fluid inclusion data in Figure 43 and Figure 44 indicate that the approximate formation temperature ranges of the Izumo, Harima and Tajima veins are 200 to 300°C, 175 to 250°C, and 150 to 250°C respectively. Figure 44 shows two trends of fluid inclusion data as described above, Harima-Tajima and Izumo, and suggests that the temperature and NaCl equivalent concentration of the initial ore solution were higher than 250°C and 2.3 weight percent for the former trend, and higher than 300°C and 4.2 weigh percent for the latter. The only possible mechanism to decrease salinity and temperature simultaneously might be mixing of the ore solution with water of lower temperature and salinity. Assuming that the temperature and salinity of the mixing counterpart correspond to the lowest measured values, they are estimated to be 160 to 210°C and 0.35 weight percent for the Harima-Tajima trend (earlier-stage mineralization), and 210 to 250°C and 0.5 weight percent for the Izumo trend (later-stage mineralization). Oxygen isotope data indicate that the mixing counterparts are geothermal water of meteoric origin, and the initial ore solutions are of deep origin, possibly magmatic (Matsuhisa et al., 1986; Matsuhisa and Yajima, 1989). Figure 44, Figure 47 and Figure 49 indicate gradational change in temperature, salinity, and mineral assemblage from the Izumo vein to the Tajima vein via the Sorachi and Soya veins during the later-stage mineralization. This implies continual invasion of ambient geothermal water into the ore solution on the way from the southeast to the north and northwest of the vein swarm. Therefore, the difference between the estimated temperatures of the mixing counterparts, the earlier and the later, presumably reflects the temperature difference of the ambient geothermal water

system.

The fluid inclusion temperatures were measured only for coarse crystals of quartz and of translucent sphalerite. Both of them are rather rare in the later veins. Estimated iron-zinc partitioning temperatures for some pairs of sphalerite and stannite or kesterite based on the equation after Nakamura and Shima (1982) are between 228 and 358°C (Ohta, 1989). The formation temperatures of arsenopyrite calculated based on the Kretschmar and Scott's data (Table 14) are applicable only when the sulfur fugacity is known. As indicated by the rare occurrence of löllingite predated by marmatite with 30 to 40 mol% of FeS of the substage A, the sulfur fugacity at the beginning of the substage B are implied to have been at around the upper limit of löllingite (Figure 48). Therefore, the maximum formation temperature of arsenopyrite seems to have been about 360°C, which is in good agreement with the maximum iron-zinc partitioning temperatures in spite of the caution denoted by Barton (1979), "there is a great deal of room for error in applying the Kretschmar and Scott's arsenopyrite geothermometer to temperatures below 400°C", and the inconsistency of calculated temperatures (about 500°C) for low-temperature (about 300°C) hydrothermal deposits recognized by Sharp et al. (1985). On the other hand, the arsenopyrite with the lowest arsenic mol% probably precipitated at the end of the substage B when the sulfur fugacity was at around the arsenopyrite - native arsenic+pyrite boundary. Consequently, Table 14 suggests that approximate formation temperature range of arsenopyrite at Toyoha is between 270 to 360°C.

The temperatures calculated based on the compositions of minerals

are significantly higher than those indicated by fluid inclusion data. In addition, the existence of the following phases suggests that a high pulse of temperature may have reached up to 400°C at the lower levels of the southeastern later veins during the substages A and B (Ohta, 1989):

1: Extremely iron-rich sphalerite (marmatite) associated with pyrrhotite.

2: The chalcopyrite-stannite solid solution and the anisotropic chalcopyrite.

3: The concentric parallel bands of the anisotropic chalcopyrite, stannite or kesterite, roquesite and mixtures of their extremely fine grains.

4: The Cu-Zn-Fe mineral within the anisotropic chalcopyrite.

Therefore it is likely that the initial ore solution of the later-stage mineralization was hotter than 400°C, and its force against the ambient geothermal water was at its maximum in the substages A and B. Meanwhile, based on the data of mineral assemblages and FeS mol% in sphalerite, approximate ranges in sulfur fugacity of the substages A, B and C are deduced as follows:

Substage A: Between the isopleth of 40 mol percent FeS in sphalerite and the pyrrhotite - pyrite boundary (maybe mostly lower than the upper limit of löllingite).

Substage B: Between the upper limit of löllingite and the arsenopyrite - pyrite+ arsenic boundaries.

Substage C: Passed through the arsenopyrite - pyrite+arsenic boundary during this substage.

It is evident that this sequence is in order of increasing sulfur fugacity and/or decreasing temperature (Figure 48).

All the mineral assemblages, chemical compositions and fluid inclusion data from Toyoha give evidence that both temperature - fs_2 and temperature - fo_2 trends of the later-stage mineralization (Figure 47, Figure 49) were shifted to the lower fugacity side in terms of mineral assemblage from those of the earlier stage. The fs_2 - temperature trends of the majority of ordinary epithermal veins such as Ohe are close to those of the earlier stage (e.g. Sato et al., 1980). Though Toyoha is similar to the tin-bearing polymetallic veins at Ikuno and Akenobe in the metal assemblage (Cu-Pb-Zn-Sn-In-W-Bi), in the overall formation temperature (Imai, 1978), and in the wall-rock alteration (Narita and Sawai, 1988; Sawai, 1988), absence of bornite, mawsonite, and stannoidite indicates lack of a high-sulfur-fugacity or low-temperature stage of tin mineralization at Toyoha.

The earlier- and the later-stage trends on the temperature - fs_2 diagram correspond to the trends of ore solutions caused by magnetite- and ilmenite-series granitoids (Tsukimura et al., 1987) respectively (Figure 50). The concordance of the trends and common existence of tin and indium in the later veins suggest that the later-stage mineraliza-

tion was initiated by an ore solution emanated from an intrusion of ilmenite-series granitoid, and the earlier veins were derived from a magnetite-series granitoid. As is described by Tsukimura et al. (1987) it is estimated that sulfur exists mostly as H_2S in ilmenite-series magmas and as SO_2 in magnetite-series, and that total abundance of sulfur in fluid phase of magmas for magnetite-series is much greater than that for ilmenite-series magmas. Accordingly, the contrast between the earlier and the later mineral assemblages are attributed mostly to the difference in the states and amounts of sulfur in the parent magmas, and the existence of tin and indium in the later veins is presumably due to the low oxygen fugacity during the magmatic differentiation in the ilmenite-series granitoid (e.g. Ishihara, 1981). The high temperature origin of the solution is also suggested by the above-mentioned oxygen isotopic data, and the extremely high iron contents in chlorite from Toyoha (Ohta and Yajima, 1988). Heinrich (1990) pointed out that an ore solution equilibrated with a granitoid magma can transport as high as thousand ppm of tin as chloride complexes, and that most efficient mechanism to deposit cassiterite from the solution is dissociation of the tin-chloride complexes by dilution of the ore solution. Kanbara et al.(1989) pointed out that saline high temperature fluid is still active in the fissures of the Shinano vein, and its chemical and oxygen isotopic compositions are similar to those of the ore solution of Toyoha estimated by Matsuhisa et al. (1986). Moreover, the current rock-temperature gradient data indicate that the high temperature fluid comes from the south of the Izumo and Shinano veins, that is, from the depth of Mount Nagaoyama (Figure 1a). This implies that the root and route of the fluid are almost in the same position with those of the ore solution.

Based on the observations and considerations, a model for the formation history of the Toyoha deposit is deduced as follows:

1: Earlier-stage mineralization of ordinary epithermal type was proceeded by an ore solution presumably derived from a latent magnetite-series granitoid stock. After the deposition of zinc and lead as essential metals, the activity of the solution decreased and the influence of the ambient geothermal water of meteoric origin extended to have deposited manganese minerals of the substage II defined by Kanbara et al. (1989).

2: Another latent granitoid stock intruded in a depth to the south of the Izumo and Shinano veins. Higher tops of the intrusion reached to the horizon of a sedimentary rock, possibly the Usubetsu Formation, and evolved to ilmenite-series magma by contamination of organic substances. Lower tops or shoulders of the intrusion, however, was not completely effected by the organic substances.

3: A hydrothermal ore solution emanated from the higher top of the intrusion was enriched with chlorine and rare metals such as tin, but depleted in sulfur which existed mostly as H_2S, and formed ore of the successive substages A and B. Part of the hematite (without argentite association) in the earlier veins may have been reduced to magnetite at this time.

4: A solution from the lower top was not enriched with the rare elements, but contained enough amounts of chlorine and sulfur to carry base metals as chloride complexes, and silver as chloride and

sulfide complexes. The solution caused intense silver mineralization which deposited silver sulfosalts, and modified part of tin and indium minerals in the earlier veins. The same mineralization reduced hematite to magnetite, and simultaneously deposited argentite in the earlier veins.

5: In either stages, the main mechanism of metal deposition was dilution of the ore solution due to mixing with the meteoric geothermal water. But oxidation of the solution by hematite also played an important roll to deposit argentite in the earlier veins.

At this time, no sample nor data is available for the granitoids that must have caused the mineralization at Toyoha. The only known igneous rocks which can be correlated to the mineralization are the Muineyama (Nagaoyama) Andesite and the dacitic lavas and pyroclastics of the Sanbonmata (Suberizawa) Formation because of their ages comparable to those of the mineralization at Toyoha. All other igneous rocks observed on the surface or in the drill holes around Toyoha are too old to be related with the formation of the Toyoha deposit (Table 1). As all data obtained from the veins at Toyoha indicate that the ore solutions came from south, it may be reasonable to conclude that the ore solutions were emanated from latent granitoid stocks under the Muineyama andesite. The andesite exhibits absolute ages as old as the beginning of the mineralization at Toyoha (Table 1), and its volume is enough to hide large granitoid stocks which could have emanated the huge amounts of ore solutions to have formed the Toyoha deposit. An extension of the shoot of the mineable uppermost levels (+30 mL at Harima, -150 mL at Izumo) to the south goes down a few kilometers beneath the peak of the

Mount Nagaoyama. That depth is believed to be most suitable for granitoid stocks to evolve ore solutions at their top (e.g. Burnham, 1979). Therefore petrological studies on the andesite, and on some granitoids detected in the drill holes done by MMAJ (Figure 1) and the Toyoha Mines Co. Ltd. should be performed to clarify the features of the igneous activities possibly related to the intense mineralization at Toyoha.

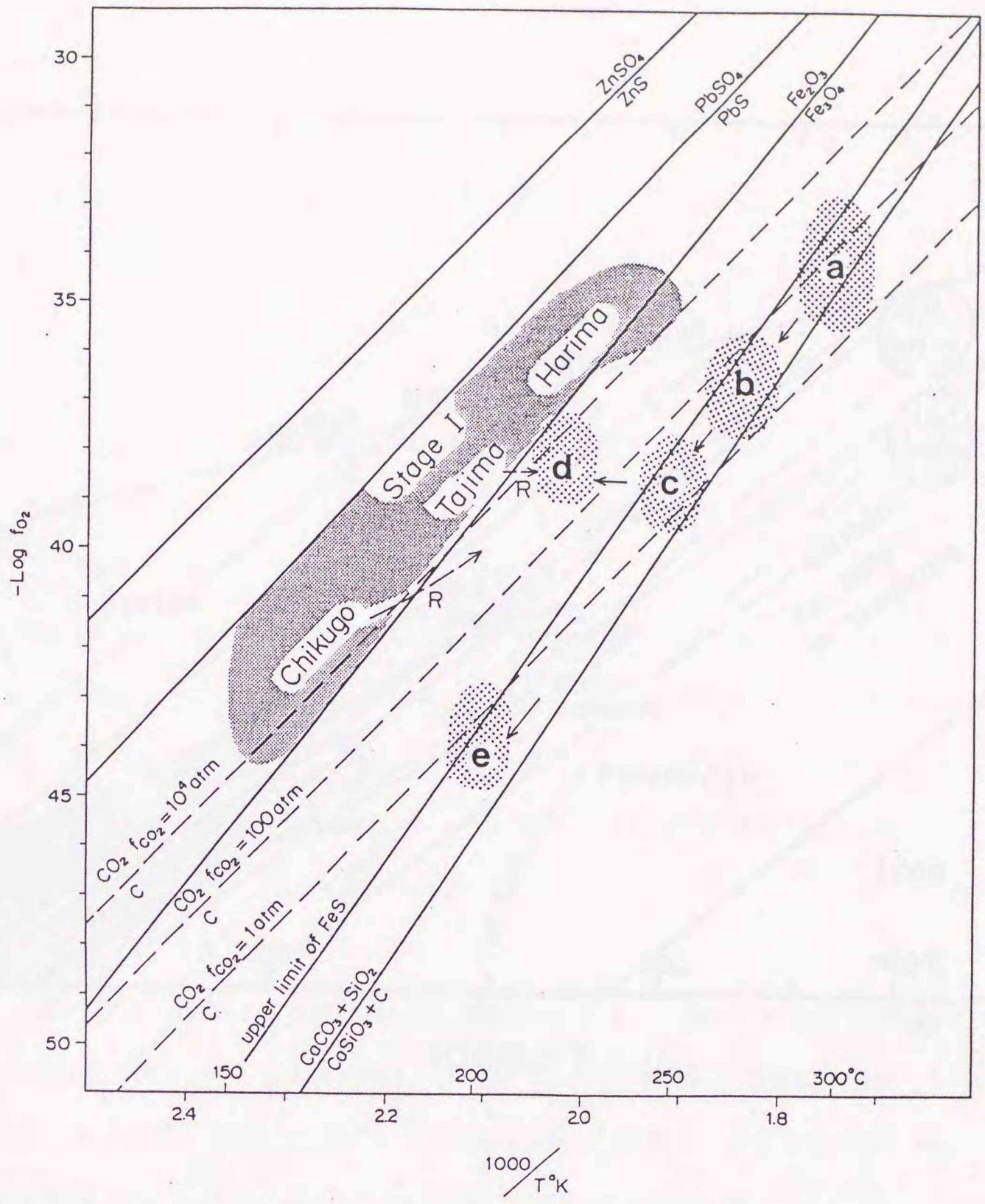

Figure 49. Diagram showing the temperature - oxygen fugacity conditions of ore formation at Toyoha (Yajima and Ohta, 1979).

Stage I: Formation conditions of hematite-pyrite ore in the earlier-stage mineralization at the Chikugo, Tajima and Harima veins.

a to e: Conditions during the substages B and C at the Izumo vein -580 mL(a) and -430 to -400 mL(b), the Sorachi vein -300 mL(c), argentite-quartz veinlets in the Tajima vein -200 mL(d), and calcite-quartz-berthierite veinlets crossing the Tajima vein -450 mL(e).

Solid arrows show a flow path of the ore solution, and broken arrows marked with R indicate reduction of the early-stage ore by the later-stage ore solution.

The diagram is based on the data in Holland (1959, 1965), and Ripley and Ohmoto (1977).

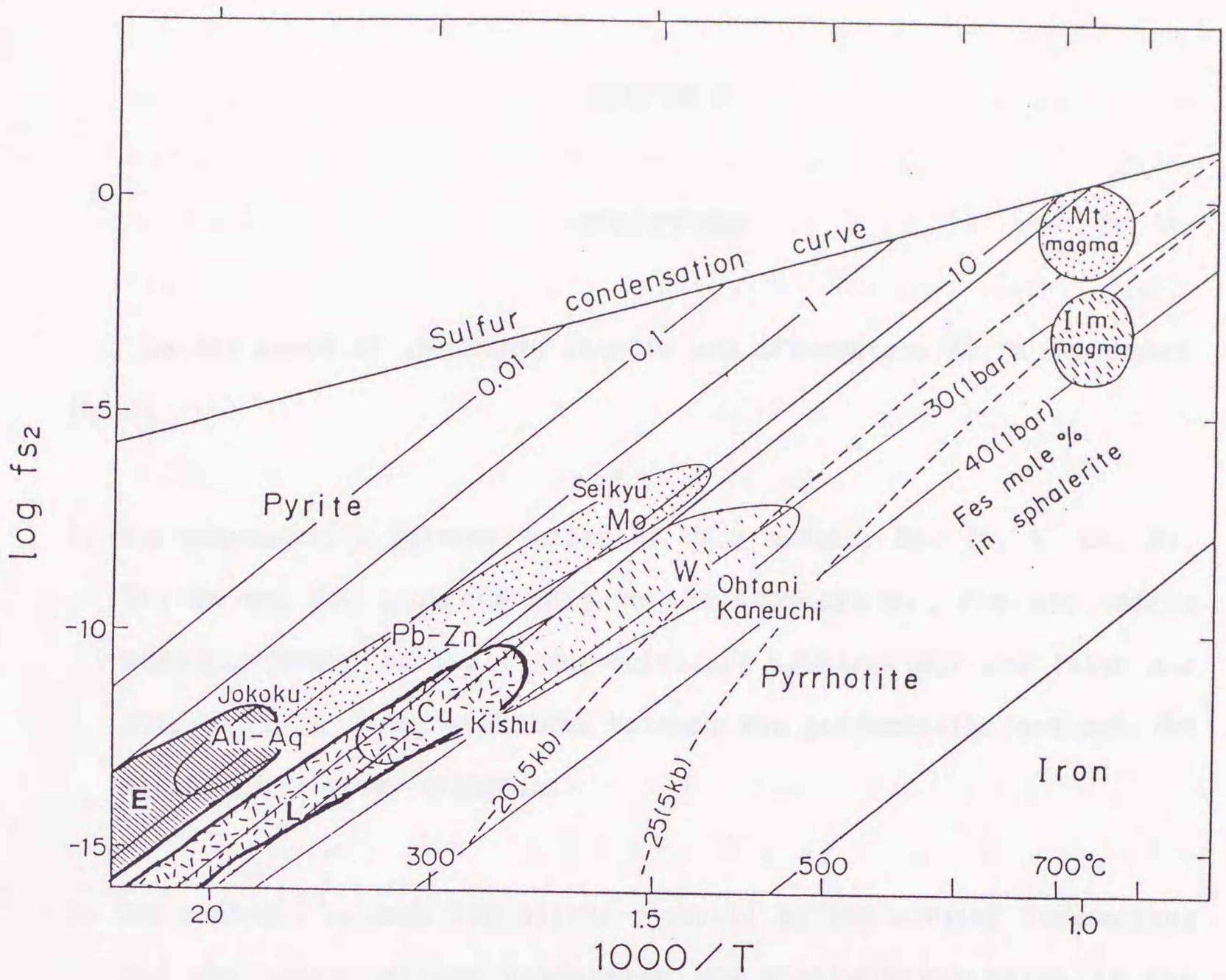

Figure 50. Diagram showing two trends of the ore solutions related to ilmenite- and magnetite-series granitoids after Tsukimura et al. (1987), and trends of the ore solutions formed the Toyoha deposit.

E: trend of the solution deposited sphalerite in the earlier-stage mineralization based on fluid inclusion data (Yajima and Ohta, 1979) and FeS mol% in sphalerite summarized in this study and in Yoshie et al. (1986).

L: trend of the solution caused the rare metal mineralization (substage B) in the later-stage mineralization based on the mineral assemblage, FeS mol% in sphalerite, and estimated formation temperatures by Yajima and Ohta (1979), Ohta (1980, 1989), Yoshie et al. (1986) and this study.

CHAPTER 6

CONCLUSIONS

On the basis of the above results and discussions it is concluded that:

1: The polymetallic mineralization of rare metals; Sn, In, W, Co, Ni, Bi, Ga and Mo; occurred only in the substage B. Tin and indium minerals formed in the silver-sulfosalt substage (C) and later are attributed to local reactions between the polymetallic ore and the later hydrothermal solutions.

2: The contrast between the silver minerals in the earlier (argentite) and the later (silver sulfosalts and freibergite) veins is due mainly to the difference of oxygen fugacities caused by the existence of hematite in the earlier veins. Deposition of both types of silver minerals proceeded simultaneously; as oxidation of silver-sulfide complexes by hematite in the earlier veins, and as dissociation of silver-chloride complexes by mixing of the ore solution with ambient geothermal water in the later veins; during the substage C.

3: The temperatures and NaCl equivalent concentrations of the initial ore solutions were higher than 250°C and 2.3 weight percent for the Harima-Tajima trend (earlier-stage mineralization), and higher than 300°C and 4.2 weigh percent for the Izumo trend (later-stage

mineralization). The chemical compositions and occurrences of rare-metal-containing minerals suggest that a pulse of high temperature may have reached up to 400°C in the course of the tin-indium mineralization of the substage B, for which an initial hydrothermal fluid at 350 to 400°C, salinity of 5 to 7 equivalent weight percent NaCl, fo_2 below the upper limit of pyrrhotite, fs_2 at around the pyrrhotite- pyrite boundary, is consistent with data of fluid inclusions and mineral assemblages at Toyoha.

4: The ore solution flew almost laterally from the southeast to the north and northwest of the Toyoha vein swarm through the Sorachi and Soya veins as major paths. In either stage, the main mechanism of metal deposition was mixing of the ore fluid from a granitic source with geothermal water of meteoric origin, except the argentite deposition in the earlier veins. The temperature and salinity of the geothermal water (mixing counterpart) are estimated to be 160 to 210°C and 0.35 weight percent for the earlier stage, and 210 to 250°C and 0.5 weight percent for the later.

5: The earlier- and the later-stage trends on the temperature versus sulfur fugacity diagram correspond to the trends caused by magnetite- and ilmenite-series granitoids respectively. This, as well as the occurrence of tin and indium in the later veins, suggest that the later-stage mineralization was initiated by an ore solution emanated from an intrusion of ilmenite-series granitoid, and that the earlier was derived from a magnetite-series granitoid. This may be attributed to local reduction of an intrusion by contamination of organic materials in the Usubetsu Formation. The chronological

data, the zonal distribution of minerals, metal grades and fluid inclusions, and the flow vector of the currently active hydrothermal solution in the Shinano vein indicate that the source of the ore solution is a latent granitoid intrusion at the root of the Muineyama Andesite.

REFERENCES

Akome, K. and Haraguchi, M. (1963): Geology and ore deposits of Toyoha mine. Mining Geol., 13, 93-99 (in Japanese with English abstract).

Akome, K. and Haraguchi, M. (1967): The characteristics of fracture and mineralization of the Toyoha mine. Mining Geol., 17, 93-100 (in Japanese with English abstract).

Barnes, H. L. (1979): Solubilities of ore minerals. In Geochemistry of Hydrothermal Ore Deposits (second edition)., H. L. Barnes ed., A Wiley-Interscience Publication, New York.

Barton, P. B. Jr. (1969): Thermochemical study of the system Fe-As-S. Geoch. Cosmoch. Act., 33, 841-857.

Barton, P. B. Jr. (1979): Sulfide mineral stabilities. In Geochemistry of Hydrothermal Ore Deposits (second edition)., H. L. Barnes ed., A Wiley-Interscience Publication, New York.

Burnham, C. W. (1979): Magmas and hydrothermal fluids. In Geochemistry of Hydrothermal Ore Deposits (second edition)., H. L. Barnes ed., A Wiley-Interscience Publication, New York.

Chang, L. Y., Wu, D. and Knowles, C. R. (1988): Phase relations in the system Ag_2S-Cu_2S-PbS-Bi_2S_3. Econ. Geol., 83, 405-418.

Craig, J. R. and Barton, P. B. Jr. (1973): Thermochemical approximations for sulphosalts. Econ. Geol., 68, 493-506.

Crerar, D. A., Wood, S. and Brantly, S. (1985): Chemical controls on solubility of ore-forming minerals in hydrothermal solutions. Can. Min., 23, 333-352.

References

Fujikawa, O., Matsueda, H. and Yui, S. (1990): Mineralization at Shinano vein in the Toyoha mine, Hokkaido (abstract). Abst. Joint Meet. Soc. Mining Geol. Japan, Mineral Soc. Japan and Japan. Assoc. Mineral. Petrol. Econ. Geol., B-10 (in Japanese).

Haraguchi, M. and Tajima, Y. (1969): Mineralization of the Toyoha Mine, with special reference to the nature and occurrence of sphalerite and behaviour of silver. Mining Geol., 19, 9-18.

Hashimoto, H., Ishizaka, T. and Ichinose, T. (1977): Recent exploration for the Izumo vein of the Toyoha mine. Mining Geol., 27, 87-97 (in Japanese with English abstract).

Heinrich C. A. (1990): The chemistry of hydrothermal tin-(tungsten) ore deposition. Econ. Geol., 85, 457-481.

Holland, H. D. (1959): Some applications of thermochemical data to problems of ore deposits I. Stability relations among the oxides, sulphides, sulphates and carbonates of ore and gangue minerals. Econ. Geol., 54, 184-233.

Holland, H. D. (1965): Some applications of thermochemical data to problems of ore deposits II. Mineral assemblages and the composition of ore-forming fluids. Econ. Geol., 60, 1101-1166.

Igarashi et al. (1978): Geological investigation of hydrothermal alteration haloes in Toyoha geothermal field, Hokkaido. Rept. Geol. Surv. Japan, 259, 9-42 (in Japanese with English abstract).

Imai, H. (1978): Geological Studies of the Mineral Deposits in Japan and East Asia. Univ. Tokyo Press. 392pp.

Ishihara, S. (1981): The granitoid series and mineralization. Econ. Geol. 75th Anniv. Vol., 458-484.

Ishiyama, D. and Matsueda, H. (1988): Modes of occurrence and chemical compositions of silver-bearing minerals and accompanied minerals from the Matahachi deposit of Jokoku mine, southwestern Hokkaido. Rept. Min. Coll. Akita Univ., 53, 17-32 (in Japanese with English abstract).

Johan, Z. and Picot, P. (1982): La pirquitasite, Ag_2ZnSnS_4, un nouveau membre du groupe de la stannite. Bull. Mineral., 105, 229-235 (in French with English abstract).

Kanbara, H. and Kumita K. (1990): Mode of occurrence and chemical composition of electrum from the Toyoha polymetallic vein-type deposits, Hokkaido, Japan. Prof. Urashima volume, 201-210 (in Japanese with English abstract).

Kanbara, H., Sanga, T., Ohura, T. and Kumita, K. (1989): Mineralization of Shinano vein in Toyoha polymetallic vein-type deposits, Hokkaido, Japan. Mining Geol. 39, 107-122 (in Japanese with English abstract).

Karup-Møller, S. (1970): Gustavite, a new sulphosalt mineral from Greenland. Can. Min., 10, 173-190.

Kase, K. (1987): Tin-bearing chalcopyrite from the Izumo Vein, Toyoha mine, Hokkaido, Japan. Can. Mineral., 25, 9-13.

Kojima, S., Kawazumi, T., Takeyama, T. and Miyaishi, O. (1979): The modes of occurrence and mineralogy of silver minerals from the Toyoha Mine. Mining Geol., 29, 197-206 (in Japanese with English abstract).

Koshimizu, S. and Narita, E. (1987): Fission-track dating of Paleogene acidic rocks from the western Jozankei area, Sapporo, Japan., Jour. Geol. Soc. Japan, 93, 439-440 (in Japanese with English abstract).

Kretschmar, U. and Scott, S. D. (1976): Phase relations involving arsenopyrite in the system Fe-As-S and their application. Can. Mineral. 14, 364-386.

Kuwahara, T., Miyazaki, T., Tani, T. and Iida, K. (1983): A characterization of the vein mineralizations at the Motoyama deposit, Toyoha mine from the viewpoint of their tectonic setting and ore assays. Mining Geol., 33, 115-129 (in Japanese with English abstract).

Matsuhisa, Y., Yajima, J. and Ohta, E. (1986): Oxygen-isotope ratio and fluid inclusions in gangue quartz from the Toyoha mine (abstract). Abst. Joint Meet. Soc. Mining Geol. Japan, Mineral Soc. Japan and Japan. Assoc. Mineral. Petrol. Econ. Geol., 26-26 (in Japanese).

Matsuhisa, Y. and Yajima, J. (1989): Magmatic contribution to the ore-forming solution of the Toyoha Polymetallic vein, Hokkaido (abstract). Deep Crust Fluid-Rock Interaction, Symposium 1, 21-21 (in Japanese).

Miyajima, T., Hakari, N. and Kita, M. (1971): Some considerations on geologic structure and mechanisms of fracturing at the Toyoha mine. Mining Geol., 21, 22-35 (in Japanese with English abstract).

MMAJ (Metal Mining Agency of Japan) (1976): Report on detailed geological survey in Jozankei district during the fiscal year Showa 50 (in Japanese).

MMAJ (1977): Report on detailed geological survey in Jozankei district during the fiscal year Showa 51 (in Japanese).

MMAJ (1988): Report on detailed geological survey in Jozankei district during the fiscal year Showa 63 (in Japanese).

MMAJ (1990): Report on detailed geological survey in Jozankei district during the fiscal year Heisei 1 (in Japanese).

Nakamura, Y. and Shima, H. (1982): Fe and Zn partitioning between stannite and sphalerite (abstract). Abst. Joint Meet. Soc. Mining Geol. Japan, Mineral. Soc. Japan, and Japan Assoc. Mineral. Petrol. Econ. Geol., A-8 (in Japanese).

Narita, E. and Sawai, O. (1988): Wall rock alteration of rhyolitic tuff in the Kanagase area, Ikuno mine, Hyogo Pref., Japan. Mining Geol. Spec. Issue, 12, 37-46.

Narita, E., Yajima, J. and Ohta, E.(1977): On the occurrence of tin and tungsten minerals from the Toyoha mine (abstract). Abst. Joint Meet. Soc. Mining Geol. Japan, Mineral. Soc. Japan, and Japan Assoc. Mineral. Petrol. Econ. Geol., C-17 (in Japanese).

Narui, E., Yoshie, T. and Kato, K. (1988): On the recent exploration results at the Toyoha polymetallic vein-type deposits, Hokkaido. Mining Geol., 38, 99-113 (in Japanese with English abstract).

NEDO (New Energy and Industrial Technology Development Organization) (1988): Report on geothermal energy exploration and development of the Toyoha area. 1156p (in Japanese).

Ohta, E. (1979): Occurrence and geochemical environment of berthierite from Toyoha Mine. Mining Geol., 29, 97-102 (in Japanese with English abstract).

Ohta, E. (1980): Mineralization of Izumo and Sorachi veins of the Toyoha mine, Hokkaido, Japan. Bull. Geol. Surv. Japan, 31, 585-597 (in Japanese with English abstract).

Ohta, E. (1989): Occurrence and chemistry of indium-containing minerals from the Toyoha Mine, Hokkaido, Japan. Mining Geol., 39, 355-372.

Ohta, E. and Marumo, K. (1985): Occurrence of apatite and associated gangue minerals in the Toyoha deposits, West Hokkaido, Japan. Proc. Japan Academy, 61, Ser. B, 99-102.

Ohta, E. and Yajima, J. (1979): New occurrence of canfieldite and berthierite from the Toyoha mine (abstract). Abst. Joint Meet. Soc. Mining Geol. Japan, Mineral. Soc. Japan, and Japan Assoc. Mineral. Petrol. Econ. Geol., 96-96 (in Japanese).

Ohta, E. and Yajima, J. (1988): Magnesium to iron ratio of chlorite as indicator of type of hydrothermal ore deposit. Mining Geol. Spec. Issue, 12, 17-22.

Ohta, E., Yajima, J. and Kanazawa, Y (1987): Chemistry of ore minerals from the Toyoha mine (abstract). Abst. Joint Meet. Soc. Mining Geol. Japan, Mineral. Soc. Japan, and Japan Assoc. Mineral. Petrol. Econ. Geol., 68 (in Japanese).

Ripley, E. M. and Ohmoto, H. (1977): Mineralogic, sulphur isotopic and fluid inclusion studies of the stratabound copper deposits at the Raul mine, Peru. Econ. Geol., 72, 1017-1041.

Sato, J., Maeda, H., Kinryu, Y. and Ono, S. (1980): Mineral paragenesis and fluid inclusion data of the Ohe polymetallic vein-type deposits, Hokkaido, Japan. Mining Geol., 30, 277-288.

Sato, J. and Ono, S. (1988): Relationship of chemical composition to reflectivity and Vickers hardness of fahlore. Mining Geol. 38, 401-406 (in Japanese with English abstract).

Sawai, O. (1986): The distribution of alteration zones in the eastern area of the Toyoha mine, Hokkaido, Japan. Mining Geol., 36, 273-288 (in Japanese with English abstract).

Sawai, O. (1988): Wall rock alteration of the Chiemon vein swarm in the Akenobe mine, Hyogo Pref., Japan. Mining Geol. Spec. Issue, 12, 23-36.

Sawai, O. and Ganzawa, Y. (1988): Fission track ages of some Neogene Tertiary acidic tuffs around the Toyoha mine, southwestern Hokkaido, Japan. Mining Geol., 38, 517-525 (in Japanese with English abstract).

Sawai, O. and Itaya, T. (1988): K-Ar ages of sericite in hydrothermally altered rocks from the Toyoha mine (abstract). Mining Geol., 38, 66-67 (in Japanese).

Sawai, O., Okada, T. and Itaya, T. (1989): K-Ar ages of sericite in hydrothermally altered rocks around the Toyoha deposits, Hokkaido, Japan. Mining Geol., 39, 191-204.

Scott, S. D. and Barnes, H. L. (1971): Sphalerite geothermometry and geobarometry. Econ. Geol., 66, 653-669.

Shikazono, N. (1975): Mineralization and chemical environment of the Toyoha lead-zinc vein-type deposits, Hokkaido, Japan. Econ. Geol., 70, 694-705.

Shimizu, M., Kato, A. and Shiozawa, T. (1986): Sakuraiite: chemical composition and extent of (Zn,Fe)In-for-CuSn substitution. Can. Mineral., 24, 405-409.

Soler, P. (1987): Variations des teneurs en éléments mineurs (Cd,In, Ge,Ga,Ag,Bi,Se,Hg,Sn) des minerais de Pb-Zn de la province polymétallique des Andes du Pérou Central. Mineral. Deposita, 22, 135-143 (in French with English abstract).

Sugaki, A. and Hayashi, K. (1986): Teallite from the Toyoha mine, Hokkaido. Jour. Japan Assoc. Miner. Petro. Econ. Geol., 81, 393-398 (in Japanese with English abstract).

Sugaki, A. and Kitakaze, A. (1988): Tin-bearing minerals from Bolivian polymetallic deposits and their mineralization stages. Mining Geol., 38, 419-435.

References

Tani, T., Iida, K., Yoshie, T. and Tamai, H. (1985): Silver in the Motoyama ore deposit, Toyoha Mine. In Gold-silver Ores in Japan, No. 3. Min. Met. Inst. Japan, 61-88 (in Japanese).

Tsukimura, K., Sato, K. and Ishihara, S. (1987): Regional and temporal variation in FeS content of sphalerite from Japan and its relation to granitoids series. Bull. Geol. Surv. Japan, 38, 227-246.

Uytenbogaardt, W. and Burke, E. A. J. (1971): Tables for Microscopic Identification of Ore Minerals. Elsevier Publishing Co., Amsterdam. 430p.

Watanabe, Y. (1990a): Pull-apart vein system of the Toyoha deposit, the most productive Ag-Pb-Zn vein-type deposit in Japan. Mining Geol., 40, 269-278.

Watanabe, Y. (1990b): Pliocene to Pleistocene volcanism and related vein-type mineralization in Sapporo-Iwanai district, southwest Hokkaido, Japan. Mining Geol., 40, 289-298.

Watanabe, Y. and Iwata, K. (1986): Miocene stratigraphy around Toyoha Mine, southwest Hokkaido. Jour. Geol. Soc. Japan, 92, 817-820 (in Japanese with English abstract).

Watanabe, Y., Iwata, K. and Hasaka, T. (1989): Stratigraphy and structure of the Miocene in the Jozankei area, southwestern Hokkaido. Earth Science, 43, 7-15 (in Japanese with English abstract).

Wu, I. and Petersen, U. (1977): Geochemistry of tetrahedrite and mineral zoning at Casapalca, Peru. Econ. Geol., 72, 993-1016.

Yajima, J. (1977): New occurrence of tin-minerals from the Toyoha mine, Hokkaido, Japan. Mining Geol., 27, 23-30 (in Japanese with English abstract).

References

Yajima, J. and Ohta, E. (1979): Two-stage mineralization and formation process of the Toyoha deposits, Hokkaido, Japan. Mining Geol., 29, 291-306.

Yajima, J. and Okabe, K. (1971): On the iron-rich banded ore from the Toyoha mine, Hokkaido. Mining Geol., 21, 221-228 (in Japanese with English abstract).

Yajima, J., Ohta, E. and Kanazawa, Y. (in press): A new mineral, toyohaite, $Ag_2FeSn_3S_8$.

Yoneda, T. (1987): Barite ores and compositional variations in tetrahedrite-tennantite of the Minamishiraoi Mine, Hokkaido, Japan. Mining Geol. 37, 323-336 (in Japanese with English abstract).

Yoshie, T., Narui, E. and Kato, K. (1986): On the process of mineralization and distribution of minor elements in the Toyoha ore deposit, Hokkaido. Mining Geol., 36, 179-193 (in Japanese with English abstract).

Inches 1 2 3 4 5 6 7 8

1 2 3 4 5 6 7 8 9 10 11 12 13 14 15 16 17 18 19

Centimetres

KODAK Color Control Patches

Kodak
LICENSED PRODUCT

Blue Cyan Green Yellow Red Magenta White 3/Color Black

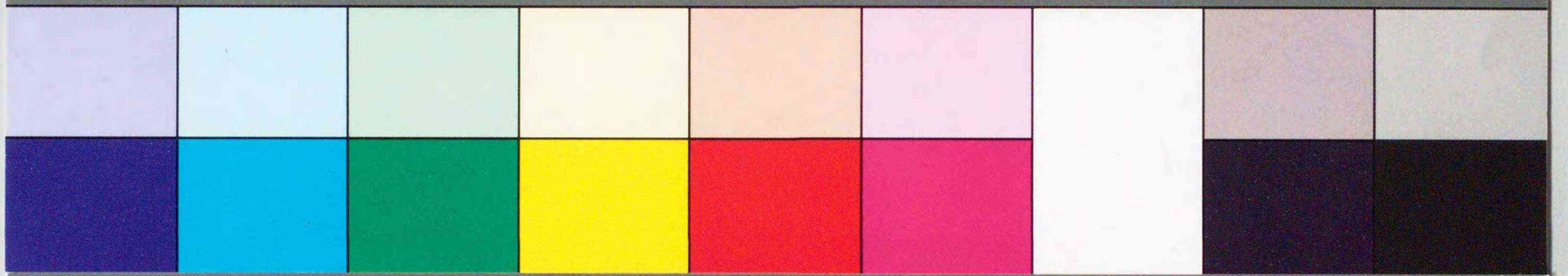

Kodak Gray Scale

C Y M

A 1 2 3 4 5 6 M 8 9 10 11 12 13 14 15 B 17 18 19